Drivers of Spatial and Temporal Heterogeneity in Vegetation Productivity, Function, and Functional Diversity on the Yamal Peninsula, Siberia, Russia

Morgan Shelby Tassone

A thesis presented to the Department of Environmental Sciences Graduate Faculty of the University of Virginia in Candidacy for the Degree of Master of Science

December 2021

Acknowledgements

Many people (and a cat) were absolutely vital to the completion of this thesis. I would first like to thank my advisor, Howard Epstein, for giving me the opportunity to work on this project and for his guidance throughout the entire process. I would also like to thank my committee members, Lauren Simkins and Xi Yang, for their helpful advice and valuable time. Amanda Armstrong and Domingo Alcaraz-Segura, members of the Ecosystem Functional Diversity project team, not only developed the Ecosystem Functional Types used in this thesis, but provided support along the way and were always willing to help me out. The technical support provided by the University of Virginia Stat Lab and Rivanna staff were also invaluable to the analyses included in this thesis. I would also like to thank Justin Braaten, a Google developer who helped Amanda and I develop the snow-free period onset date dataset and a tutorial so that other researchers are able to use this variable in future analyses. Lastly, I could have not completed this project without the ongoing support of my husband Spencer, my work buddy/cat Olive, my friends and family, and my fellow Environmental Sciences graduate students. Funds for this project were provided by the NASA Biodiversity and Ecological Forecasting GEO-BON Work Programme and the University of Virginia. Being a part of the University of Virginia Environmental Sciences Department and a NASA-funded project are some of my proudest accomplishments, and I'm thankful for this opportunity that has not only helped advance my career as an Environmental Scientist, but provided a trove of invaluable life lessons.

Abstract

The understanding of Arctic vegetation patterns and dynamics is necessary to accurately assess carbon gains and ecosystem resistance under projected warming. Uncertainties in determining the relative importance of physical and biological drivers of Arctic vegetation productivity remain, and the potential drivers of vegetation function and functional diversity as determined by Ecosystem Functional Types (EFTs) have not yet been evaluated for the Arctic. This thesis analyzed the climatic, geologic, biologic, and anthropogenic drivers of vegetation productivity, function, and functional diversity across the Yamal Peninsula, a region within the northwestern Siberian tundra, between 2001 and 2018. Productivity was assessed using the Normalized Difference Vegetation Index (NDVI), a proxy for primary productivity and aboveground biomass. Specifically, Max NDVI (representative of peak growing season aboveground biomass) and time-integrated (TI)-NDVI (representative of total growing season productivity) were used. Vegetation function was assessed using NDVI-based EFTs that represent discrete areas with similar carbon gain dynamics, and functional diversity was quantified as EFT richness (the number of unique EFTs within a discrete area).

The spatial distributions of Max NDVI, TI-NDVI, and EFTs were primarily influenced by long-term climate patterns (particularly Summer Warmth Index, the sum of April – September monthly mean temperatures > 0 °C) on the Yamal Peninsula, while spatial patterns of EFT richness were best predicted by the degree of landscape heterogeneity in an area. Max and TI-NDVI increased while EFT richness exhibited no trend across a majority of the Yamal Peninsula between 2001 and 2018, indicating that functional diversity was maintained despite increases in peak aboveground biomass and total productivity. Positive Max NDVI, TI-NDVI, and EFT richness trends were best predicted by distance from the coast, but climate-induced permafrost disturbances, elevation, and human modification were also important predictors of

positive trends. Findings indicated that the most extreme warming on the Yamal Peninsula could cause increases in peak aboveground biomass and total productivity but decrease functional diversity. As a whole, this thesis contributes to the knowledge base needed to disentangle the effects of environmental and anthropogenic drivers on Arctic vegetation productivity, function, and functional diversity. Chapter 1 provides insight into the potential future of Arctic regions undergoing warming, moisture regime shifts, and increasing human modification, while Chapter 2 articulates that Arctic regions with heterogeneous landscapes shaped by permafrost disturbance regimes are more likely to experience increases in functional diversity under changing climate conditions.

Introduction

Arctic vegetation plays a critical role in global climate feedbacks (Pearson et al., 2013), permafrost dynamics (Blok et al., 2010), and the distribution of herbivore populations connected to the livelihood of Arctic communities (Forbes and Kumpula, 2009). Despite a net increase in Arctic vegetation productivity between 1982 and 2019 (Frost et al., 2020), the direction and magnitude of productivity trends have exhibited substantial spatiotemporal heterogeneity across multiple scales (e.g., local to continental, inter-annual to decadal) (Berner et al., 2020; Dutrieux et al., 2012; Elmendorf et al., 2012; Frost et al., 2020; Lara et al., 2018). This spatiotemporal heterogeneity is likely due to complex vegetation interactions with climatic, geologic, biologic, and anthropogenic drivers (Frost et al., 2019; Walker et al., 2009). While understanding Arctic vegetation dynamics is necessary to accurately model future climate scenarios (Pearson et al., 2013), there are uncertainties in determining the relative importance of drivers across regions with varying climatological conditions, landscapes, and vegetation responses (Bhatt et al., 2021; Dutrieux et al., 2012; Epstein et al., 2004; Lara et al., 2018; Walker et al., 2006; Walker et al., 2009; Yu et al., 2017).

Shifts in the seasonal dynamics of productivity (aboveground biomass accumulation and phenology) have also been reported throughout the Arctic (Berner et al., 2020; Elmendorf et al., 2012; Frost et al., 2020; Post et al., 2016; Prevéy et al., 2019; Zeng et al., 2011). These seasonal dynamics of productivity can be used to define Ecosystem Functional Types (EFTs), patches of the landscape with similar carbon gain dynamics (Alcaraz-Segura et al., 2013; Armstrong et al., in prep.; Cabello et al., 2013; Cazorla et al., 2021; Ivits et al., 2013; Paruelo et al., 2001; Pérez-Hoyos et al., 2014; Villarreal et al., 2018). EFT richness, the number of unique EFTs within a prescribed area, represents functional diversity (Alcaraz-Segura et al., 2013; Cabello et al., 2013; Cazorla et al., 2021; Paruelo et al., 2001). EFTs can be used to determine which conditions cause Arctic vegetation communities to have differential functionality, while functional diversity provides insight into ecosystem resistance through differential responses to environmental changes and disturbances. However, the drivers of EFT distribution and EFT richness have not yet been evaluated for the Arctic, and it is unclear if EFT richness is increasing or decreasing in response to climate change.

The goal of this thesis was to examine the effects of environmental and anthropogenic drivers on the vegetation productivity, function, and functional diversity of the Yamal Peninsula, Siberia, Russia between 2001 and 2018 in order to increase understanding of the heterogeneous response of Arctic vegetation to climate change. The Yamal Peninsula was chosen as the study site, because it is characterized by a unique combination of features (e.g., steep climate and geological gradients, ice-rich continuous permafrost, diverse Arctic vegetation, indigenous reindeer herding, and natural resource extraction operations) that make it representative of current and future conditions in other Arctic regions (Macias-Fauria et al., 2012; Walker et al., 2009). In Chapter 1, Yamal Peninsula productivity was assessed using the Normalized

Difference Vegetation Index (NDVI), a remotely-sensed proxy for primary productivity and aboveground biomass (Berner et al., 2018, 2020; Epstein et al., 2012, 2021; Jia et al., 2006; Raynolds et al., 2012; Reichle et al., 2018). In Chapter 2, Yamal Peninsula vegetation function and functional diversity were assessed using NDVI-based EFTs developed by Armstrong et al. (in prep.) for the circumpolar Arctic. In both chapters, a suite of climatic, geologic, biologic, and anthropogenic drivers were used as explanatory variables in spatial and temporal analyses. Together, these chapters provide the first comprehensive assessment of how these drivers influence vegetation productivity, function, and functional diversity over space and time in the Arctic. Independently, these chapters contribute to the base of knowledge necessary for predicting Arctic carbon balance under projected warming (IPCC, 2021) and outline a methodology for assessing the individual impacts of interacting drivers on Arctic vegetation dynamics.

References

Alcaraz-Segura, D., Paruelo, J., Epstein, H., & Cabello, J. (2013). Environmental and Human Controls of Ecosystem Functional Diversity in Temperate South America. *Remote Sensing*, *5*(1), 127–154. https://doi.org/10.3390/rs5010127

Armstrong et al. (in preparation). Ecosystem Functional Types of the circumpolar arctic tundra based on the seasonal dynamics of vegetation productivity.

Berner, L. T., Jantz, P., Tape, K. D., & Goetz, S. J. (2018). Tundra plant above-ground biomass and shrub dominance mapped across the North Slope of Alaska. *Environmental Research Letters*, 13(3), 035002. https://doi.org/10.1088/1748-9326/aaaa9a

Berner, L. T., Massey, R., Jantz, P., Forbes, B. C., Macias-Fauria, M., Myers-Smith, I., Kumpula, T., Gauthier, G., Andreu-Hayles, L., Gaglioti, B. V., Burns, P., Zetterberg, P., D'Arrigo, R., & Goetz, S. J. (2020). Summer warming explains widespread but not uniform greening in the Arctic tundra biome. *Nature Communications*, 11(1), 4621. https://doi.org/10.1038/s41467-020-18479-5

Bhatt, U. S., Walker, D. A., Raynolds, M. K., Walsh, J. E., Bieniek, P. A., Cai, L., Comiso, J. C., Epstein, H. E., Frost, G. V., Gersten, R., Hendricks, A. S., Pinzon, J. E., Stock, L., &

Tucker, C. J. (2021). Climate drivers of Arctic tundra variability and change using an indicators framework. *Environmental Research Letters*, *16*(5), 055019. https://doi.org/10.1088/1748-9326/abe676

Blok, D., Heijmans, M. M. P. D., Schaepman-Strub, G., Kononov, A. V., Maximov, T. C., & Berendse, F. (2010). Shrub expansion may reduce summer permafrost thaw in Siberian tundra. *Global Change Biology*, *16*(4), 1296–1305. https://doi.org/10.1111/j.1365-2486.2009.02110.x

Cabello, J., Lourenço, P., Reyes, A., Alcaraz-Segura, D. (2013). Chapter 9: Ecosystem Services Assessment of National Parks Networks for Functional Diversity and Carbon Conservation Strategies Using Remote Sensing, Earth Observation of Ecosystem Services (1st ed). CRC Press. https://doi.org/10.1201/b15628

Cazorla, B. P., Cabello, J., Peñas, J., Garcillán, P. P., Reyes, A., & Alcaraz-Segura, D. (2021). Incorporating Ecosystem Functional Diversity into Geographic Conservation Priorities Using Remotely Sensed Ecosystem Functional Types. *Ecosystems*, 24(3), 548–564. https://doi.org/10.1007/s10021-020-00533-4

Dutrieux, L. P., Bartholomeus, H., Herold, M., & Verbesselt, J. (2012). Relationships between declining summer sea ice, increasing temperatures and changing vegetation in the Siberian Arctic tundra from MODIS time series (2000–11). *Environmental Research Letters*, *7*(4), 044028. https://doi.org/10.1088/1748-9326/7/4/044028

Elmendorf, S. C., Henry, G. H. R., Hollister, R. D., Björk, R. G., Boulanger-Lapointe, N., Cooper, E. J., Cornelissen, J. H. C., Day, T. A., Dorrepaal, E., Elumeeva, T. G., Gill, M., Gould, W. A., Harte, J., Hik, D. S., Hofgaard, A., Johnson, D. R., Johnstone, J. F., Jónsdóttir, I. S., Jorgenson, J. C., … Wipf, S. (2012). Plot-scale evidence of tundra vegetation change and links to recent summer warming. *Nature Climate Change*, *2*(6), 453–457. https://doi.org/10.1038/nclimate1465

Epstein, H. E., Beringer, J., Gould, W. A., Lloyd, A. H., Thompson, C. D., Chapin, F. S., Michaelson, G. J., Ping, C. L., Rupp, T. S., & Walker, D. A. (2004). The nature of spatial transitions in the Arctic. *Journal of Biogeography*, *31*(12), 1917–1933. https://doi.org/10.1111/j.1365-2699.2004.01140.x

Epstein, H. E., Raynolds, M. K., Walker, D. A., Bhatt, U. S., Tucker, C. J., & Pinzon, J. E. (2012). Dynamics of aboveground phytomass of the circumpolar Arctic tundra during the past three decades. *Environmental Research Letters*, *7*(1), 015506. https://doi.org/10.1088/1748-9326/7/1/015506

Epstein, H. E., Walker, D. A., Frost, G. V., Raynolds, M. K., Bhatt, U., Daanen, R., Forbes, B., Geml, J., Kaärlejarvi, E., Khitun, O., Khomutov, A., Kuss, P., Leibman, M., Matyshak, G., Moskalenko, N., Orekhov, P., Romanovsky, V. E., & Timling, I. (2021). Spatial patterns of arctic tundra vegetation properties on different soils along the Eurasia Arctic Transect, and insights for a changing Arctic. *Environmental Research Letters*, *16*(1),

014008. https://doi.org/10.1088/1748-9326/abc9e3

Forbes, B. C., & Kumpula, T. (2009). The Ecological Role and Geography of Reindeer (*Rangifer tarandus*) in Northern Eurasia: Ecology/geography of Eurasian reindeer. *Geography Compass*, *3*(4), 1356–1380. https://doi.org/10.1111/j.1749-8198.2009.00250.x

Frost, G. V., Bhatt, U. S., Epstein, H. E., Walker, D. A., Raynolds, M. K., Berner, L. T., Bjerke, J. W., Breen, A. L., Forbes, B. C., Goetz, S. J., Iverson, C. M., Lara, M. J., Macander, M. J., Phoenix, G. K., Rocha, A.V., Salmon, V.G., Thorton, P. E., Tommervik, H., & Wullschleger, S. D. (2019). Tundra Greenness. In: Arctic Report Card: Update for 2019. NOAA, Silver Spring, MD. Retrieved from https://arctic.noaa.gov/Report-Card/Report-Card-2019/ArtMID/7916/ArticleID/838/Tundra-Greenness

Frost, G. V., Bhatt, U. S., Epstein, H. E., Myers-Smith, I., Phoenix, G. K., Berner, L. T., Bjerke, J. W., Forbes, B. C., Goetz, S. J., Kerby, J. T., Macander, M. J., Park, T., Raynolds, M. K., Tommervik, H., and Walker, D. A. (2020). Tundra Greenness. In: Arctic Report Card: Update for 2020. NOAA, Silver Spring, MD. Retrieved from https://arctic.noaa.gov/Report-Card/Report-Card-2020/ArtMID/7975/ArticleID/879/Tundra-Greenness

IPCC, 2021: *Climate Change 2021: The Physical Science Basis. Contribution of Working Group I to the Sixth Assessment Report of the Intergovernmental Panel on Climate Change* [Masson-Delmotte, V., P. Zhai, A. Pirani, S. L. Connors, C. Péan, S. Berger, N. Caud, Y. Chen, L. Goldfarb, M. I. Gomis, M. Huang, K. Leitzell, E. Lonnoy, J. B.R. Matthews, T. K. Maycock, T. Waterfield, O. Yelekçi, R. Yu and B. Zhou (eds.)]. Cambridge University Press. In Press.

Ivits, E., Cherlet, M., Horion, S., & Fensholt, R. (2013). Global Biogeographical Pattern of Ecosystem Functional Types Derived From Earth Observation Data. *Remote Sensing*, *5*(7), 3305–3330. https://doi.org/10.3390/rs5073305

Jia, G. J., Epstein, H. E., & Walker, D. A. (2006). Spatial heterogeneity of tundra vegetation response to recent temperature changes: SPATIAL HETEROGENEITY OF TUNDRA DYNAMICS. *Global Change Biology*, *12*(1), 42–55. https://doi.org/10.1111/j.1365-2486.2005.01079.x

Lara, M. J., Nitze, I., Grosse, G., Martin, P., & McGuire, A. D. (2018). Reduced arctic tundra productivity linked with landform and climate change interactions. *Scientific Reports*, *8*(1), 2345. https://doi.org/10.1038/s41598-018-20692-8

Macias-Fauria, M., Forbes, B. C., Zetterberg, P., & Kumpula, T. (2012). Eurasian Arctic greening reveals teleconnections and the potential for structurally novel ecosystems. *Nature Climate Change*, *2*(8), 613–618. https://doi.org/10.1038/nclimate1558

Paruelo, J. M., Jobbágy, E. G., & Sala, O. E. (2001). Current Distribution of Ecosystem Functional Types in Temperate South America. *Ecosystems*, *4*(7), 683–698.

https://doi.org/10.1007/s10021-001-0037-9

Pearson, R. G., Phillips, S. J., Loranty, M. M., Beck, P. S. A., Damoulas, T., Knight, S. J., & Goetz, S. J. (2013). Shifts in Arctic vegetation and associated feedbacks under climate change. *Nature Climate Change*, *3*(7), 673–677. https://doi.org/10.1038/nclimate1858

Pérez-Hoyos, A., Martínez, B., García-Haro, F., Moreno, Á., & Gilabert, M. (2014). Identification of Ecosystem Functional Types from Coarse Resolution Imagery Using a Self-Organizing Map Approach: A Case Study for Spain. *Remote Sensing*, *6*(11), 11391–11419. https://doi.org/10.3390/rs61111391

Post, E., Kerby, J., Pedersen, C., & Steltzer, H. (2016). Highly individualistic rates of plant phenological advance associated with arctic sea ice dynamics. Biology Letters, 12(12), 20160332. https://doi.org/10.1098/rsbl.2016.0332

Prevéy, J. S., Rixen, C., Rüger, N., Høye, T. T., Bjorkman, A. D., Myers-Smith, I. H., Elmendorf, S. C., Ashton, I. W., Cannone, N., Chisholm, C. L., Clark, K., Cooper, E. J., Elberling, B., Fosaa, A. M., Henry, G. H. R., Hollister, R. D., Jónsdóttir, I. S., Klanderud, K., Kopp, C. W., … Wipf, S. (2019). Warming shortens flowering seasons of tundra plant communities. *Nature Ecology & Evolution*, *3*(1), 45–52. https://doi.org/10.1038/s41559-018-0745-6

Raynolds, M. K., Walker, D. A., Epstein, H. E., Pinzon, J. E., and Tucker C. J. (2012). A new estimate of tundra-biome phytomass from trans-Arctic field data and AVHRR NDVI *Remote Sens. Lett.* 3, 403–11. https://doi.org/10.1080/01431161.2011.609188

Raynolds, M., Comiso, J., Walker, D., & Verbyla, D. (2008). Relationship between satellite-derived land surface temperatures, arctic vegetation types, and NDVI. *Remote Sensing of Environment*, *112*(4), 1884–1894. https://doi.org/10.1016/j.rse.2007.09.008

Reichle, L. M., Epstein, H. E., Bhatt, U. S., Raynolds, M. K., & Walker, D. A. (n.d.). Spatial Heterogeneity of the Temporal Dynamics of Arctic Tundra Vegetation. Geophysical Research Letters, 10.

Villarreal, S., Guevara, M., Alcaraz-Segura, D., Brunsell, N. A., Hayes, D., Loescher, H. W., & Vargas, R. (2018). Ecosystem functional diversity and the representativeness of environmental networks across the conterminous United States. *Agricultural and Forest Meteorology*, 262, 423–433. https://doi.org/10.1016/j.agrformet.2018.07.016

Walker, D. A., Leibman, M. O., Epstein, H. E., Forbes, B. C., Bhatt, U. S., Raynolds, M. K., Comiso, J. C., Gubarkov, A. A., Khomutov, A. V., Jia, G. J., Kaarlejärvi, E., Kaplan, J. O., Kumpula, T., Kuss, P., Matyshak, G., Moskalenko, N. G., Orekhov, P., Romanovsky, V. E., Ukraientseva, N. G., & Yu, Q. (2009). Spatial and temporal patterns of greenness on the Yamal Peninsula, Russia: Interactions of ecological and social factors affecting the Arctic normalized difference vegetation index. *Environmental Research Letters*, *4*(4), 045004. https://doi.org/10.1088/1748-9326/4/4/045004

Walker, M. D., Wahren, C. H., Hollister, R. D., Henry, G. H. R., Ahlquist, L. E., Alatalo, J. M., Bret-Harte, M. S., Calef, M. P., Callaghan, T. V., Carroll, A. B., Epstein, H. E., Jonsdottir, I.S., Klein, J.A., Magnusson, B., Molau, U., Oberbauer, S.F., Rewa, S.P., Robinson, C.H., … Wookey, P.A. (2006). Plant community responses to experimental warming across the tundra biome. *Proceedings of the National Academy of Sciences*, 103(5), 1342-1346. DOI: 10.1073/pnas.0503198103.

Yu, Q., Epstein, H., Engstrom, R., & Walker, D. (2017). Circumpolar arctic tundra biomass and productivity dynamics in response to projected climate change and herbivory. *Global Change Biology*, *23*(9), 3895–3907. https://doi.org/10.1111/gcb.13632

Zeng, H., Jia, G., & Epstein, H. (2011). Recent changes in phenology over the northern high latitudes detected from multi-satellite data. *Environmental Research Letters*, *6*(4), 045508. https://doi.org/10.1088/1748-9326/6/4/045508

Chapter 1: Drivers of Spatial and Temporal Heterogeneity in Vegetation Productivity on the Yamal Peninsula, Siberia, Russia

1.0 Abstract

The direction and magnitude of Arctic vegetation productivity trends inferred from the Normalized Difference Vegetation Index (NDVI) have exhibited spatiotemporal heterogeneity over recent decades, which has led to uncertainty in the future of global climate feedbacks, permafrost stability, and herbivore populations under continued warming. The mechanisms behind this heterogeneity are unclear; however, determining the relative importance of climatic, geologic, biologic, and anthropogenic drivers across regions with varying climatological conditions, landscapes, and vegetation responses can provide insight into the variable spatial and temporal patterns of Arctic vegetation productivity. In this study, I examined the spatial and temporal drivers of peak growing season aboveground biomass (represented by Max NDVI) and total growing season productivity (represented by time-integrated [TI]-NDVI) on the Yamal Peninsula, Siberia, Russia between 2001 and 2018.

Summer Warmth Index (SWI), the timing of snowmelt, and physiognomic vegetation unit best explained the spatial distribution of Max and TI-NDVI on the Yamal Peninsula, with the highest mean Max and TI-NDVI occurring where summer temperatures were higher, snowmelt occurred earlier, and erect shrub and wetland vegetation communities were dominant. Max and TI-NDVI trends were positive across the majority of the Peninsula (57.4% [5.0% significant] and 97.7% [13.8% significant], respectively) between 2001 and 2018, and divergent trends in some areas could be the result of a shift from shrub to graminoid dominance. Max and TI-NDVI trends had variable relationships with drivers and were primarily influenced by coastal-inland gradients in summer warmth and soil moisture. Max and TI-NDVI trend relationships with SWI, soil moisture, and precipitation trends were possibly tied to the influence that these drivers have on permafrost degradation and subsequent shifts in hydrological conditions that have differential effects on Arctic growth forms. Both Max and TI-NDVI trends were negatively impacted by

human modification, highlighting how human disturbances are becoming an increasingly important driver of Arctic vegetation dynamics in remote but developing areas. Overall, these findings provide insight into the potential future of Arctic regions experiencing warming, moisture regime shifts, and human modification, and demonstrate the usefulness of considering multiple NDVI metrics to disentangle the effects of individual drivers across heterogeneous landscapes.

2.0 Introduction

Arctic vegetation plays a critical role in global climate feedbacks (Pearson et al., 2013), permafrost dynamics (Blok et al., 2010), and the distribution of herbivore populations connected to the livelihood of Arctic communities (Forbes and Kumpula, 2009). Changes in Arctic vegetation since the 1980s have been monitored using the Normalized Difference Vegetation Index (NDVI) (Frost et al., 2020), a proxy for primary productivity that remotely quantifies photosynthetically-active green vegetation (Jia et al., 2006; Reichle et al., 2018). Several studies have provided evidence of a strong relationship between Arctic aboveground biomass and NDVI, allowing *in situ* vegetation changes to be inferred from NDVI metrics (Berner et al., 2018; Epstein et al., 2012, 2021; Jia et al., 2006; Raynolds et al., 2012). Max NDVI (the greatest intra-annual NDVI value) represents peak growing season aboveground biomass, whereas time-integrated (TI)-NDVI (the sum of growing season NDVI values > 0.10) represents total growing season productivity (Bhatt et al., 2021; Frost et al., 2020; Jia et al., 2006).

Despite a net increase in Max and TI-NDVI between 1982 and 2019 (Frost et al., 2020), the direction and magnitude of Arctic vegetation productivity trends exhibit substantial spatiotemporal heterogeneity across multiple scales (e.g., local to continental, inter-annual to decadal) (Berner et al., 2020; Dutrieux et al., 2012; Elmendorf et al., 2012; Frost et al., 2020;

Lara et al., 2018). This spatiotemporal heterogeneity is likely due to complex vegetation interactions with climatic, geologic, biologic, and anthropogenic drivers (Frost et al., 2019; Walker et al., 2009). While some of these relationships are well-studied, there are uncertainties in determining the relative importance of drivers across regions with varying climatological conditions, landscapes, and vegetation responses (Bhatt et al., 2021; Dutrieux et al., 2012; Epstein et al., 2004; Lara et al., 2018; Walker et al., 2006; Walker et al., 2009; Yu et al., 2017).

Arctic vegetation productivity is generally limited by summer warmth (Raynolds et al., 2008); however, increased productivity in response to warming has not been uniform across the Arctic, indicating the presence of other limiting drivers (Berner et al., 2020; Bhatt et al., 2021; Dutrieux et al., 2012). Other climatic drivers such as precipitation, soil moisture, and the timing of snow melt mediate the response of Arctic vegetation to warming through their influence on water availability (Campbell et al., 2021; Gamon et al., 2013; Li et al., 2016; Myers-Smith et al., 2015; Tape et al., 2012) and the stability of ice-rich permafrost (Leibman et al., 2014; Macias-Fauria et al., 2012; Walker et al., 2009; Zhang, 2005). Additionally, the timing of snowmelt determines the start of the growing season (Bieniek et al. 2015). Climatic drivers can be mediated by others that influence temperature and precipitation, such as sea ice concentration/extent (Bhatt et al., 2010, 2013) and elevation (Raynolds et al., 2006), in addition to glacial history (Raynolds and Walker, 2009; Walker et al., 1995), soil texture (Epstein et al., 2021; Macias-Fauria et al., 2012), substrate chemistry (Raynolds et al., 2006), vegetation type (Elmendorf et al., 2012; Epstein et al., 2021; Walker et al., 2006), and the extent of human disturbance (Forbes, 1999; Johnstone and Kokelj, 2008; Walker and Everett 1987; Walker et al., 1987, 2010).

The goal of this study was to examine the effects of environmental and anthropogenic drivers on the spatial and temporal patterns of vegetation productivity on the Yamal Peninsula, Siberia, Russia. The Yamal Peninsula is located in one of the warmer regions of the Arctic (Raynolds et al., 2008), has steep climate and geologic gradients, ice-rich continuous permafrost, diverse Arctic vegetation, indigenous reindeer herding, and natural resource (gas) operations (Figures 1 and 2; Walker et al., 2009). These conditions allowed it to serve as a case study for determining the critical drivers of Arctic vegetation productivity (Macias-Fauria et al., 2012) under projected warming (IPCC, 2021), increasing oil/gas development (UNEP, 2001; Walker et al., 2010), and ongoing herbivory. Specifically, I aimed to answer the following questions:

1) Which environmental and anthropogenic drivers exerted the greatest influence on the spatial distribution of Max and TI-NDVI across the Yamal Peninsula between 2001 and 2018?

2) What were the direction and magnitude of Yamal Peninsula Max and TI-NDVI temporal trends between 2001 and 2018?

3) Which drivers best predicted variations in Max and TI-NDVI temporal trends across the Yamal Peninsula?

These questions were addressed using Max and TI-NDVI derived from the Moderate Resolution Imaging Spectroradiometer (MODIS) Vegetation Indices product and a suite of climatic, geologic, biologic, and anthropogenic drivers (Table 1). Climatic drivers considered included Summer Warmth Index (SWI, sum of April – September monthly mean temperatures > 0 °C), mean growing season (April – September) precipitation and soil moisture (hereafter, precipitation and soil moisture), and snow-free period onset date (first day of the year with 0%

snow cover). Geologic drivers included coast distance (a proxy for sea ice influence on temperature), elevation, landscape age (time since last glaciation), soil texture, and substrate chemistry. The biologic driver considered was physiognomic vegetation unit (as determined by the Circumpolar Arctic Vegetation Map) (Walker and Raynolds 2018). While reindeer herbivory is common throughout on the Yamal Peninsula, a lack of quantitative data and exclusion areas limited the potential for a meaningful assessment of reindeer effects as a biologic driver (Walker et al., 2009). The anthropogenic driver considered was human modification, a cumulative measure of the area impacted by natural resource extraction, infrastructure, and settlements (Kennedy et al., 2019).

I expected the spatial and temporal drivers of Yamal Peninsula vegetation productivity to differ. First, it was hypothesized that the climatic drivers and physiognomic vegetation unit would best explain the spatial distribution of Max and TI-NDVI, because of the influence of long-term climate patterns and growth form-specific physiological requirements on Arctic vegetation distribution (Raynolds et al., 2008; Walker et al., 2002). It was hypothesized that both Max and TI-NDVI temporal trends would be positive across a majority of the Yamal Peninsula; however, spatial heterogeneity in trend magnitude and direction was also expected due to the variable climatological and landscape conditions of the Peninsula. Last, it was hypothesized that geologic and anthropogenic drivers would best explain variations in Max and TI-NDVI trends due to their ability to mediate the effects of climate on vegetation productivity.

3.0 Methods

3.1 Study Area

The Yamal Peninsula, located within the Arctic tundra of northwestern Siberia, Russia, is approximately 600 km long (including Belyy Island in the north) and up to 250 km wide (Figure 1, Walker et al., 2009). Between 2001-2018, the mean annual temperature ranged from -13 to -8

°C (Wan et al., 2015), and mean annual precipitation ranged from 240 to 367 mm (Abatzoglou et al., 2018). The Yamal Peninsula has predominantly flat topography, with a majority of slopes < 7°, and elevations reaching 86 m above sea level (Figure 1; Leibman et al., 2014; Rizzoli et al., 2017). The landscape is underlain by ice-rich continuous permafrost and dominated by river networks, sandy ridges, and lowland valleys with abundant thermokarst lakes, drained thermokarst lake basins, and polygonal peatlands (Walker et al., 2009; Verdonen et al., 2020). Cryogenic landslides controlled by summer thaw depth and soil water content are the primary landscape forming process on the Yamal Peninsula (Leibman, 1995; Leibman et al., 2014; Macias-Fauria et al., 2012). Landslides occur when heavy precipitation and/or summer thawing expose ice-rich sediments (Leibman, 1995; Leibman et al., 2014), but are also common along the eroded banks of seasonally-flooded rivers and streams (Lemenkova, 2015; Walker et al., 2009).

The Peninsula was last glaciated during the late Pleistocene, with a majority (84%) of the Peninsula deglaciating ~25,000 years ago (Figure 2a; Walker and Raynolds, 2018). Yamal Peninsula soils are comprised of nutrient-poor marine sands, nutrient-rich clays, and primarily acidic substrates; however, circumneutral and saline substrates are present in the central and northern regions (Figure 2b; Walker and Raynolds, 2018; Yu et al., 2011). The dominant soil textures are loam (53%), silt loam (32%), and sandy loam (12%) (Figure 2c; FAO et al., 2012). Vegetation transitions from erect low shrub tundra in the south to sedge, dwarf prostrate shrub, and moss tundra in the north (Figure 2d; Walker et al., 2009). Shrubs are present throughout the Yamal Peninsula, but increase in abundance from north to south (Epstein et al., 2021).

3.2 Data Sources and Pre-Processing

Pre-processing was completed using a combination of Google Earth Engine (GEE), ArcGIS (Redlands, CA), and R version 4.0.0 (R Core Team, 2020). GEE allows for cloud-based

pre-processing of spatial data from a variety of sources. Max and TI-NDVI, precipitation, soil moisture, snow-free period onset date, SWI, and human modification driver datasets were derived from products available through GEE (Table 1). All other driver datasets were downloaded from their respective sources and uploaded to GEE for pre-processing. Pre-processing was tailored to each driver dataset, but generally entailed evaluating pixel quality, masking surface water, deriving the parameter of interest for the 2001-2018 study period, resampling to a 1-km spatial resolution, and developing georeferenced tables for statistical analysis. Product developers evaluated data quality, and when applicable removed low-quality pixels affected by cloud cover, aerosols, and viewing angle (Abatzoglou et al., 2018; Didan, 2015; FAO et al., 2012; Hall et al., 2016; Kennedy et al., 2019; Rizzoli et al., 2017; Walker and Raynolds, 2018; Wan et al., 2015). Marginal-quality pixels were used to supplement the spatial coverage of snow-free period onset, SWI, Max NDVI, and TI-NDVI datasets when high-quality data were unavailable. Permanent surface water bodies were masked using the GlobCover Global Land Cover Map available through GEE (ESA and UC Louvain, 2010). When required, mean aggregation was used to decrease spatial resolution in GEE, while bilinear interpolation or nearest neighbor resampling was used to increase spatial resolution in ArcGIS. Georeferenced tables were developed using the terra package in R (Hijmans, 2021).

3.3 Max and TI-NDVI Calculation

The MODIS Vegetation Indices product (MOD13Q1.006) provides NDVI calculated using the equation (NIR – R)/(NIR + R), where NIR equals the spectral reflectance of near-infrared radiation (0.7 - 1.1 μm), and R equals the spectral reflectance of visible red radiation (0.6 - 0.7 μm) (Didan, 2015). Annual Max and TI-NDVI values were derived from 16-day maximum value composites (i.e., representative images of the 16-day maximum NDVI values) (Didan, 2015). Max NDVI for each pixel was determined by selecting the maximum NDVI value

from composites covering June 26 - September 13 (period of peak vegetation productivity on the Yamal Peninsula). Barren, snow-covered, and ephemeral water-covered land surfaces were excluded by masking pixels with Max NDVI values below 0.1. TI-NDVI for each pixel was calculated by summing NDVI values above 0.1 from composites covering the entire growing season (April – September). Each composite included in the Max and TI-NDVI calculations had variable spatial coverage due to the exclusion of low-quality pixels. At the pixel scale, this resulted in variable intra-annual coverage and a bias toward artificially low Max and TI-NDVI values. This bias was removed by developing spatially-consistent composite masks for each year, ensuring that annual Max and TI-NDVI were only calculated when all composites considered were available.

3.4 Spatial Analyses

Spatial correlations among Max NDVI, TI-NDVI, and continuous drivers

Pairwise Spearman's correlation was used to determine the direction and significance of the spatial relationships among Max NDVI, TI-NDVI, and the continuous drivers (Table 1). The 2001-2018 means of Max NDVI, TI-NDVI, and climatic drivers were included as inputs. All other included variables (coast distance, elevation, and human modification) were constant over the 2001-2018 study period. The Bonferroni correction was applied to account for multiple comparisons. Spearman's correlations were also run on stratified random samples using 2/3 and 1/2 of the input dataset. Spearman's correlation was implemented using the psych package in R (R Core Team, 2020; Revelle, 2020).

Spatial correlations among Max/TI-NDVI and categorical drivers

Chi-Square (χ^2) Tests of Independence were employed to determine if there were significant spatial associations among mean Max/TI-NDVI and categorical drivers (Table 1).

Mean Max and TI-NDVI were divided into high, mid-, and low categories using the Jenk's natural breaks classification method (implemented using the BAMMtools package in R) (R Core Team, 2020; Rabosky et al., 2014). Chi-Square Tests of Independence were also run on stratified random samples using 2/3 and 1/2 of the input datasets. The χ^2 test statistics and residuals were compared to determine the direction and significance of the spatial associations.

3.5 Temporal Analyses

Max NDVI, TI-NDVI, and climatic driver trend detection

Mann-Kendall trend tests were implemented to detect the presence of pixel-scale monotonic trends in Max NDVI, TI-NDVI, and climatic drivers between 2001 and 2018. Pixels with fewer than 15 years of data were excluded from the analyses. First, the Durbin-Watson test was used to test residuals for lag-1 serial autocorrelation, which can result in the erroneous detection of significant trends (Kulkarni and von Storch, 1995). Modified Mann-Kendall trend tests that applied pre-whitening to input time series were also run to verify that pixels with significant serial autocorrelation (< 5% of pixels) did not affect trend significance. Non-parametric Sen's slope estimation was used to determine the direction and magnitude of Max NDVI, TI-NDVI, and climatic driver trends. Trend detection analyses were completed using the car (Fox and Weisberg, 2019), Kendall (McLeod, 2011), modifiedmk (Patakamuri and O'Brien, 2020), and trend packages (Pohlert, 2020) in R. To facilitate an illustrative examination of changes in Max and TI-NDVI, GEE was used to calculate 2001-2008 and 2009-2018 mean NDVI values for each growing season composite.

Drivers of Max and TI-NDVI trends

Random Forest regression models were used to determine the most important drivers (i.e., the best predictors) of Max and TI-NDVI trends (Sen's slopes) across the Yamal Peninsula.

All drivers were included as explanatory variables in the models, and the Sen's slopes of climatic drivers were also used (Table 1). A pairwise Spearman's correlation was used to confirm that multicollinearity ($r > 0.75$ or < -0.75) was not present among the continuous input drivers (Berner et al., 2020; Oliveira et al., 2012). Random Forest regression is a non-parametric machine-learning method that utilizes independent decision tree models of bootstrapped data (Breiman, 2001; Liaw and Wiener, 2002). Data excluded from the trees, or out-of-bag (OOB) data, were used to determine prediction accuracy (inferred from mean square error [MSE]) and variable importance (inferred from mean decrease in accuracy [% IncMSE]) (Liaw and Wiener, 2002; Oliveira et al., 2012). Models were repeatedly fit to determine the number of randomized drivers considered at each tree node (mtry) that resulted in the lowest MSE (Oliveira et al., 2012). The % IncMSE metric determined variable importance by measuring the decrease in prediction accuracy when OOB data for a given variable were permuted in the model (Liaw and Wiener, 2002). Random Forest regression modelling was completed using the University of Virginia's high-performance computing system (Rivanna) along with the caret (Kuhn, 2020), randomForest (Liaw and Wiener, 2002), and doParallel packages (Microsoft and Weston, 2020) in R.

The relationships between Max/TI-NDVI trends and the six most important drivers identified by the Random Forest regression models were evaluated using partial dependence plots and Spearman's correlations. Partial dependence plots were used to evaluate the average predicted relationships between Max/TI-NDVI Sen's slopes and individual drivers across their range of values while still considering the average effects of the other drivers (Goldstein et al., 2014). Pixel-scale Spearman's correlations were run between linearly-detrended Max/TI-NDVI and precipitation, soil moisture, and SWI time series to assess their interannual covariation

irrespective of trends. These analyses were completed using the pdp (Greenwell, 2017), pracma (Borchers, 2019), and psych packages (Revelle, 2020) in R.

4.0 Results

4.1 Spatial Analyses

Spatial correlations among Max NDVI, TI-NDVI, and continuous drivers

There was a significant (p-value < 0.05), strong, and positive spatial correlation between 2001-2018 mean Max and TI-NDVI (r = 0.93, Figures 3 and 4). Mean Max NDVI exhibited significant spatial correlations with all of the continuous drivers except for elevation, and spatial correlations with mean SWI, mean precipitation, and mean snow-free period onset date were the strongest. Mean Max NDVI was positively correlated with mean SWI (r = 0.40) and mean precipitation (r = 0.39), and negatively correlated with mean snow-free period onset date (r = -0.40). Therefore, areas with high Max NDVI coincided with high SWI, high precipitation, and earlier snowmelt. Additionally, mean Max NDVI was positively correlated with human modification (r = 0.27) and weakly correlated with mean soil moisture (r = 0.02) and coast distance (r = -0.02). Mean TI-NDVI exhibited similar spatial relationships with the continuous drivers; however, mean TI-NDVI was not significantly correlated with mean soil moisture, and was better correlated with mean SWI, mean precipitation, mean snow-free period onset date, human modification, coast distance, and elevation than mean Max NDVI (Figure 3). Results were similar for analyses run on stratified random samples using 2/3 and 1/2 of the input dataset.

Notable spatial correlations among the continuous drivers were present. Mean precipitation was positively correlated with mean SWI (r = 0.88), and both mean precipitation and mean SWI were negatively correlated with mean snow-free period onset date (r = -0.86 and -0.85, respectively; Figures 3 and 5). Human modification was positively correlated with mean

SWI (r = 0.32) and mean precipitation (r = 0.47), and negatively correlated with mean snow-free period onset date (r = -0.44). Additionally, coast distance was positively correlated with elevation (r = 0.63) and mean SWI (r = 0.40), and negatively correlated with mean soil moisture (r = -0.72).

Spatial correlations among Max/TI-NDVI and categorical drivers

Of the categorical drivers, vegetation unit had the strongest spatial association with mean Max NDVI categories (χ^2 = 10,674), followed by substrate chemistry (χ^2 = 5,672), soil texture (χ^2 = 2,337), and landscape age (χ^2 = 128, Table 2). Similarly, vegetation unit had the strongest spatial association with mean TI-NDVI categories (χ^2 = 25,781), followed by soil texture (χ^2 = 3,771), substrate chemistry (χ^2 = 3,017), and landscape age (χ^2 = 1,774). Overall, Max and TI-NDVI exhibited similar relationships with the categorical drivers, and results were similar for analyses run on stratified random samples using 2/3 and 1/2 of the input datasets (Table 3). High mean Max and TI-NDVI were associated with erect shrub and wetland vegetation (a combination of sedges, mosses, and erect shrubs) (Raynolds et al., 2006), whereas low mean Max and TI-NDVI were associated with graminoid and prostrate shrub vegetation. High mean Max and TI-NDVI were associated with circumneutral substrates, whereas low mean Max and TI-NDVI were associated with acidic and saline substrates. Last, high mean Max and TI-NDVI were associated with clay loam and silt loam soil textures, whereas low mean Max and TI-NDVI were associated with loam, sand, and sandy loam soil textures. Mean Max and TI-NDVI exhibited slightly different relationships with landscape age. High mean Max NDVI was associated with older landscapes (~70,000 years old), and low mean Max NDVI was associated with younger (~25,000 years old) and recently disturbed landscapes (~1,000 years old). Mid-mean TI-NDVI was associated with older landscapes (result not shown), and low mean TI-NDVI

was associated with younger and recently disturbed landscapes. However, high mean TI-NDVI was also associated with younger landscapes.

4.2 Temporal Analyses

Max NDVI, TI-NDVI, and climatic driver trends

Max and TI-NDVI increased across a majority of the Yamal Peninsula between 2001 and 2018 (Figure 6). Max NDVI trends were positive across 57.4% of the Peninsula (5.0% significant positive trends [p-value < 0.05]) and negative across 17.8% (0.6% significant negative trends). Additionally, 25.4% of the Peninsula exhibited no Max NDVI trend (p-value > 0.05 and Sen's slope = 0.000). Max NDVI Sen's slope ranged from -0.022 to 0.045 yr^{-1}, with the mode between 0.000 and 0.001 yr^{-1}. TI-NDVI trends were positive across 97.7% of the Peninsula (13.8% significant positive trends) and negative across 1.9% (< 0.1% significant negative trends). Only 0.3% of the Peninsula exhibited no TI-NDVI trend. TI-NDVI Sen's slope ranged from -0.144 to 0.244 yr^{-1}, with the mode between 0.020 and 0.030 yr^{-1}. Overall, 71.2% of the Yamal Peninsula exhibited simultaneous increases in Max and TI-NDVI, while 26.7% saw divergent trends in Max and TI-NDVI (Figure 7).

The direction and magnitude of climatic driver trends were variable (Figure 8). SWI trends were positive across 84.1% of the Yamal Peninsula (1.5% significant positive trends). Precipitation trends exhibited more variability than SWI trends, but increased across a slight majority (50.6%) of the Yamal Peninsula (no significant trends). Generally, positive precipitation trends were stronger where SWI also increased (r = 0.41). Snow-free period onset date trends were negative across 78.3% of the Peninsula (5.1% significant negative trends), indicating trends toward earlier snow melt. Negative snow-free period onset date trends were stronger where SWI

increased (r = -0.42). Soil moisture trends were negative across 85.3% of the Yamal Peninsula (3.9% significant negative trends), and were less negative where SWI increased (r = 0.44).

Drivers of Max and TI-NDVI Trends

The Max NDVI Random Forest regression model explained 65% of Max NDVI Sen's slope variance. The most important drivers of Max NDVI trends were coast distance, human modification, soil moisture Sen's slope, precipitation Sen's slope, elevation, and SWI Sen's slope (Figure 9). On average, positive Max NDVI trends were strongest further inland, at higher elevations, and where SWI trends exceeded approximately 0.5 °C months yr^{-1} (Figure 10). However, some strong, positive Max NDVI trends occurred along the southeastern coastline at elevations between -15 m and -13 m (< 1.0% of pixels). Additionally, only 1.7% of the Yamal Peninsula experienced increases in SWI greater than 0.5 °C months yr^{-1} (equivalent to a cumulative SWI increase of greater than 9 °C months). Prior to reaching this threshold, Max NDVI and SWI trends exhibited a slightly negative relationship. The covariation between detrended Max NDVI and SWI time series was variable, with 53.9% of pixels exhibiting a negative correlation (4.9% significant, p-value < 0.05) and 46.1% exhibiting a positive correlation (3.5% significant) (Figure 11).

On average, positive Max NDVI trends were strongest where human modification was limited, soil moisture trends were negative, and precipitation trends were negative (Figure 10). Most pixels had less than 3% of their area modified by gas operations, infrastructure, and/or human settlement; however, pixels comprised of 30% or more modified area exhibited negative Max NDVI trends. Detrended Max NDVI and soil moisture time series were negatively correlated across 68.5% of the Peninsula (4.5% significant) and positively correlated across 31.5% (1.5% significant) (Figure 12). Similarly, detrended Max NDVI and precipitation time

series were negatively correlated across 62.8% of the Peninsula (4.3% significant) and positively correlated across 37.2% (1.6% significant) (Figure 13). These correlations, although spatially variable, indicate that above-average Max NDVI co-occurred with below-average soil moisture and precipitation across a majority of the Yamal Peninsula.

The TI-NDVI Random Forest regression model explained 69% of TI-NDVI Sen's slope variance. Max and TI-NDVI Sen's slopes were best predicted by the same six variables; however, the importance of these variables varied (Figure 9). The most important drivers of TI-NDVI trends were coast distance, precipitation Sen's slope, elevation, human modification, SWI Sen's slope, and soil moisture Sen's slope. On average, positive TI-NDVI trends were strongest at higher elevations, where SWI trends exceeded approximately 0.1 °C months yr^{-1}, and where soil moisture trends were slightly positive around 0.5 mm yr^{-1} (Figure 14). The positive relationship between TI-NDVI and SWI trends became stronger after SWI Sen's slopes reached 0.5 °C months yr^{-1}. Detrended TI-NDVI and SWI time series were positively correlated across 99.9% of the Yamal Peninsula (76.9% significant), indicating that annual TI-NDVI and SWI positively covaried across nearly the entire Peninsula (Figure 15). Positive TI-NDVI trends were consistently stronger where soil moisture Sen's slopes were less negative and approaching 0 mm yr^{-1}. Detrended TI-NDVI and soil moisture time series were negatively correlated across 66.3% of the Peninsula (9.7% significant) and positively correlated across 33.7% (2.3% significant) (Figure 16). Therefore, although TI-NDVI and soil moisture trends exhibited a positive relationship, they did not positively covary interannually across a majority of the Peninsula.

On average, positive TI-NDVI trends were strongest closer to the coast, where precipitation trends were negative, and where human modification was limited (Figure 14). TI-NDVI trends fluctuated with distance from the coast, but were strongest between 0 and 75 km

inland. The relationship between TI-NDVI and precipitation trends was unimodal, with the strongest TI-NDVI trends occurring where precipitation decreased by approximately 0.5 mm yr^{-1}. Detrended TI-NDVI and precipitation time series were positively correlated across 74.0% of the Peninsula (2.3% significant) and negatively correlated across 26.0% (0.1% significant); therefore, TI-NDVI and precipitation positively covaried interannually across a majority of the Peninsula despite the trends exhibiting a negative relationship where precipitation trends were greater than -0.5 mm yr^{-1} (Figure 17). As with Max NDVI trends, positive TI-NDVI trends were weakest where 30% or more of the area had been modified by humans.

5.0 Discussion

5.1. Spatial Drivers of Peak Biomass and Total Productivity

Climatic drivers (except soil moisture) and physiognomic vegetation unit best explained the spatial distribution of peak aboveground biomass and total productivity on the Yamal Peninsula. On average, areas with higher Max and TI-NDVI coincided with warmer summer temperatures, higher precipitation, earlier snow melt, and vegetation units dominated by erect shrubs and wetland vegetation. Although soil moisture has been found to influence Arctic vegetation distribution (Raynolds et al., 2008; van der Kolk et al., 2016; Walker et al., 2001) and has a more direct effect on water availability than precipitation, it did not exhibit a spatial correlation with Max or TI-NDVI. This implies that the positive spatial correlations among Max/TI-NDVI and precipitation may have been driven by the strong spatial relationship precipitation had with SWI and snow-free period onset date, rather than spatial patterns of water availability. In addition to influencing water availability (Gamon et al., 2013), the timing of snow melt determines when the growing season can begin (Bieniek et al. 2015). Vegetation distribution may have been more limited by summer warmth and growing season onset than water availability because the continuous permafrost underlying the Yamal Peninsula restricts

drainage and generally facilitates high soil moisture conditions (Bieniek et al., 2015). Additionally, our results are consistent with findings that more productive Arctic vegetation with higher aboveground biomass is found where growth is not limited by low temperatures or shorter growing seasons (Epstein et al. 2021; Jia et al., 2006; Raynolds et al., 2006). The positive spatial correlations between Max/TI-NDVI and human modification were likely the result of warmer areas with earlier snowmelt also coinciding with more human activity. However, re-vegetated off-road vehicle tracks on the Yamal Peninsula near concentrated areas of infrastructure have been found to have higher aboveground biomass than surrounding undisturbed areas approximately 20 years after revegetation (Forbes et al., 2009).

Although less important than vegetation unit, the other categorical variables considered (substrate chemistry, soil texture, and landscape age) also influenced spatial patterns of peak aboveground biomass and total productivity. Max and TI-NDVI were highest on nutrient-rich circumneutral substrates as well as clay loam and silt loam soil textures, similar to other studies from the region (Epstein et al., 2021; Macias-Fauria et al., 2012; Walker et al., 2005). The weak positive association with high TI-NDVI and younger landscapes was unexpected because older landscapes can have greater nutrient availability and erect shrub coverage after the development of fine-grained soils and stream networks, vegetation succession, and peat accumulation (Walker et al., 1995). However, the negative spatial association between high TI-NDVI and younger landscapes was much stronger and drove the significance of the spatial relationship between TI-NDVI and landscape age.

5.2. Peak Biomass and Total Productivity Trends

Peak aboveground biomass and total productivity increased across a majority of the Yamal Peninsula between 2001 and 2018. The magnitude and direction of the trends were

spatially variable, with most pixels exhibiting insignificant (p-value > 0.05) change. Max NDVI has consistently increased across a majority of the Yamal Peninsula for the past three decades (Berner et al., 2020; Bhatt et al., 2021; Frost et al., 2020; Myers-Smith et al., 2020), while the nearly uniform increase in TI-NDVI indicates a recent shift from negative to positive TI-NDVI trends in some areas (Bhatt et al., 2021; Frost et al., 2020). The co-occurrence of negative Max NDVI and positive TI-NDVI trends could be explained by the different aspects of productivity and phenology that these variables represent (Jia et al., 2006). Max NDVI better identifies the contribution of the growth form with the greatest aboveground biomass at the peak of the growing season (erect shrubs across a majority of the Peninsula) than TI-NDVI, which better captures the contributions of all growth forms (shrubs, graminoids, forbs, lichens, and mosses) by summing NDVI values across the entire growing season (Bhatt et al., 2021; Frost et al., 2020; Jia et al., 2006; Mikola et al., 2018). Therefore, areas with divergent Max and TI-NDVI trends likely experienced total productivity increases despite potential decreases in peak erect shrub biomass due to the expansion of graminoids (Forbes et al., 2009; Kumpula et al., 2011; Magnússon et al., 2021; Raynolds et al., 2006; van der Kolk et al., 2016). This shift in community composition has been reported for the central Yamal Peninsula following disturbance from off-road vehicle tracks and heavy reindeer grazing (Forbes et al., 2009; Kumpula et al., 2011), but could not be confirmed for other areas without ground verification (Myers-Smith et al., 2020). However, Max NDVI has been found to have a strong relationship ($r^2 = 0.82$) with shrub aboveground biomass (Berner et al., 2018).

5.3. Temporal Drivers of Peak Biomass and Total Productivity

The six drivers that best predicted peak aboveground biomass and total productivity trends were a combination of geologic (coast distance and elevation), anthropogenic (human modification), and climatic (precipitation trends, soil moisture trends, and SWI trends) drivers.

Positive Max and TI-NDVI trends exhibited similar relationships with precipitation trends, elevation, and human modification but had opposing relationships with the most important driver (coast distance), soil moisture trends, and SWI trends less than 0.5 °C months yr^{-1}. These relationships could be due to erect shrubs and other growth forms in the vegetation community having differential responses to some drivers and coordinated responses to others. While these findings elucidated the relationships between positive Max/TI-NDVI trends and the drivers, they also provide insight into the potential causes of divergent Max and TI-NDVI trends.

Coast distance captured the effect of coastal-inland gradients in SWI on the Yamal Peninsula. The consistently cooler coastal temperatures influenced by sea ice (Bhatt et al., 2010) and maritime air flow (Bhatt et al., 2021) potentially facilitated graminoid, forb, moss, and lichen growth (indicated by stronger positive TI-NDVI trends) and limited shrub growth (indicated by weaker positive Max NDVI trends) (Walker et al., 2005). As coastal temperatures increase due to melting sea ice (Bhatt et al., 2021), shrub growth may become less limited near the Yamal Peninsula coastline. The spatial relationship between coast distance and mean soil moisture may also point to the influence of other factors, such as nutrient availability, on Yamal Peninsula vegetation productivity trends. Graminoids are able to take advantage of low nutrients in high soil moisture conditions that can limit shrub growth (van der Kolk et al., 2016), and soil organic nitrogen content has been found to limit increased shrub growth in response to warming on the Yamal Peninsula (Yu et al., 2011). Additionally, limited shrub growth along the coast would facilitate moss and lichen growth by decreasing light competition and burial under litter (van Wijk et al., 2003).

The opposing relationships between Max/TI-NDVI trends, soil moisture trends, and SWI trends indicate that climate-induced permafrost degradation may have driven moisture regime

shifts that favored shrub growth and positive Max NDVI trends where drying was more pronounced, but graminoid, forb, and moss growth and positive TI-NDVI trends where drying was less pronounced or wetting occurred (Jorgenson et al., 2015; Magnússon et al., 2020, 2021; van der Kolk et al., 2016). Warming has been found to increase shrub, graminoid, and forb growth (Elmendorf et al., 2012; Walker et al., 2006; Yu et al., 2011) and would be expected to have a positive relationship with Max and TI-NDVI trends without the influence of other limiting factors (Berner et al., 2020; Bhatt et al., 2021; Dutrieux et al., 2012). Prior to reaching the 0.5 °C months yr^{-1} threshold that resulted in the strongest positive relationships between Max/TI-NDVI trends and SWI trends, the influence of positive SWI trends on permafrost thaw and subsequent soil moisture conditions was likely more important than their direct effects on vegetation growth. Ice wedge degradation and the expansion of thermokarst features (lakes, gullies, and pits) could have countered negative soil moisture trends through surface wetting that caused shrub death and the succession of graminoids, forbs, and mosses (Frost and Epstein, 2014; Jorgenson et al., 2015; Magnússon et al., 2020, 2021; Osterkamp et al., 2009; van der Kolk et al., 2016). Conversely, thermokarst that causes lake drainage and the drying of areas adjacent to depressions could have contributed to strong negative soil moisture trends that favored shrub growth (Jin et al., 2020; Lantz, 2017; Loiko et al., 2020; Osterkamp et al., 2009; van der Kolk et al., 2016). Ice wedges, thermokarst features, and drained thermokarst lakes have been observed on the Yamal Peninsula (Leibman et al., 2014; Nitze et al., 2018; Verdonen et al., 2020; Walker et al., 2009), and the above processes have been reported elsewhere in the Eurasian (Frost and Epstein, 2014; Loiko et al., 2020; Magnússon et al., 2020, 2021) and North American (Jorgenson et al., 2015; Lantz, 2017; Osterkamp et al., 2009) Arctic. However, further research using *in situ* or high-resolution remote measurements of ice wedge degradation and thermokarst processes are

needed to confirm their influence on Yamal Peninsula peak aboveground biomass and total productivity trends. The negative relationship between positive Max NDVI trends and soil moisture trends could also be the result of spectral contamination within pixels with high soil moisture (Myers-Smith et al., 2020); however, I would have expected a similar impact on TI-NDVI trends if this were the case.

Increasing precipitation has been found to benefit graminoid growth over shrub growth in mixed vegetation communities; however, positive Max and TI-NDVI trends had a negative relationship with precipitation trends (van der Kolk et al., 2016). These similar relationships could have been associated with the effect of precipitation on the frequency of cryogenic landslides (Leibman et al., 2014) and/or an increase in early growing season rain-on-snow events (Bartsch et al., 2010; Phoenix and Bjerke, 2016). Increased precipitation is the primary cause of cryogenic landslides (Leibman et al., 2014) that result in shear surfaces that remain bare or sparsely vegetated for decades before recolonization by shrubs (Verdonen et al., 2020; Walker et al., 2009). Additionally, April rain-on-snow events followed by below-freezing temperatures have been recorded on the Yamal Peninsula during the study period (Bartsch et al., 2010) and can result in the death of vegetation due to ice encasement and the formation of ice crusts (Bartsch et al., 2010; Phoenix and Bjerke, 2016).

While the observed relationships revealed how overall change in the most important climatic drivers influenced overall change in Max and TI-NDVI, their degree of positive or negative interannual covariation provided insight into the more immediate responses of vegetation to fluctuating SWI, soil moisture, and precipitation conditions that may or may not be reflected by the average trend relationships (Myers-Smith et al., 2020). For example, detrended TI-NDVI and precipitation were positively correlated across 74.0% of the Yamal Peninsula, but positive TI-

NDVI trends had a negative relationship with precipitation trends greater than -0.5 mm yr^{-1}. Higher precipitation during any given year could have immediate beneficial effects on TI-NDVI by limiting water stress (Epstein et al., 2018; Opala-Owczarek et al., 2018), whereas increases in precipitation over time could cause an increase in landslides (Leibman et al., 2014; Verdonen et al., 2020) and/or early growing season rain-on-snow events (Bartsch et al., 2010; Phoenix and Bjerke, 2016) that would weaken positive TI-NDVI trends. Additionally, the correlations among Max/TI-NDVI and SWI, soil moisture, and precipitation detrended time series revealed spatial heterogeneity in the direction and magnitude of covariation, with concentrated areas of strong positive and negative covariation occurring throughout the Yamal Peninsula. For instance, strong positive covariation between Max NDVI and SWI occurred along the central western coastline, while strong negative covariation occurred in the central northern region of the Peninsula (Figure 11). This heterogeneity is reflective of the spatiotemporal variation in the suite of drivers that influence Arctic vegetation productivity, and highlights the difficulty in generalizing the effects of individual drivers on Arctic vegetation productivity across large regions.

5.4. Summary and Conclusions

These findings indicate that spatial patterns of peak aboveground biomass and total productivity were similarly influenced by SWI, growing season onset, and vegetation type, whereas peak aboveground biomass and total productivity trends had variable relationships with drivers and were primarily influenced by coastal-inland gradients in SWI and soil moisture. Max and TI-NDVI increased across a majority of the Yamal Peninsula, and TI-NDVI trends may have recently shifted from negative to positive in some areas (Bhatt et al., 2021; Frost et al., 2020) despite some concurrent decreases in Max NDVI. Relationships among Max/TI-NDVI trends and climatic driver trends pointed to the potential influence of permafrost degradation on Max and TI-NDVI via changes in hydrological conditions. While remote sensing analyses can miss

the impact of fine-scale landscape features related to permafrost degradation (Myers-Smith et al., 2020), the comparison of Max and TI-NDVI trend relationships indicated that permafrost processes may be causing differential vegetation responses and divergent trends. Divergent trends were likely caused by a shift from shrub to graminoid dominance (Forbes et al., 2009; Kumpula et al., 2011; Magnússon et al., 2021; Raynolds et al., 2006; van der Kolk et al., 2016), which can occur following heavy reindeer grazing (Forbes et al., 2009; Olofsson et al., 2009). Additional research detailing the interaction between permafrost degradation and reindeer herbivory is needed to determine their combined effects on Yamal Peninsula peak aboveground biomass and total productivity. Further, the importance of the negative relationships between Max/TI-NDVI trends and human modification indicates that anthropogenic disturbances are becoming an increasingly important mediator of Yamal Peninsula vegetation responses to changing climate and landscape conditions (Walker et al., 2009). This study provides insight into the potential future of Arctic regions undergoing warming, moisture regime shifts, and increasing human modification, and demonstrates the usefulness of considering multiple NDVI metrics to disentangle the effects of individual drivers across heterogeneous landscapes.

6.0 Figures

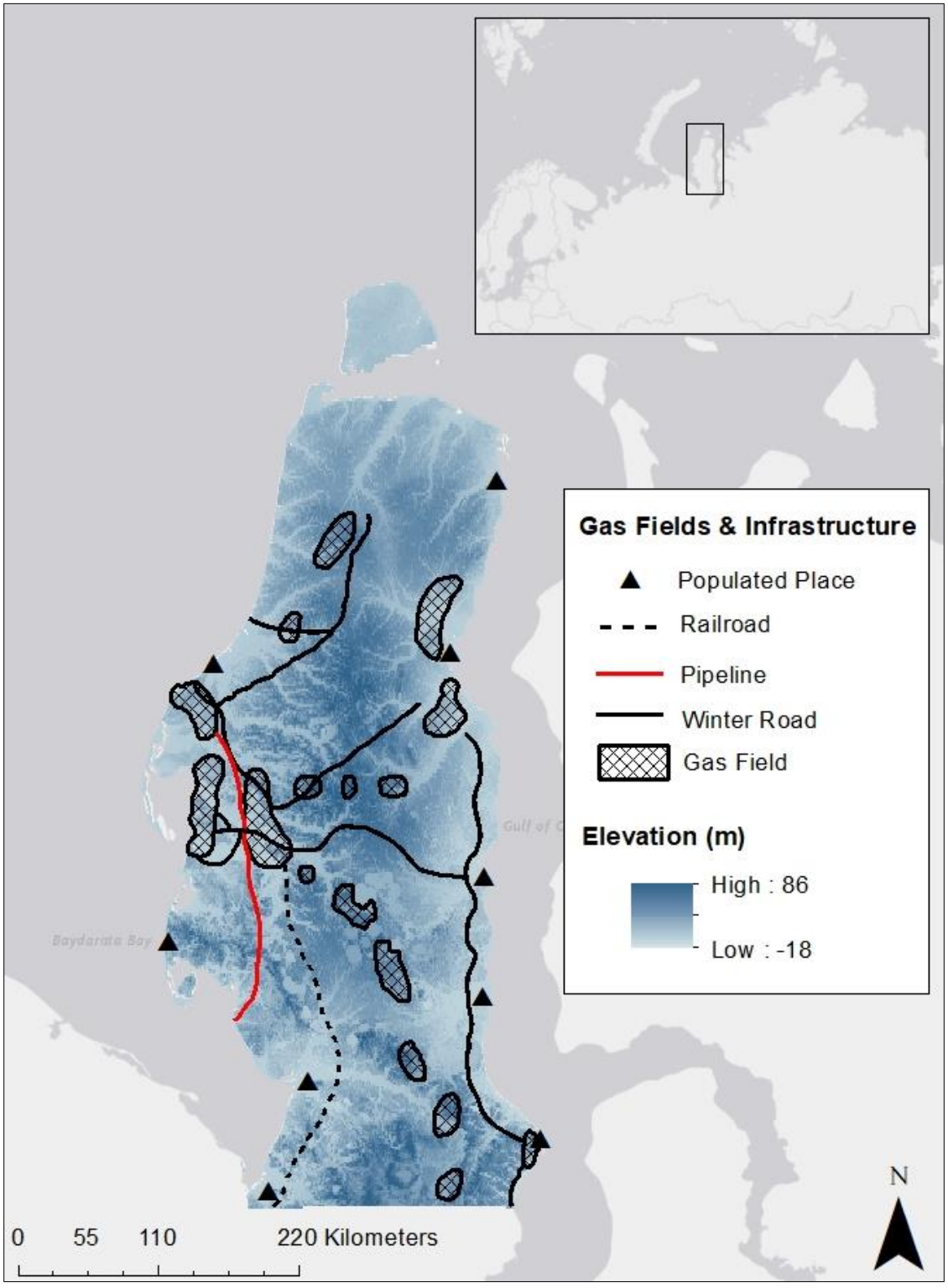

Figure 1. The Yamal Peninsula with elevation (m above sea level) and locations of population centers, infrastructure, and gas fields (adapted from Forbes 1999 and Gazprom 2021). The inset map shows the location of the Yamal Peninsula (outlined by the black box).

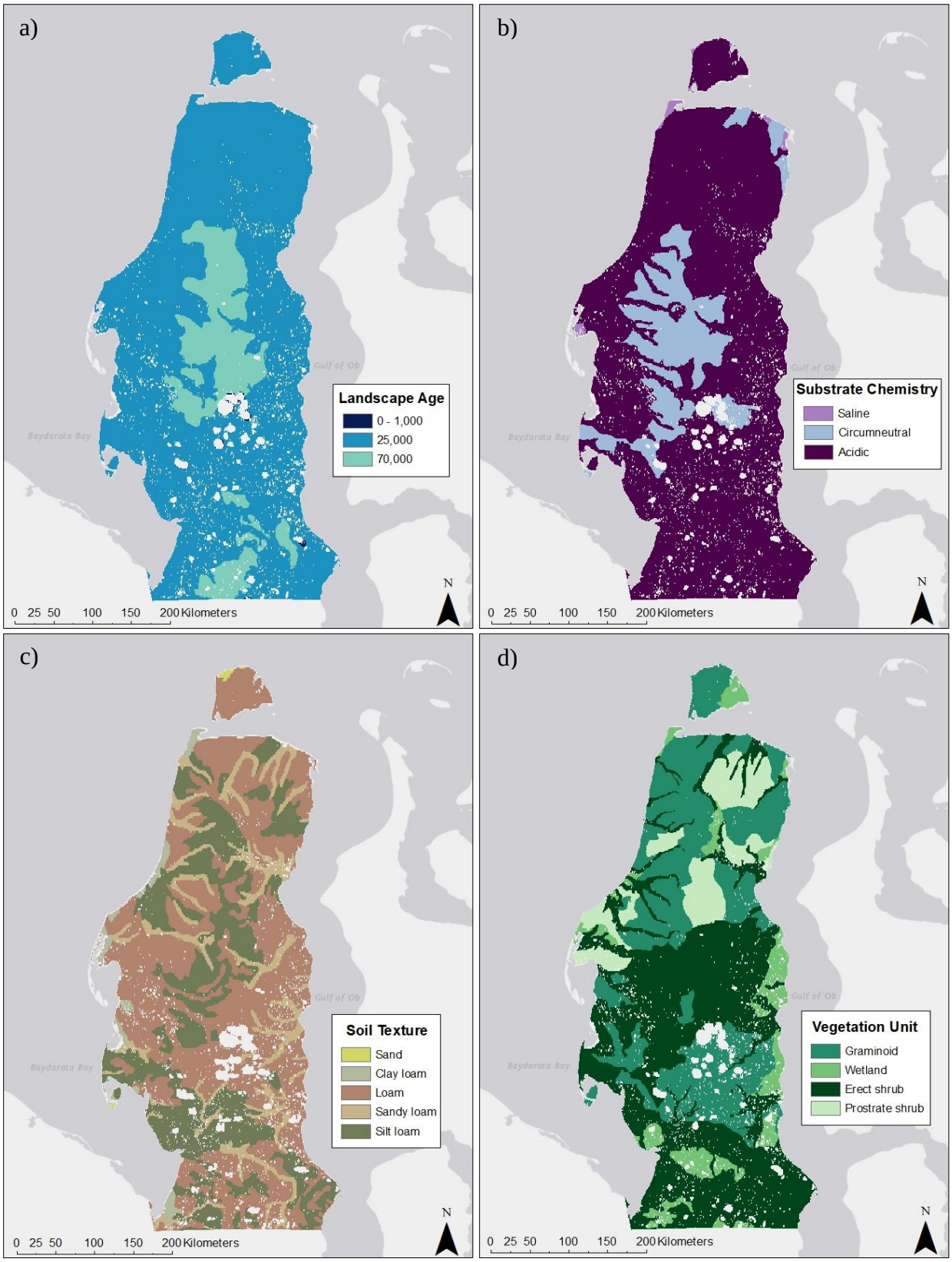

Figure 2. Yamal Peninsula (a) landscape age, or time since last glaciation, (b) substrate chemistry, (c) soil texture, and (d) physiognomic vegetation unit representing the dominant vegetation type. Permanent surface water bodies are masked.

Table 1. Datasets included in the analyses and their respective types, years collected, native spatial resolutions, and sources.

Data Type	Year(s) Collected	Dataset(s)	Native Resolution	Source
Continuous	NA	Distance from the Coast	1 kilometer	Circumpolar Arctic Vegetation Map
	2010 - 2015	Elevation	90 meters	TanDEM-X 90m Digital Elevation Model
	2014, 2016	Human Modification	1 kilometer	Conservation Science Partners
	2000-2019	Max and TI-NDVI	250 meters	Terra MODIS Vegetation Indices (MOD13Q1.006)
	1958-2018	Mean Growing Season Precipitation and Soil Moisture	2.5 arc minutes	TerraClimate: Monthly Climate and Climatic Water Balance for Global Terrestrial Surfaces, University of Idaho
	2000-2019	Snow-Free Period Onset	500 meters	Terra MODIS Snow Cover (MOD10A1.006)
	2000-2019	Summer Warmth Index	1 kilometer	Terra MODIS Land Surface Temperature and Emissivity (MOD11A1.006)
Categorical	2009	Landscape Age	1 kilometer	Circumpolar Arctic Vegetation Map
	2003	Physiognomic Vegetation Unit	1 kilometer	Circumpolar Arctic Vegetation Map
	1971 - 2010	Soil Texture	1 kilometer	Harmonized World Soil Database
	2003	Substrate Chemistry	1 kilometer	Circumpolar Arctic Vegetation Map

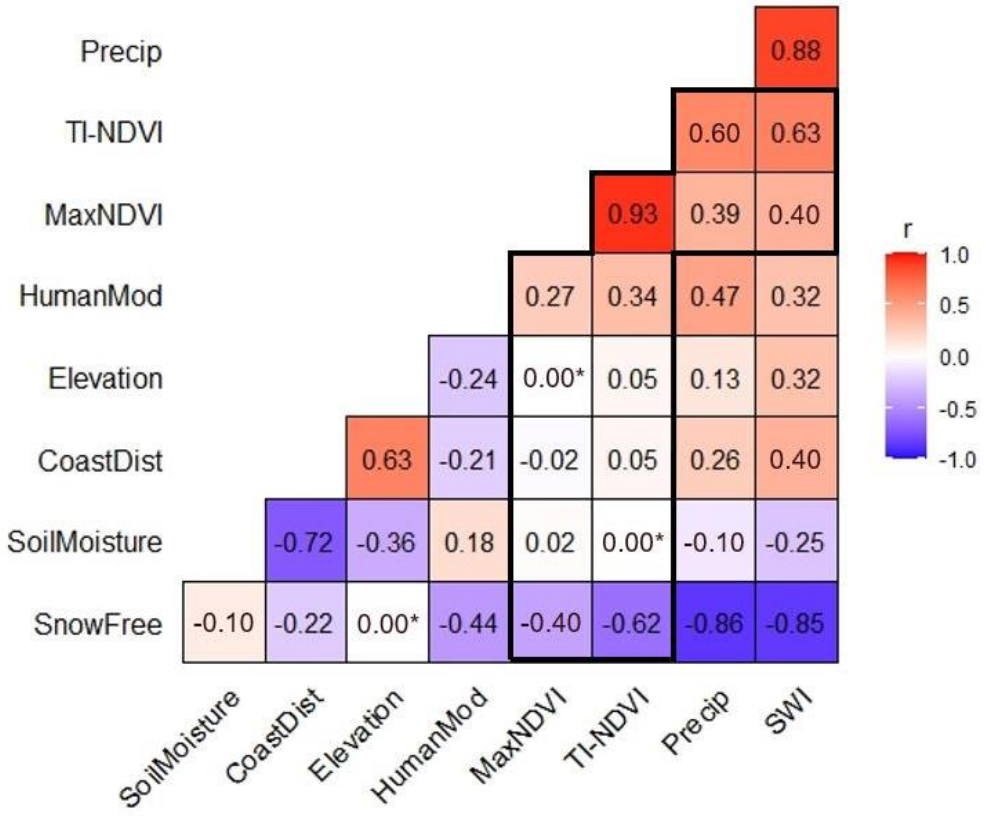

Figure 3. Spearman's correlation coefficients (r) for correlations between Max NDVI, TI-NDVI, and continuous drivers. The 2001-2018 means of Max NDVI, TI-NDVI, precipitation (Precip), snow-free period onset date (SnowFree), soil moisture, and Summer Warmth Index (SWI) were used. Human modification (HumanMod), elevation, and coast distance (CoastDist) values included were constant over the study period. Max and TI-NDVI correlations are highlighted by the thicker black boxes. *Insignificant at the 95% confidence level.

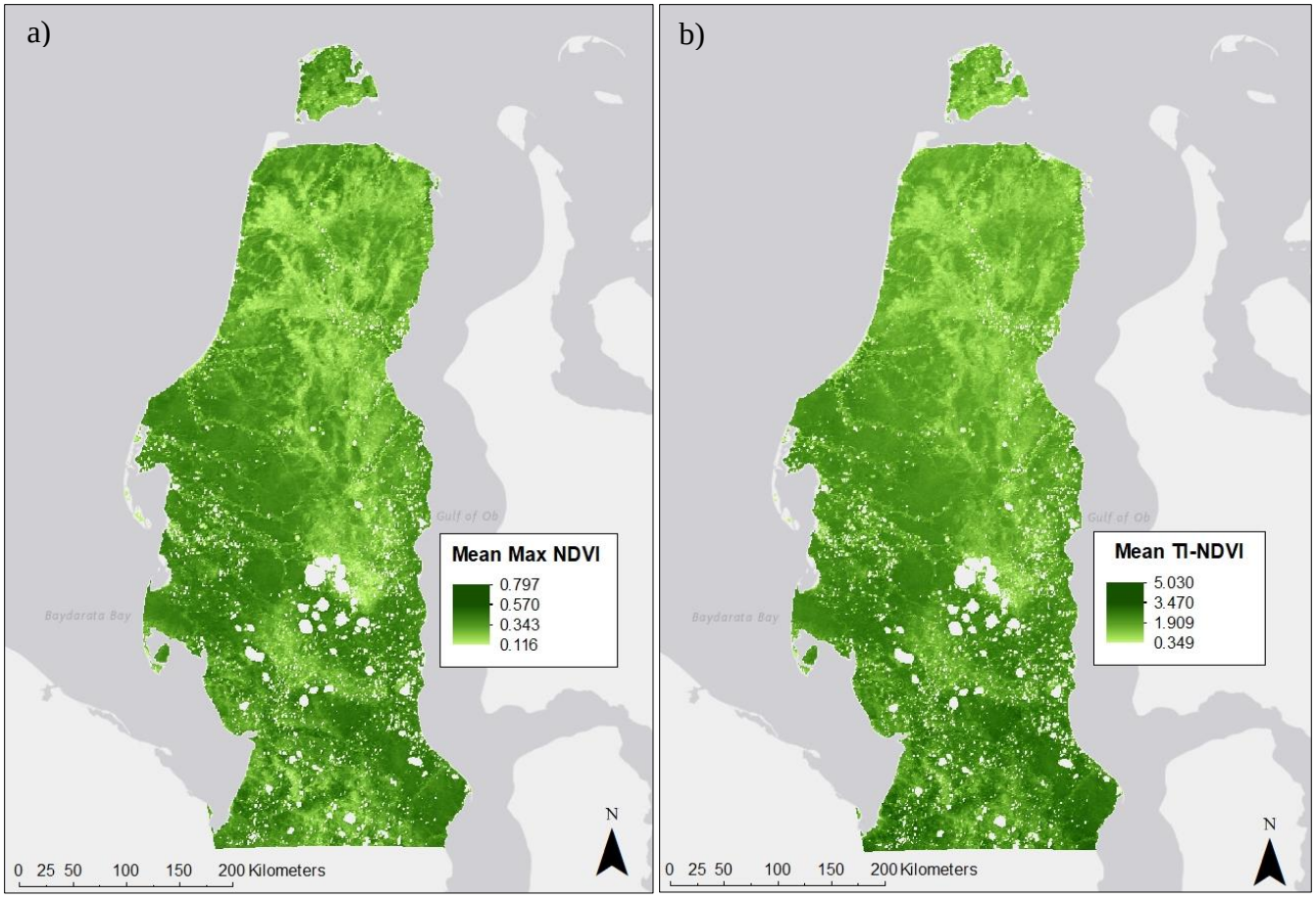

Figure 4. Yamal Peninsula 2001-2018 mean (a) Max NDVI and (b) TI-NDVI. Max NDVI is the maximum NDVI value, and represents peak growing season aboveground biomass. TI-NDVI is the sum of all NDVI values > 0.01 and represents total growing season productivity.

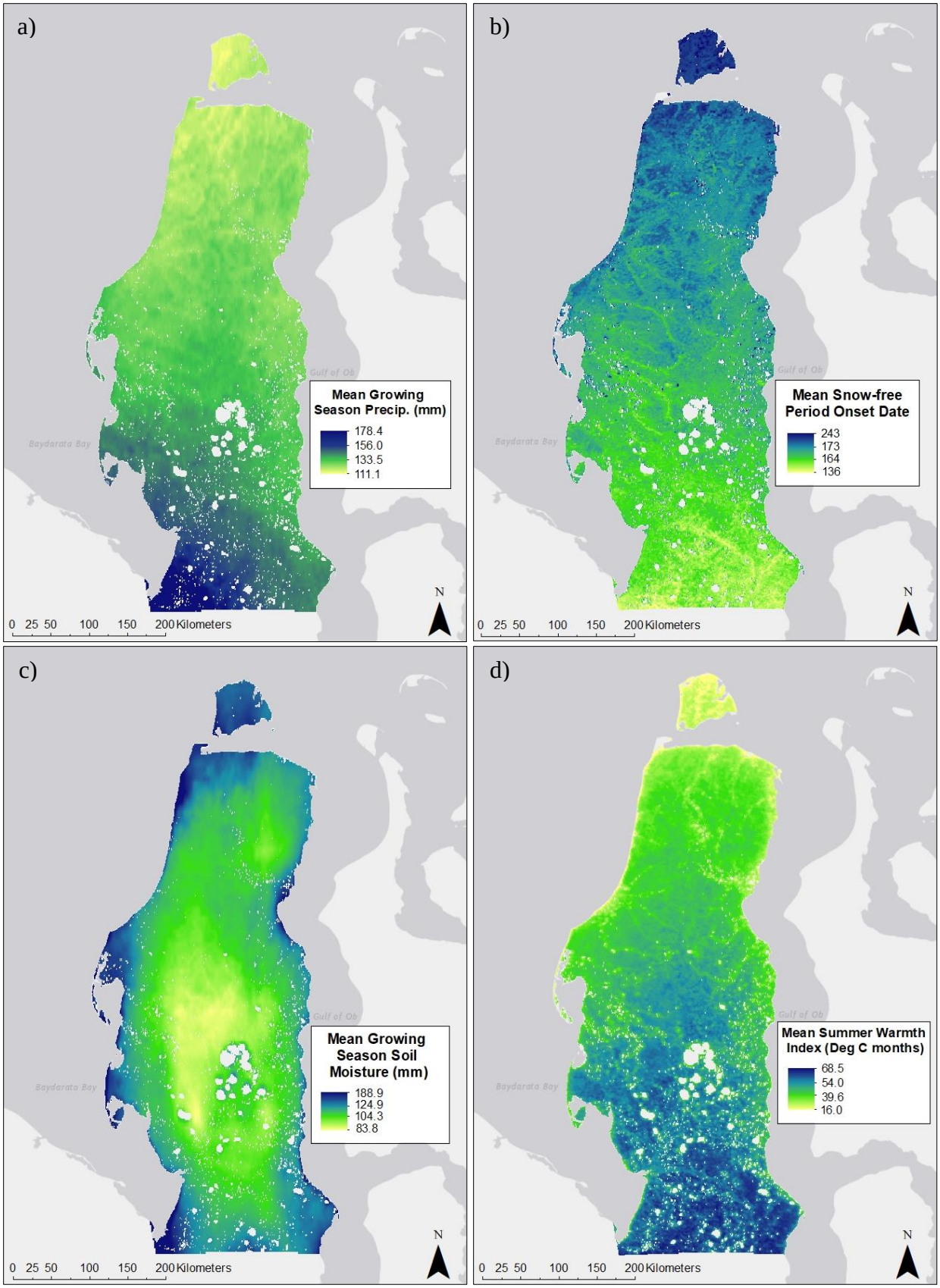

Figure 5. Yamal Peninsula 2001-2018 mean (a) mean growing season precipitation, (b) snow-free period onset date (Julian date), (c) mean growing season soil moisture, and (d) Summer Warmth Index (SWI).

Table 2. Chi-Square Test of Independence results. All tests were significant at the 95% confidence level. A larger χ^2 value indicates a stronger spatial association. Bolded residual values with the largest absolute values had the greatest influence on the spatial associations. Positive residuals indicate a positive relationship, and negative residuals indicate a negative relationship. The mid- mean Max and TI-NDVI categories are excluded because the most influential relationships were associated with high and low mean Max and TI-NDVI categories.

Drivers			Chi-Square Test of Independence Residuals			
			Mean Max NDVI		Mean TI-NDVI	
			High	Low	High	Low
Vegetation Unit	(χ^2 = 10,674)	Erect Shrub	41.0	-43.8	**77.2**	-66.1
		Graminoid	-30.3	33.5	-66.4	48.3
		Prostrate Shrub	-43.5	**49.5**	-57.4	65.5
		Wetland	9.5	-15.9	21.8	-9.1
Substrate Chemistry	(χ^2 = 5,672)	Acidic	-22.4	15.8	-2.8	17.9
		Circumnuetral	**50.7**	-36.5	7.0	**-41.8**
		Saline	-0.9	5.3	-4.9	10.6
Soil Texture	(χ^2 = 2,337)	Clay Loam	7.2	-10.1	7.5	-6.2
		Loam	-2.3	5.1	-11.2	5.0
		Sand	-4.4	8.0	-9.7	11.8
		Sandy Loam	**-28.1**	16.5	-30.9	20.7
		Silt Loam	18.8	-14.8	**32.2**	-18.3
Landscape Age	(χ^2 = 128)	Older	3.9	-5.6	-2.4	**-28.6**
		Younger	-1.7	2.1	1.1	12.2
		Recently Disturbed	-0.9	**7.3**	-0.8	9.2

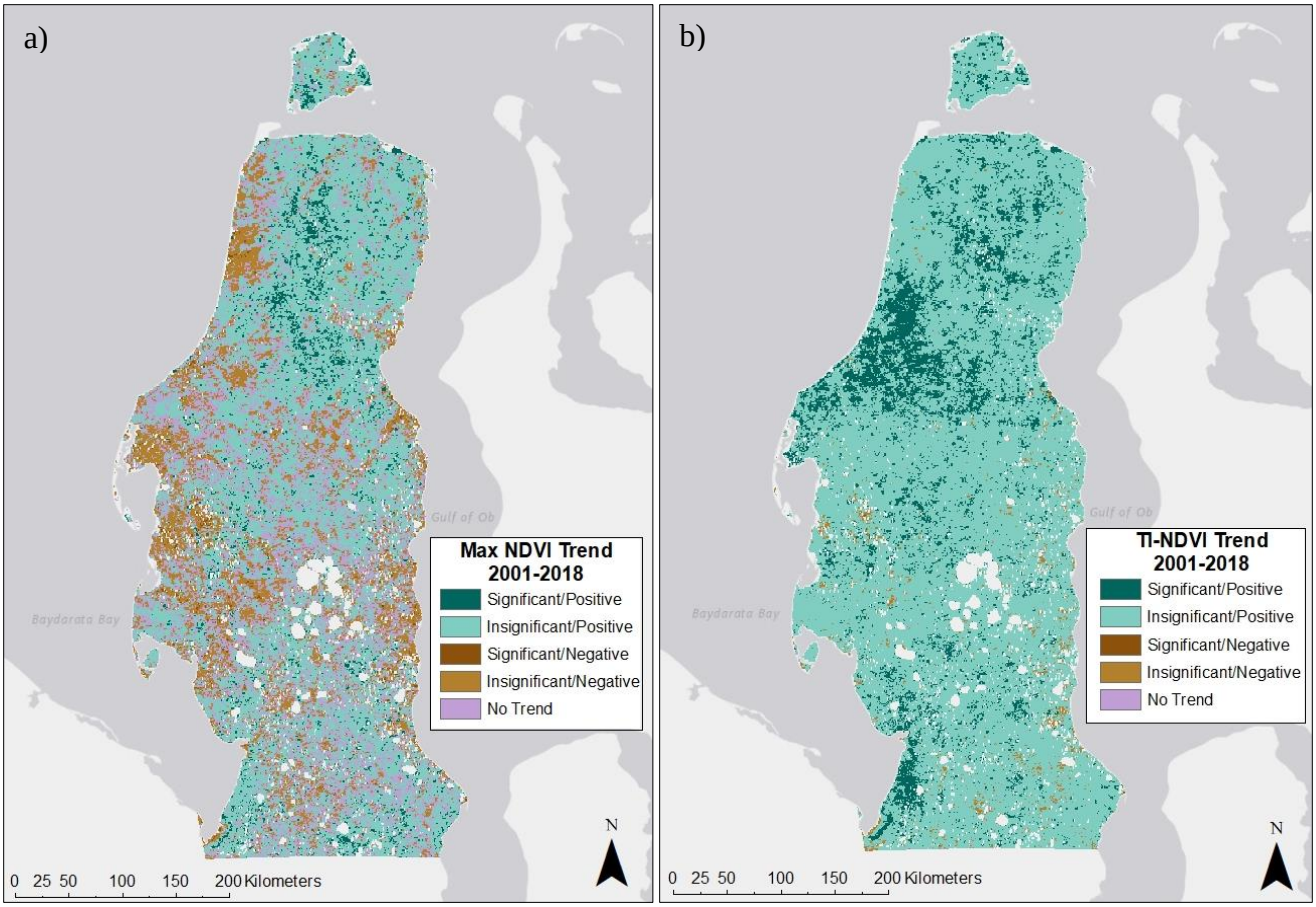

Figure 6. Trends in (a) Max NDVI and (b) TI-NDVI inferred from Mann-Kendall trend tests and Sen's slope estimation. Pixels were classified based on trend significance at the 95% confidence level and Sen's slope direction. Pixels classified as no trend had insignificant trends and Sen's slopes = 0.000. Permanent water bodies and pixels with < 15 years of data (due to low quality data or conditions preventing vegetation growth) were masked.

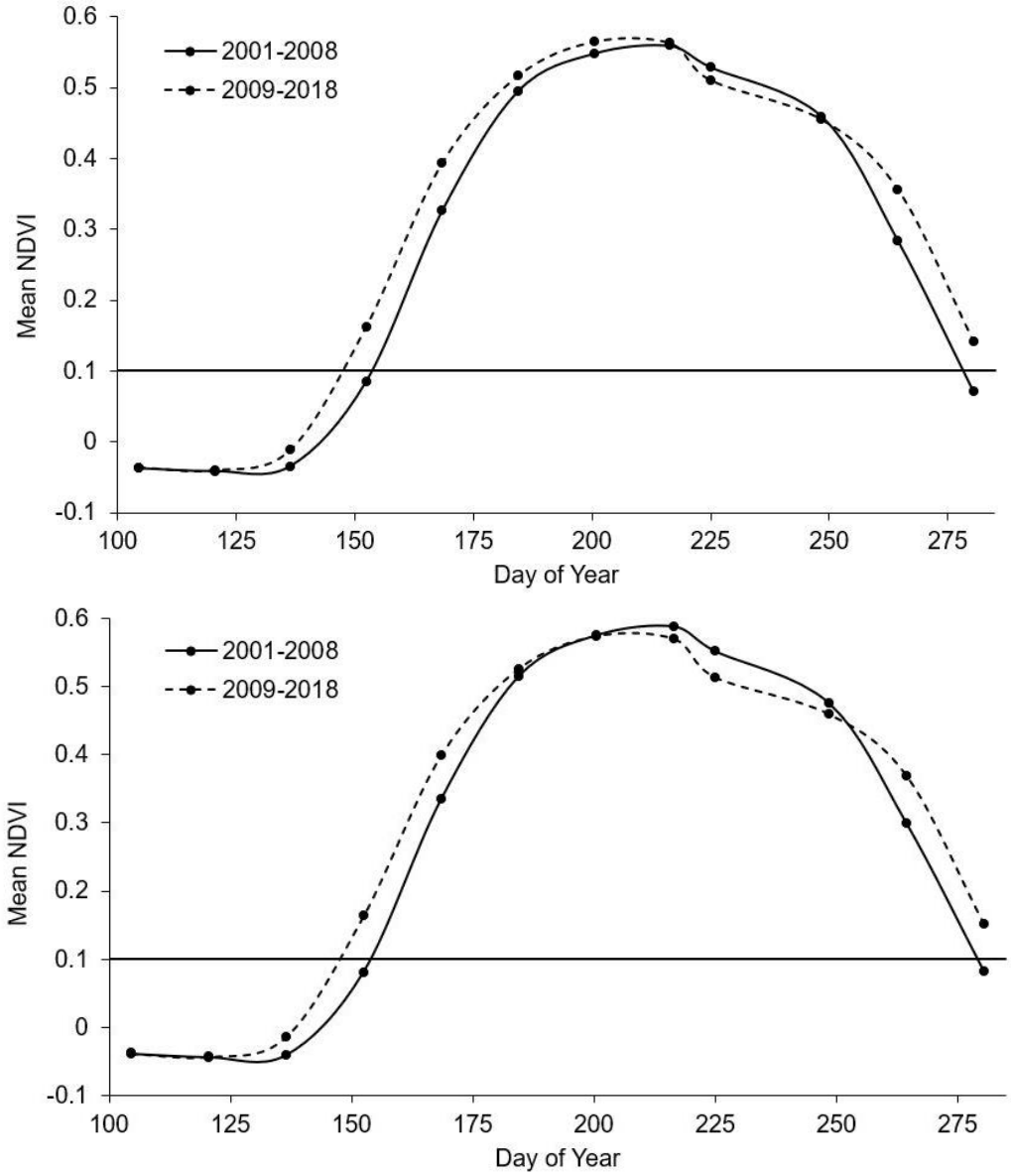

Figure 7. Phenology curves for pixels where a) Max and TI-NDVI increased and b) where Max NDVI decreased while TI-NDVI increased. Mean 2001-2008 and 2009-2018 NDVI values were calculated for each 16-day growing season composite image to assess how Max and TI-NDVI shifted between the first and second halves of the study period. Max NDVI is represented by the peak mean NDVI value at the top of each curve, and TI-NDVI is represented by the area under the curve. The line at mean NDVI = 0.1 indicates the minimum threshold for NDVI values included in TI-NDVI calculation.

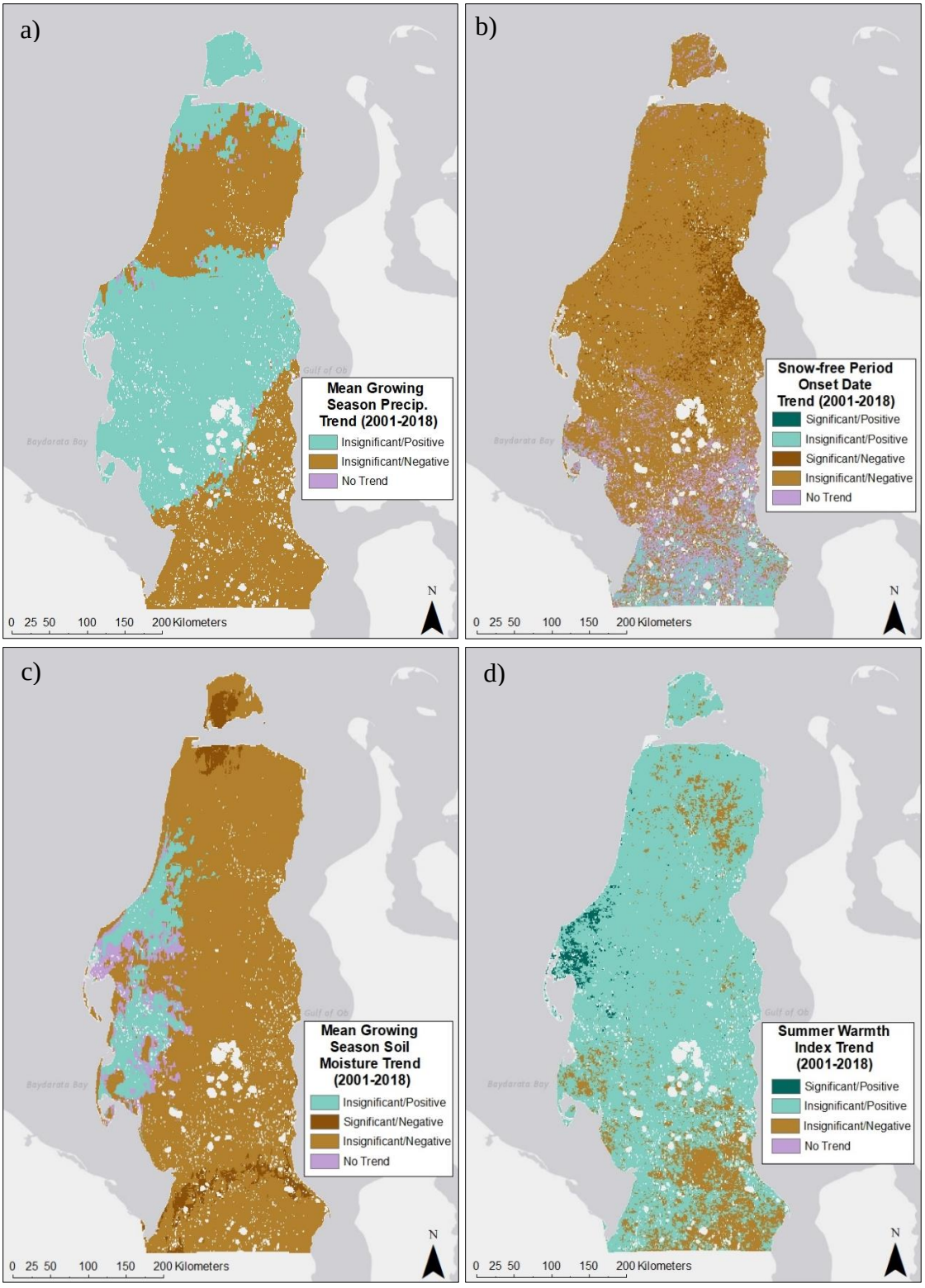

Figure 8. Trends in (a) mean growing season precipitation, (b) snow-free period onset date, (c) mean growing season soil moisture, and (d) Summer Warmth Index (SWI) inferred from Mann-Kendall trend tests and Sen's slope estimation. Pixels were classified based on trend significance at the 95% confidence level and Sen's slope direction. Pixel with marginal significance had p-values = 0.05. Pixels classified as no trend had insignificant trends and Sen's slopes = 0.000. Permanent water bodies and pixels with < 15 years of data (due to low quality data or conditions preventing vegetation growth) were masked.

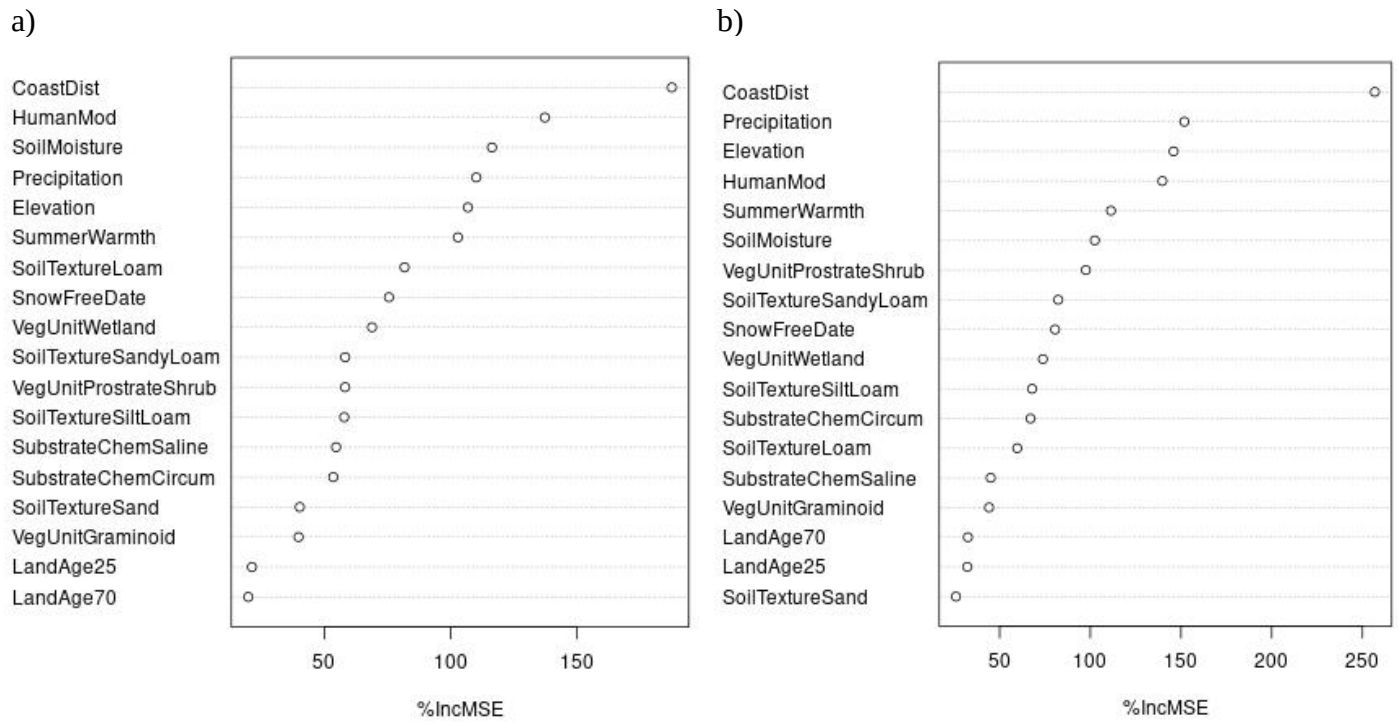

Figure 9. Variable importance for the prediction of a) Max NDVI Sen's slope and b) TI-NDVI Sen's slope. Variable importance was determined by the Random Forest regression models and quantified with %Inc MSE parameter. %Inc MSE measures the percent increase in MSE when a predictor variable is permuted in the out-of-bag (OOB) data while all other predictor variables remain unchanged (Liaw and Wiener 2002). A higher %Inc MSE value indicates greater importance.

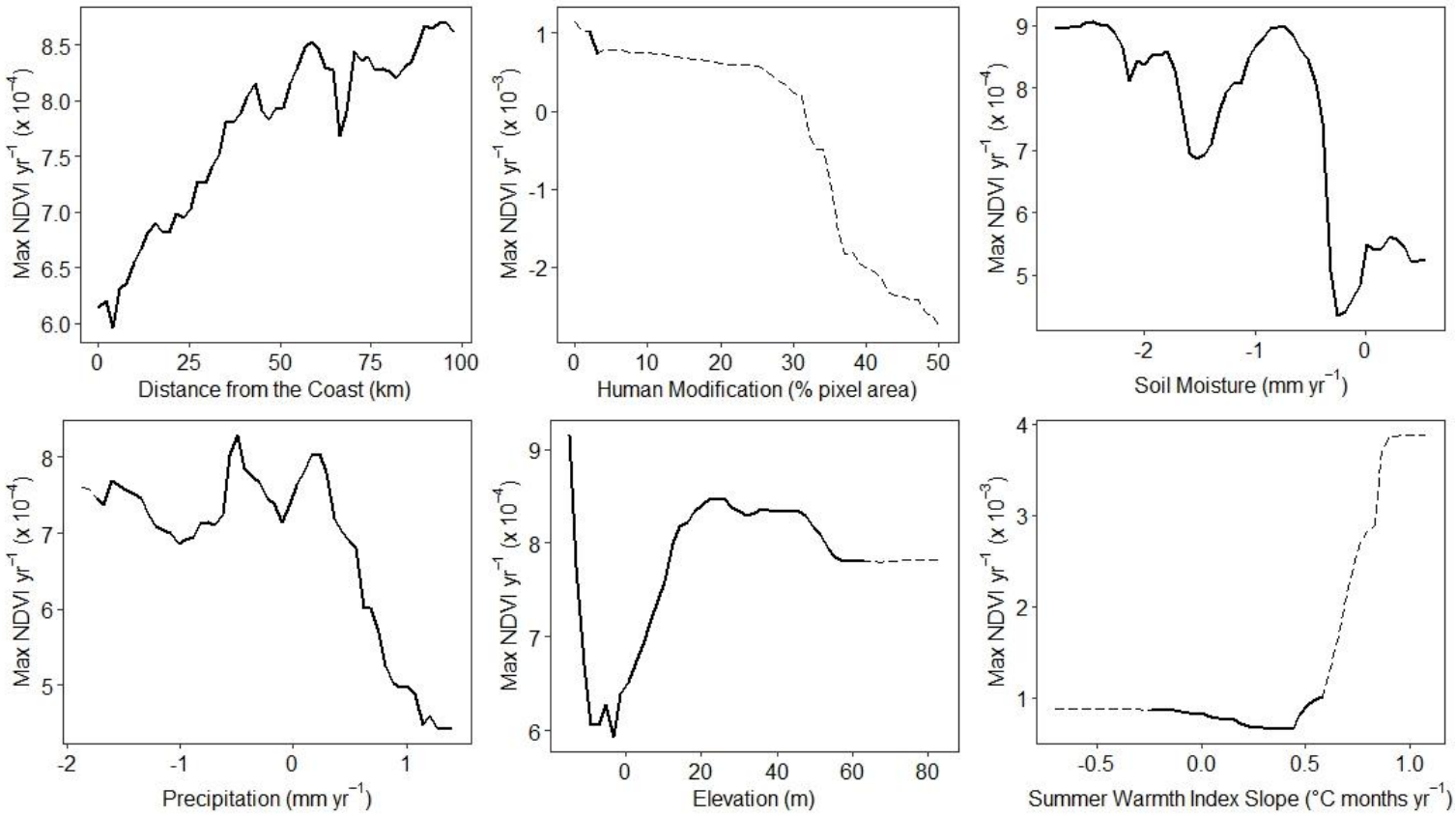

Figure 10. Partial dependence plots for the six most important drivers of Max NDVI Sen's slope: distance from the coast, human modification, mean growing season soil moisture Sen's slope, mean growing season precipitation Sen's slope, elevation, and Summer Warmth Index (SWI) Sen's slope. Partial dependence plots display the average predicted relationships between Max-NDVI trends and individual drivers across their range of values while still considering the average effects of the other drivers (Goldstein et al., 2014). Dashed lines indicate outlier driver variable values.

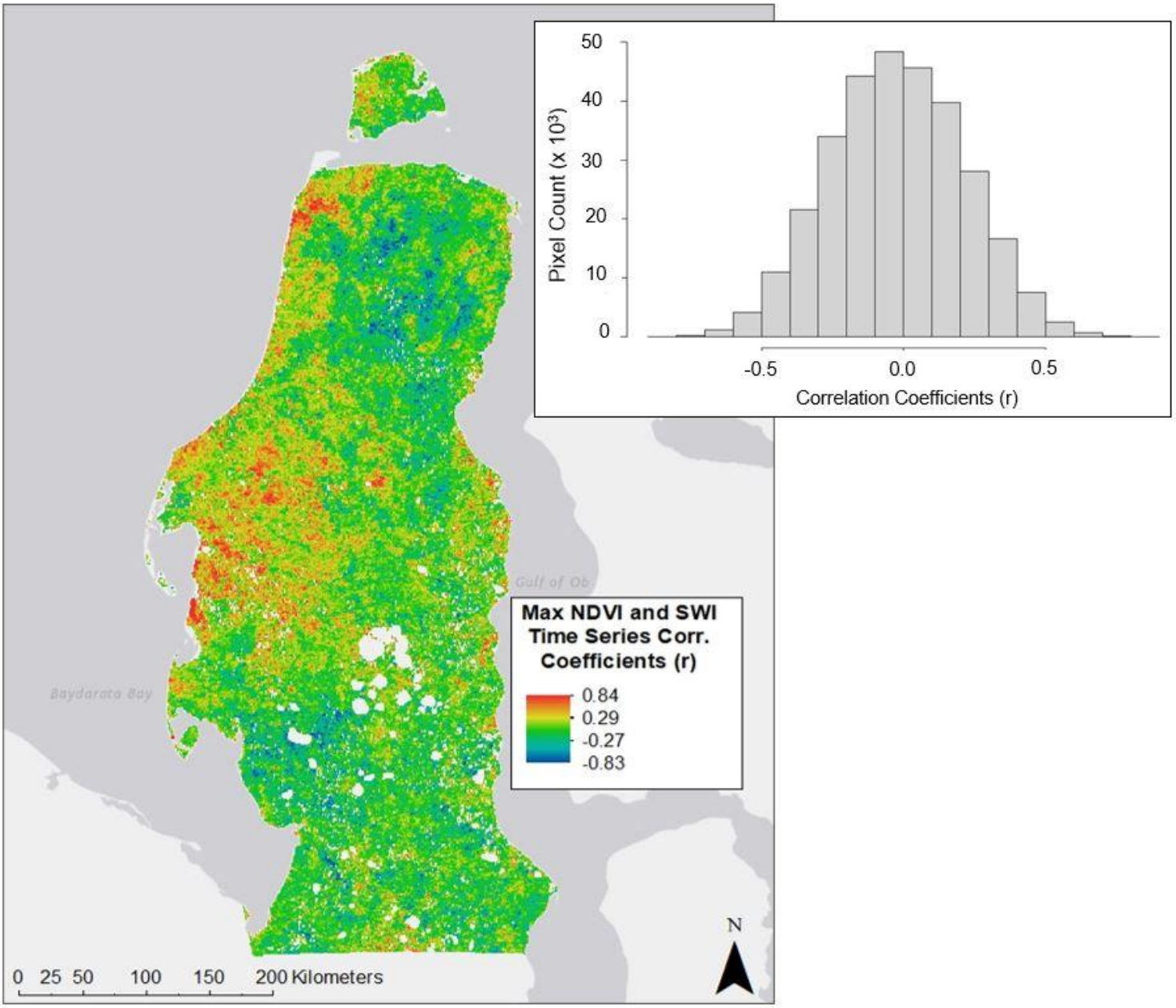

Figure 11. Map of Spearman's correlation coefficients (r) for pixel-wise correlations between linearly detrended Max NDVI and SWI time series (2001 – 2018). The inset histogram displays the frequency of r values across the Yamal Peninsula.

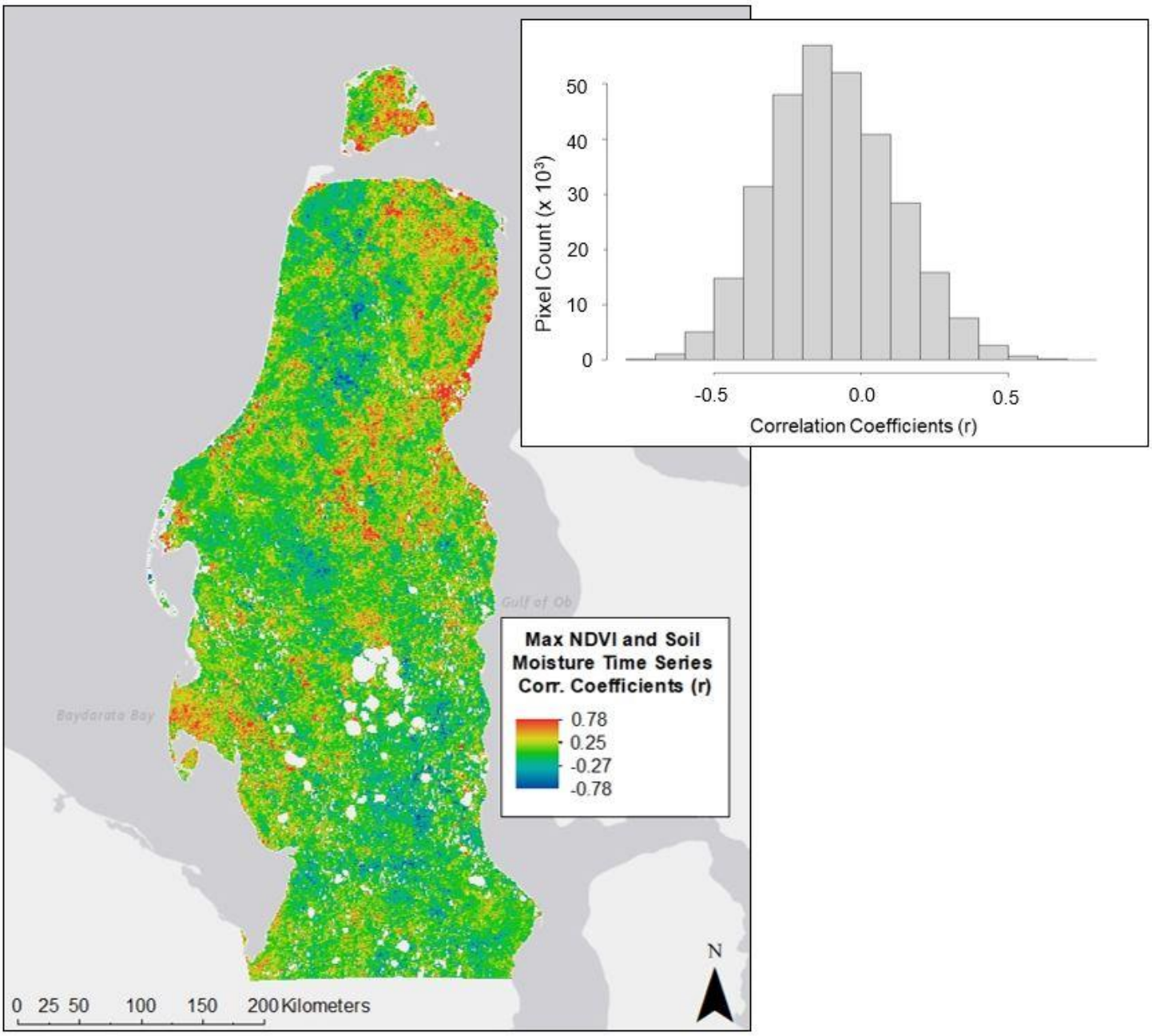

Figure 12. Map of Spearman's correlation coefficients (r) for pixel-wise correlations between linearly detrended Max NDVI and mean growing season soil moisture time series (2001 – 2018). The inset histogram displays the frequency of r values across the Yamal Peninsula.

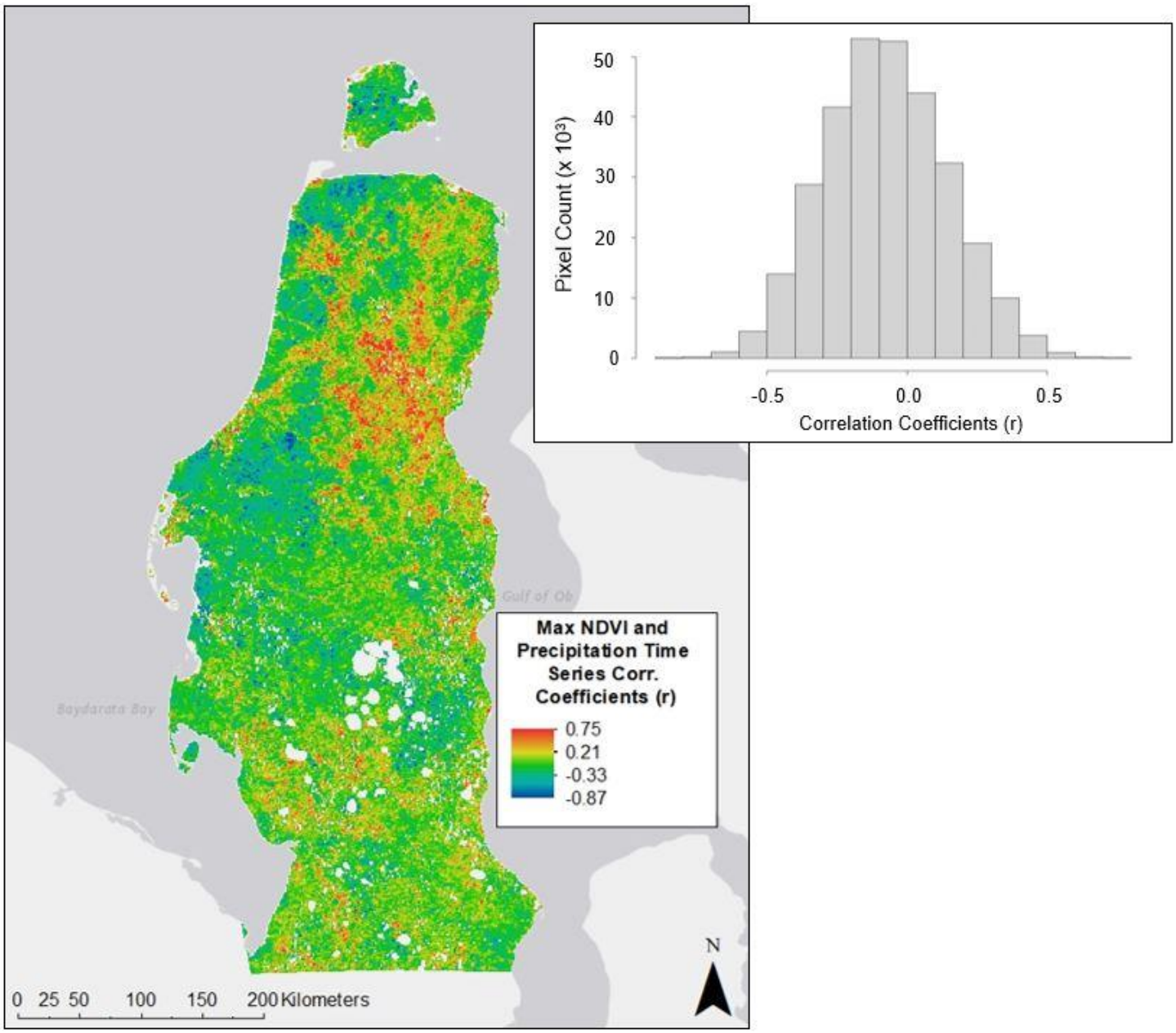

Figure 13. Map of Spearman's correlation coefficients (r) for pixel-wise correlations between linearly detrended Max NDVI and mean growing season precipitation time series (2001 – 2018). The inset histogram displays the frequency of r values across the Yamal Peninsula.

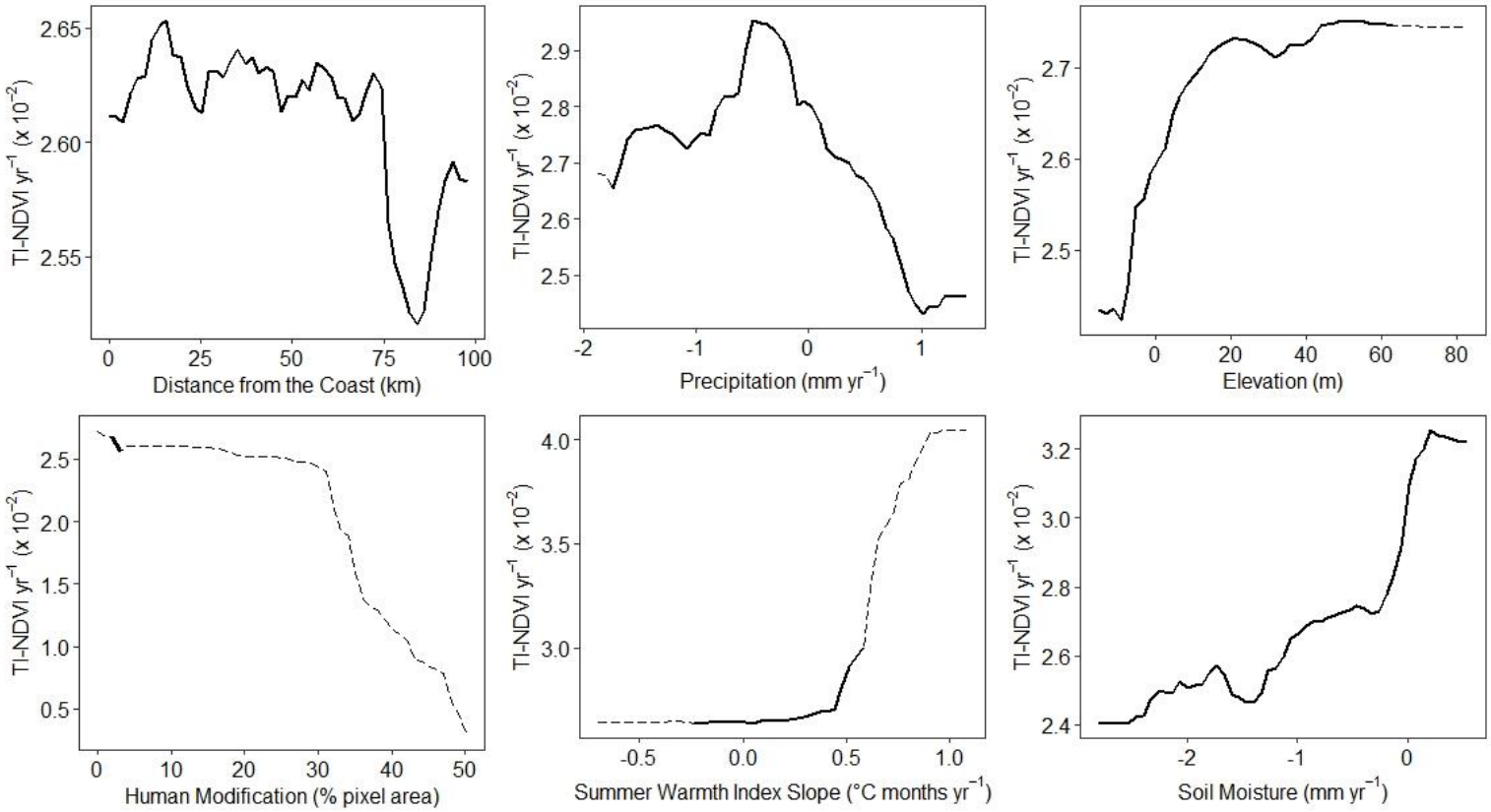

Figure 14. Partial dependence plots for the six most important drivers of TI-NDVI Sen's slope: distance from the coast, mean growing season precipitation Sen's slope, elevation, human modification, Summer Warmth Index (SWI) Sen's slope, and mean growing season soil moisture Sen's slope. Partial dependence plots display the average predicted relationships between TI-NDVI trends and individual drivers across their range of values while still considering the average effects of the other drivers (Goldstein et al., 2014). Dashed lines indicate outlier driver variable values.

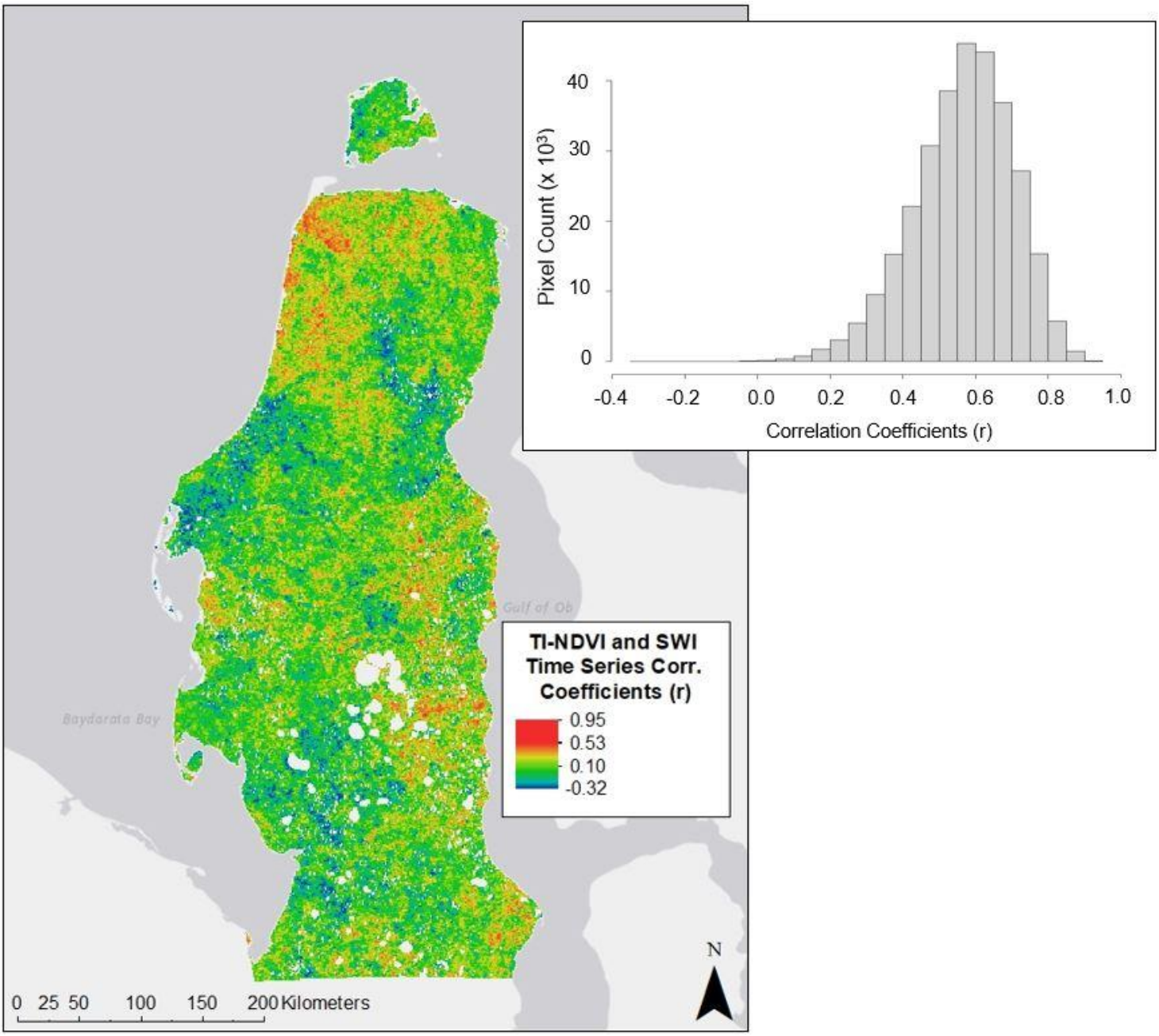

Figure 15. Map of Spearman's correlation coefficients (r) for pixel-wise correlations between linearly detrended TI-NDVI and SWI time series (2001 – 2018). The inset histogram displays the frequency of r values across the Yamal Peninsula.

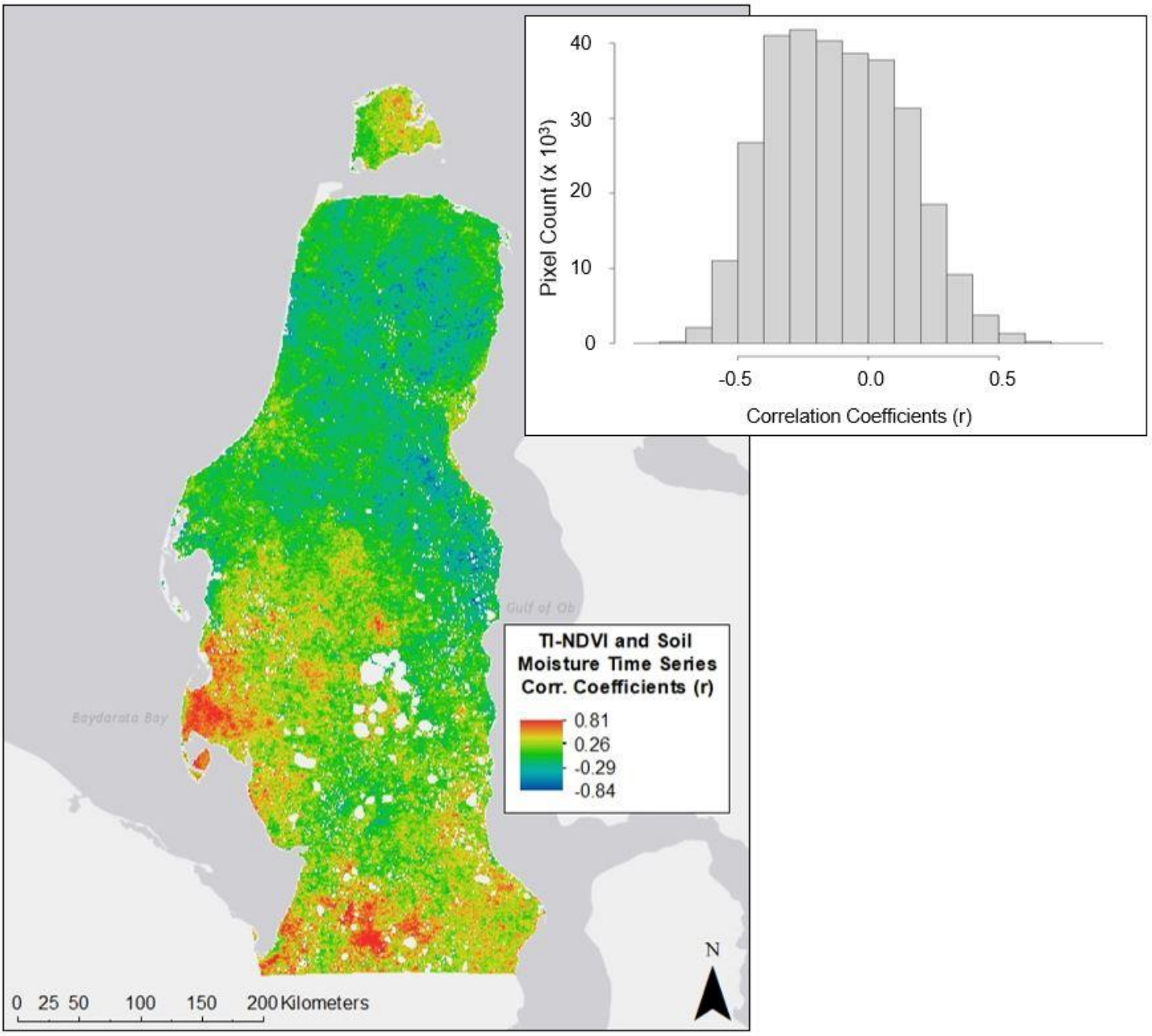

Figure 16. Map of Spearman's correlation coefficients (r) for pixel-wise correlations between linearly detrended TI-NDVI and mean growing season soil moisture time series (2001 – 2018). The inset histogram displays the frequency of r values across the Yamal Peninsula.

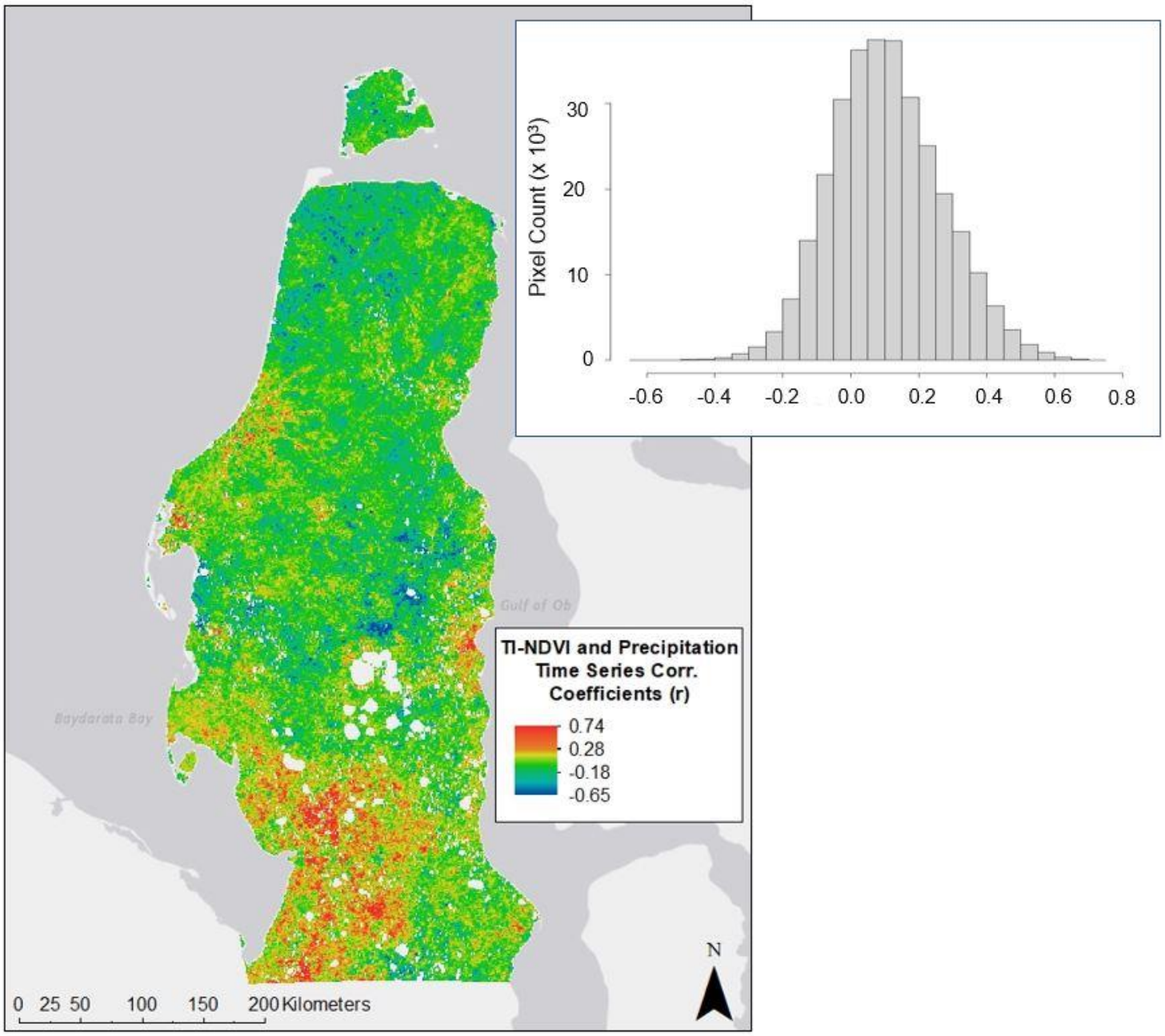

Figure 17. Map of Spearman's correlation coefficients (r) for pixel-wise correlations between linearly detrended TI-NDVI and mean growing season precipitation time series (2001 – 2018). The inset histogram displays the frequency of r values across the Yamal Peninsula.

7.0 References

Abatzoglou, J. T., Dobrowski, S. Z., Parks, S. A., & Hegewisch, K. C. (2018). TerraClimate, a high-resolution global dataset of monthly climate and climatic water balance from 1958–2015. *Scientific Data*, *5*(1), 170191. https://doi.org/10.1038/sdata.2017.191

Bartsch, A., Kumpula, T., Forbes, B. C., & Stammler, F. (2010). Detection of snow surface thawing and refreezing in the Eurasian Arctic with QuikSCAT: Implications for reindeer herding. *Ecological Applications*, *20*(8), 2346–2358. https://doi.org/10.1890/09-1927.1

Berner, L. T., Jantz, P., Tape, K. D., & Goetz, S. J. (2018). Tundra plant above-ground biomass and shrub dominance mapped across the North Slope of Alaska. *Environmental Research Letters*, *13*(3), 035002. https://doi.org/10.1088/1748-9326/aaaa9a

Berner, L. T., Massey, R., Jantz, P., Forbes, B. C., Macias-Fauria, M., Myers-Smith, I., Kumpula, T., Gauthier, G., Andreu-Hayles, L., Gaglioti, B. V., Burns, P., Zetterberg, P., D'Arrigo, R., & Goetz, S. J. (2020). Summer warming explains widespread but not uniform greening in the Arctic tundra biome. *Nature Communications*, *11*(1), 4621. https://doi.org/10.1038/s41467-020-18479-5

Bhatt, U. S., Walker, D. A., Raynolds, M. K., Comiso, J. C., Epstein, H. E., Jia, G., Gens, R., Pinzon, J. E., Tucker, C. J., Tweedie, C. E., & Webber, P. J. (2010). *Circumpolar Arctic Tundra Vegetation Change Is Linked to Sea Ice Decline*. 21.

Bhatt, U., Walker, D., Raynolds, M., Bieniek, P., Epstein, H., Comiso, J., Pinzon, J., Tucker, C., & Polyakov, I. (2013). Recent Declines in Warming and Vegetation Greening Trends over Pan-Arctic Tundra. *Remote Sensing*, *5*(9), 4229–4254. https://doi.org/10.3390/rs5094229

Bhatt, U. S., Walker, D. A., Raynolds, M. K., Walsh, J. E., Bieniek, P. A., Cai, L., Comiso, J. C., Epstein, H. E., Frost, G. V., Gersten, R., Hendricks, A. S., Pinzon, J. E., Stock, L., & Tucker, C. J. (2021). Climate drivers of Arctic tundra variability and change using an indicators framework. *Environmental Research Letters*, *16*(5), 055019. https://doi.org/10.1088/1748-9326/abe676

Bieniek, P. A., Bhatt, U. S., Walker, D. A., Raynolds, M. K., Comiso, J. C., Epstein, H. E., Pinzon, J. E., Tucker, C. J., Thoman, R. L., Tran, H., Mölders, N., Steele, M., Zhang, J., & Ermold, W. (2015). Climate Drivers Linked to Changing Seasonality of Alaska Coastal Tundra Vegetation Productivity. *Earth Interactions*, *19*(19), 1–29. https://doi.org/10.1175/EI-D-15-0013.1

Blok, D., Heijmans, M. M. P. D., Schaepman-Strub, G., Kononov, A. V., Maximov, T. C., & Berendse, F. (2010). Shrub expansion may reduce summer permafrost thaw in Siberian tundra. *Global Change Biology*, *16*(4), 1296–1305. https://doi.org/10.1111/j.1365-2486.2009.02110.x

Borchers, H.W. (2019). pracma: Practical Numerical Math Functions. R package version 2.2.9.

https://CRAN.R-project.org/package=pracma

Breiman, L. (2001). Random Forests. Machine Learning, 45, pp. 5-32.

Cai, L., Lee, H., Westermann, S., & Aas, K. S. (2019). *Projecting Circum-Arctic Excess Ground Ice Melt with a sub-grid representation in the Community Land Model* [Preprint]. Frozen ground/Frozen Ground. https://doi.org/10.5194/tc-2019-230

Campbell, T. K. F., Lantz, T. C., Fraser, R. H., & Hogan, D. (2021). High Arctic Vegetation Change Mediated by Hydrological Conditions. *Ecosystems*, *24*(1), 106–121. https://doi.org/10.1007/s10021-020-00506-7

Didan, K. (2015). MOD13Q1 MODIS/Terra Vegetation Indices 16-Day L3 Global 250m SIN Grid V006 [Data set]. NASA EOSDIS Land Processes DAAC. DOI: 10.5067/MODIS/MOD13Q1.006

Dutrieux, L. P., Bartholomeus, H., Herold, M., & Verbesselt, J. (2012). Relationships between declining summer sea ice, increasing temperatures and changing vegetation in the Siberian Arctic tundra from MODIS time series (2000–11). *Environmental Research Letters*, *7*(4), 044028. https://doi.org/10.1088/1748-9326/7/4/044028

Elmendorf, S. C., Henry, G. H. R., Hollister, R. D., Björk, R. G., Boulanger-Lapointe, N., Cooper, E. J., Cornelissen, J. H. C., Day, T. A., Dorrepaal, E., Elumeeva, T. G., Gill, M., Gould, W. A., Harte, J., Hik, D. S., Hofgaard, A., Johnson, D. R., Johnstone, J. F., Jónsdóttir, I. S., Jorgenson, J. C., … Wipf, S. (2012). Plot-scale evidence of tundra vegetation change and links to recent summer warming. *Nature Climate Change*, *2*(6), 453–457. https://doi.org/10.1038/nclimate1465

Epstein, H. E., Beringer, J., Gould, W. A., Lloyd, A. H., Thompson, C. D., Chapin, F. S., Michaelson, G. J., Ping, C. L., Rupp, T. S., & Walker, D. A. (2004). The nature of spatial transitions in the Arctic. *Journal of Biogeography*, *31*(12), 1917–1933. https://doi.org/10.1111/j.1365-2699.2004.01140.x

Epstein, H. E., Raynolds, M. K., Walker, D. A., Bhatt, U. S., Tucker, C. J., & Pinzon, J. E. (2012). Dynamics of aboveground phytomass of the circumpolar Arctic tundra during the past three decades. *Environmental Research Letters*, *7*(1), 015506. https://doi.org/10.1088/1748-9326/7/1/015506

Epstein, H., Bhatt, U., Raynolds, M., Walker, D., Forbes, B., Phoenix, G., Jia, G. (2018). Tundra Greenness. In: Arctic Report Card: Update for 2018. NOAA, Silver Spring, MD. Retrieved from https://arctic.noaa.gov/Report-Card/Report-Card-2018/ArtMID/7878/ArticleID/777/Tundra-Greenness

Epstein, H. E., Walker, D. A., Frost, G. V., Raynolds, M. K., Bhatt, U., Daanen, R., Forbes, B., Geml, J., Kaärlejarvi, E., Khitun, O., Khomutov, A., Kuss, P., Leibman, M., Matyshak, G., Moskalenko, N., Orekhov, P., Romanovsky, V. E., & Timling, I. (2021). Spatial

patterns of arctic tundra vegetation properties on different soils along the Eurasia Arctic Transect, and insights for a changing Arctic. *Environmental Research Letters*, *16*(1), 014008. https://doi.org/10.1088/1748-9326/abc9e3

European Space Agency (ESA) and Université Catholique de Louvain (UC Louvain). (2010). GlobCover 2009 (Global Land Cover Map). http://due.esrin.esa.int/page_globcover.php.

FAO/IIASA/ISRIC/ISS-CAS/JRC (2012). Harmonized World Soil Database (version 1.2). FAO, Rome, Italy and IIASA, Laxenburg, Austria.

Forbes, B. C. (1999). Land use and climate change on the Yamal Peninsula of north-west Siberia: Some ecological and socio-economic implications. *Polar Research*, *18*(2), 367–373. https://doi.org/10.3402/polar.v18i2.6597

Forbes, B. C., & Kumpula, T. (2009). The Ecological Role and Geography of Reindeer (*Rangifer tarandus*) in Northern Eurasia: Ecology/geography of Eurasian reindeer. *Geography Compass*, *3*(4), 1356–1380. https://doi.org/10.1111/j.1749-8198.2009.00250.x

Forbes, B. C., Stammler, F., Kumpula, T., Meschtyb, N., Pajunen, A., & Kaarlejärvi, E. (2009). High resilience in the Yamal-Nenets social–ecological system, West Siberian Arctic, Russia. *Proceedings of the National Academy of Sciences*, *106*(52), 22041–22048. https://doi.org/10.1073/pnas.0908286106

Fox, J. and Weisberg, S. (2019). An {R} Companion to Applied Regression, Third Edition. Thousand Oaks CA: Sage. URL: https://socialsciences.mcmaster.ca/jfox/Books/Companion/

Frost, G. V., & Epstein, H. E. (2014). Tall shrub and tree expansion in Siberian tundra ecotones since the 1960s. *Global Change Biology*, *20*(4), 1264–1277. https://doi.org/10.1111/gcb.12406

Frost, G. V., Bhatt, U. S., Epstein, H. E., Walker, D. A., Raynolds, M. K., Berner, L. T., Bjerke, J. W., Breen, A. L., Forbes, B. C., Goetz, S. J., Iverson, C. M., Lara, M. J., Macander, M. J., Phoenix, G. K., Rocha, A.V., Salmon, V.G., Thorton, P. E., Tommervik, H., & Wullschleger, S. D. (2019). Tundra Greenness. In: Arctic Report Card: Update for 2019. NOAA, Silver Spring, MD. Retrieved from https://arctic.noaa.gov/Report-Card/Report-Card-2019/ArtMID/7916/ArticleID/838/Tundra-Greenness

Frost, G. V., Bhatt, U. S., Epstein, H. E., Myers-Smith, I., Phoenix, G. K., Berner, L. T., Bjerke, J. W., Forbes, B. C., Goetz, S. J., Kerby, J. T., Macander, M. J., Park, T., Raynolds, M. K., Tommervik, H., and Walker, D. A. (2020). Tundra Greenness. In: Arctic Report Card: Update for 2020. NOAA, Silver Spring, MD. Retrieved from https://arctic.noaa.gov/Report-Card/Report-Card-2020/ArtMID/7975/ArticleID/879/Tundra-Greenness

Gamon, J. A., Huemmrich, K. F., Stone, R. S., & Tweedie, C. E. (2013). Spatial and temporal

variation in primary productivity (NDVI) of coastal Alaskan tundra: Decreased vegetation growth following earlier snowmelt. *Remote Sensing of Environment*, *129*, 144–153. https://doi.org/10.1016/j.rse.2012.10.030

Gazprom. (2021). Yamal. https://www.gazprom.com/projects/yamal/

Goldstein, A., Kapelner, A., Bleich, J., & Pitkin, E. (2014). Peeking Inside the Black Box: Visualizing Statistical Learning with Plots of Individual Conditional Expectation. *ArXiv:1309.6392 [Stat]*. http://arxiv.org/abs/1309.6392

Greenwell, B.M. (2017). pdp: An R Package for Constructing Partial Dependence Plots. The R Journal, 9(1), 421--436. URL: https://journal.r-project.org/archive/2017/RJ-2017-016/index.html.

Hall, D. K., et al. (2016). MODIS/Terra Snow Cover Daily L3 Global 500m Grid. Version 6. Boulder, Colorado USA: NASA National Snow and Ice Data Center Distributed Active Archive Center.

Hijmans, R.J. (2021). terra: Spatial Data Analysis. R package version 1.0-10. https://CRAN.R-project.org/package=terra

IPCC, 2021: *Climate Change 2021: The Physical Science Basis. Contribution of Working Group I to the Sixth Assessment Report of the Intergovernmental Panel on Climate Change* [Masson-Delmotte, V., P. Zhai, A. Pirani, S. L. Connors, C. Péan, S. Berger, N. Caud, Y. Chen, L. Goldfarb, M. I. Gomis, M. Huang, K. Leitzell, E. Lonnoy, J. B.R. Matthews, T. K. Maycock, T. Waterfield, O. Yelekçi, R. Yu and B. Zhou (eds.)]. Cambridge University Press. In Press.

Jia, G. J., Epstein, H. E., & Walker, D. A. (2006). Spatial heterogeneity of tundra vegetation response to recent temperature changes: SPATIAL HETEROGENEITY OF TUNDRA DYNAMICS. *Global Change Biology*, *12*(1), 42–55. https://doi.org/10.1111/j.1365-2486.2005.01079.x

Jin, X.-Y., Jin, H.-J., Iwahana, G., Marchenko, S. S., Luo, D.-L., Li, X.-Y., & Liang, S.-H. (2021). Impacts of climate-induced permafrost degradation on vegetation: A review. *Advances in Climate Change Research*, *12*(1), 29–47. https://doi.org/10.1016/j.accre.2020.07.002

Johnstone, J. F., & Kokelj, S. V. (2009). Environmental Conditions and Vegetation Recovery at Abandoned Drilling Mud Sumps in the Mackenzie Delta Region, Northwest Territories, Canada. *ARCTIC*, *61*(2), 199–211. https://doi.org/10.14430/arctic35

Jorgenson, M. T., Kanevskiy, M., Shur, Y., Moskalenko, N., Brown, D. R. N., Wickland, K., Striegl, R., & Koch, J. (2015). Role of ground ice dynamics and ecological feedbacks in recent ice wedge degradation and stabilization. *Journal of Geophysical Research: Earth Surface*, *120*(11), 2280–2297. https://doi.org/10.1002/2015JF003602

Kennedy, C.M., et al. (2019). Managing the middle: A shift in conservation priorities based on the global human modification gradient. Global Change Biology, 25, pp. 811-826. DOI: https://doi.org/10.1111/gcb.14549

Kuhn, M. (2020). caret: Classification and Regression Training. R package version 6.0-86. https://CRAN.R-project.org/package=caret

Kulkarni, A., & Storch, H. V. (1995). Monte Carlo experiments on the effect of serial correlation on the Mann-Kendall test of trend. *Kurzberichte*, 4.

Kumpula, T., Pajunen, A., Kaarlejarvi, E., Forbes, B. C., Stammler, F. (2011). Land use and land cover change in Arctic Russia: Ecological and social implications of industrial development. *Global Environmental Change*, 21(2), 550-562. https://doi.org/10.1016/j.gloenvcha.2010.12.010

Lantz, T. C. (2017). Vegetation Succession and Environmental Conditions following Catastrophic Lake Drainage in Old Crow Flats, Yukon. *ARCTIC*, *70*(2), 177. https://doi.org/10.14430/arctic4646

Lara, M. J., Nitze, I., Grosse, G., Martin, P., & McGuire, A. D. (2018). Reduced arctic tundra productivity linked with landform and climate change interactions. *Scientific Reports*, *8*(1), 2345. https://doi.org/10.1038/s41598-018-20692-8

Leibman, M. O. (1995). Cryogenic landslides on the Yamal Peninsula, Russia: Preliminary observations. *Permafrost Periglac. Process*. 6, pp. 259-264.

Leibman, M., Khomutov, A., & Kizyakov, A. (2014). Cryogenic Landslides in the West-Siberian Plain of Russia: Classification, Mechanisms, and Landforms. In W. Shan, Y. Guo, F. Wang, H. Marui, & A. Strom (Eds.), *Landslides in Cold Regions in the Context of Climate Change* (pp. 143–162). Springer International Publishing. https://doi.org/10.1007/978-3-319-00867-7_11

Lemenkova, P. (2015). The Vulnerability and Environmental Resilience of Ecosystems in Yamal, Russian Arctic. In *Problems of the Sustainable Development of the Russian Regions. Tyumen, Russia*. Tyumen State Oil and Gas University (TuymGNGU). DOI: 10.6084/m9.figshare.7211645.hal-01986797

Li, B., Heijmans, M. M. P. D., Berendse, F., Blok, D., Maximov, T., & Sass-Klaassen, U. (2016). The role of summer precipitation and summer temperature in establishment and growth of dwarf shrub Betula nana in northeast Siberian tundra. *Polar Biology*, *39*(7), 1245–1255. https://doi.org/10.1007/s00300-015-1847-0

Liaw, A., & Wiener, M. (2002). Classification and Regression by randomForest. R News, 2(3).

Loiko, S., Klimova, N., Kuzmina, D., & Pokrovsky, O. (2020). Lake Drainage in Permafrost Regions Produces Variable Plant Communities of High Biomass and Productivity.

Plants, *9*(7), 867. https://doi.org/10.3390/plants9070867

Macias-Fauria, M., Forbes, B. C., Zetterberg, P., & Kumpula, T. (2012). Eurasian Arctic greening reveals teleconnections and the potential for structurally novel ecosystems. *Nature Climate Change*, *2*(8), 613–618. https://doi.org/10.1038/nclimate1558

Magnússon, R. Í., Limpens, J., Huissteden, J., Kleijn, D., Maximov, T. C., Rotbarth, R., Sass-Klaassen, U., & Heijmans, M. M. P. D. (2020). Rapid Vegetation Succession and Coupled Permafrost Dynamics in Arctic Thaw Ponds in the Siberian Lowland Tundra. *Journal of Geophysical Research: Biogeosciences*, *125*(7). https://doi.org/10.1029/2019JG005618

Magnússon, R. Í., Limpens, J., Kleijn, D., van Huissteden, K., Maximov, T. C., Lobry, S., & Heijmans, M. M. P. D. (2021). Shrub decline and expansion of wetland vegetation revealed by very high resolution land cover change detection in the Siberian lowland tundra. *Science of The Total Environment*, *782*, 146877. https://doi.org/10.1016/j.scitotenv.2021.146877

McLeod, A.I. (2011). Kendall: Kendall rank correlation and Mann-Kendall trend test. R package version 2.2. https://CRAN.R-project.org/package=Kendall

Microsoft Corporation (Microsoft) and Weston, S. (2020). doParallel: Foreach Parallel Adaptor for the 'parallel' Package. R package version 1.0.16. https://CRAN.R-project.org/package=doParallel

Mikola, J., Virtanen, T., Linkosalmi, M., Vähä, E., Nyman, J., Postanogova, O., Räsänen, A., Kotze, D. J., Laurila, T., Juutinen, S., Kondratyev, V., & Aurela, M. (2018). Spatial variation and linkages of soil and vegetation in the Siberian Arctic tundra – coupling field observations with remote sensing data. *Biogeosciences*, *15*(9), 2781–2801. https://doi.org/10.5194/bg-15-2781-2018

Myers-Smith, I. H., Elmendorf, S. C., Beck, P. S. A., Wilmking, M., Hallinger, M., Blok, D., Tape, K. D., Rayback, S. A., Macias-Fauria, M., Forbes, B. C., Speed, J. D. M., Boulanger-Lapointe, N., Rixen, C., Lévesque, E., Schmidt, N. M., Baittinger, C., Trant, A. J., Hermanutz, L., Collier, L. S., … Vellend, M. (2015). Climate sensitivity of shrub growth across the tundra biome. *Nature Climate Change*, *5*(9), 887–891. https://doi.org/10.1038/nclimate2697

Myers-Smith, I. H., Kerby, J. T., Phoenix, G. K., Bjerke, J. W., Epstein, H. E., Assmann, J. J., John, C., Andreu-Hayles, L., Angers-Blondin, S., Beck, P. S. A., Berner, L. T., Bhatt, U. S., Bjorkman, A. D., Blok, D., Bryn, A., Christiansen, C. T., Cornelissen, J. H. C., Cunliffe, A. M., Elmendorf, S. C., … Wipf, S. (2020). Complexity revealed in the greening of the Arctic. *Nature Climate Change*, *10*(2), 106–117. https://doi.org/10.1038/s41558-019-0688-1

Nitze, I., Grosse, G., Jones, B. M., Romanovsky, V. E., & Boike, J. (2018). Remote sensing

quantifies widespread abundance of permafrost region disturbances across the Arctic and Subarctic. *Nature Communications*, *9*(1), 5423. https://doi.org/10.1038/s41467-018-07663-3

Oliveira, S., Oehler, F., San-Miguel-Ayanz, J., Camia, A., & Pereira, J. M. C. (2012). Modeling spatial patterns of fire occurrence in Mediterranean Europe using Multiple Regression and Random Forest. *Forest Ecology and Management*, *275*, 117–129. https://doi.org/10.1016/j.foreco.2012.03.003

Olofsson, J., Oksanen, L., Callaghan, T., Hulme, P. E., Oksanen, T., & Suominen, O. (2009). Herbivores inhibit climate-driven shrub expansion on the tundra: *Global Change Biology*, *15*(11), 2681–2693. https://doi.org/10.1111/j.1365-2486.2009.01935.x

Opala-Owczarek, M., Pirożnikow, E., Owczarek, P., Szymański, W., Luks, B., Kępski, D., Szymanowski, M., Wojtuń, B., & Migała, K. (2018). The influence of abiotic factors on the growth of two vascular plant species (*Saxifraga oppositifolia* and *Salix polaris*) in the High Arctic. *Catena*, 163(2018), 219-232. DOI: 10.1016/j.catena.2017.12.018

Osterkamp, T. E., Jorgenson, M. T., Schuur, E. A. G., Shur, Y. L., Kanevskiy, M. Z., Vogel, J. G., & Tumskoy, V. E. (2009). Physical and ecological changes associated with warming permafrost and thermokarst in Interior Alaska: Physical and Ecological Changes Associated with Thermokarst. *Permafrost and Periglacial Processes*, *20*(3), 235–256. https://doi.org/10.1002/ppp.656

Patakamuri, S.K. and O'Brien, N. (2020). modifiedmk: Modified Versions of Mann Kendall and Spearman's Rho Trend Tests. R package version 1.5.0. https://CRAN.R-project.org/package=modifiedmk

Pearson, R. G., Phillips, S. J., Loranty, M. M., Beck, P. S. A., Damoulas, T., Knight, S. J., & Goetz, S. J. (2013). Shifts in Arctic vegetation and associated feedbacks under climate change. *Nature Climate Change*, *3*(7), 673–677. https://doi.org/10.1038/nclimate1858

Phoenix, G. K., & Bjerke, J. W. (2016). Arctic browning: Extreme events and trends reversing arctic greening. *Global Change Biology*, *22*(9), 2960–2962. https://doi.org/10.1111/gcb.13261

Pohlert, T. (2020). trend: Non-Parametric Trend Tests and Change-Point Detection. R package version 1.1.2. https://CRAN.R-project.org/package=trend

R Core Team (2020). R: A language and environment for statistical computing. R Foundation for Statistical Computing, Vienna, Austria. URL https://www.R-project.org/.

Rabosky, D.L., et al. (2014). BAMMtools: an R package for the analysis of evolutionary dynamics on phylogenetic trees. Methods in Ecology and Evolution 5:701-707.

Raynolds, M. K., Walker, D. A., & Maier, H. A. (2006). NDVI patterns and phytomass

distribution in the circumpolar Arctic. *Remote Sensing of Environment*, *102*(3–4), 271–281. https://doi.org/10.1016/j.rse.2006.02.016

Raynolds, M., Comiso, J., Walker, D., & Verbyla, D. (2008). Relationship between satellite-derived land surface temperatures, arctic vegetation types, and NDVI. *Remote Sensing of Environment*, *112*(4), 1884–1894. https://doi.org/10.1016/j.rse.2007.09.008

Raynolds, M. K., Walker, D. A., Epstein, H. E., Pinzon, J. E., and Tucker C. J. (2012). A new estimate of tundra-biome phytomass from trans-Arctic field data and AVHRR NDVI *Remote Sens. Lett.* 3, 403–11. https://doi.org/10.1080/01431161.2011.609188

Raynolds, M. K., & Walker, D. A. (2009). Effects of deglaciation on circumpolar distribution of arctic vegetation. *Canadian Journal of Remote Sensing*, *35*(2), 12.

Reichle, L. M., Epstein, H. E., Bhatt, U. S., Raynolds, M. K., & Walker, D. A. (n.d.). Spatial Heterogeneity of the Temporal Dynamics of Arctic Tundra Vegetation. *Geophysical Research Letters*, 10.

Revelle, W. (2020). psych: Procedures for Personality and Psychological Research, Northwestern University, Evanston, Illinois, USA, https://CRAN.R-project.org/package=psych Version = 2.0.9.

Rizzoli, P. et al. (2017). Generation and performance assessment of the global TanDEM-X digital elevation model. ISPRS Journal of Photogrammetry and Remote Sensing, 132, pp. 119-139.

Tape, K. D., Hallinger, M., Welker, J. M., & Ruess, R. W. (2012). Landscape Heterogeneity of Shrub Expansion in Arctic Alaska. *Ecosystems*, *15*(5), 711–724. https://doi.org/10.1007/s10021-012-9540-4

United Nations Environment Program (UNEP). (2001). GLOBIO Global methodology for mapping human impacts on the biosphere: the Arctic 2050 scenario and global application. United Nations Environment Programme.

van der Kolk, H.J., Heijmans, M. M. P. D., van Huissteden, J., Pullens, J. W. M., & Berendse, F. (2016). Potential Arctic tundra vegetation shifts in response to changing temperature, precipitation and permafrost thaw. *Biogeosciences*, *13*(22), 6229–6245. https://doi.org/10.5194/bg-13-6229-2016

van Wijk, M. T., Clemmensen, K. E., Shaver, G. R., Williams, M., Callaghan, T. V., Chapin, F. S., Cornelissen, J. H. C., Gough, L., Hobbie, S. E., Jonasson, S., Lee, J. A., Michelsen, A., Press, M. C., Richardson, S. J., & Rueth, H. (2004). Long-term ecosystem level experiments at Toolik Lake, Alaska, and at Abisko, Northern Sweden: Generalizations and differences in ecosystem and plant type responses to global change. *Global Change Biology*, *10*(1), 105–123. https://doi.org/10.1111/j.1365-2486.2003.00719.x

Verdonen, M., Berner, L. T., Forbes, B. C., & Kumpula, T. (2020). Periglacial vegetation dynamics in Arctic Russia: Decadal analysis of tundra regeneration on landslides with time series satellite imagery. *Environmental Research Letters*, *15*(10), 105020. https://doi.org/10.1088/1748-9326/abb500

Walker, D. A., & Everett, K. R. (1987). Road Dust and Its Environmental Impact on Alaskan Taiga and Tundra. *Arctic and Alpine Research*, *19*(4), 479. https://doi.org/10.2307/1551414

Walker, D. A., Webber, P. J., Binnian, E. F., Everett, K. R., Lederer, N. D., Nordstrand, E. A., & Walker, M. D. (1987). Cumulative Impacts of Oil Fields on Northern Alaskan Landscapes. *Science*, *238*(4828), 757–761. https://doi.org/10.1126/science.238.4828.757

Walker, D. A., Auerbach, N. A., & Shippert, M. M. (1995). NDVI, biomass, and landscape evolution of glaciated terrain in northern Alaska. *Polar Record*, *31*(177), 169–178. https://doi.org/10.1017/S003224740001367X

Walker, D. A., Bockheim, J. G., Chapin, F. S., Eugster, W., Nelson, F. E., & Ping, C. L. (2001). Calcium-rich tundra, wildlife, and the Mammoth Steppe. *Quaternary Science Reviews*, 20, 149−163.

Walker, D. A., Gould, W. A., Maier, H. A., & Raynolds, M. K. (2002). The Circumpolar Arctic Vegetation Map: AVHRR-derived base maps, environmental controls, and integrated mapping procedures. *International Journal of Remote Sensing*, *23*(21), 4551–4570. https://doi.org/10.1080/01431160110113854

Walker, D. A., Raynolds, M. K., Daniëls, F. J. A., Einarsson, E., Elvebakk, A., Gould, W. A., Katenin, A. E., Kholod, S. S., Markon, C. J., Melnikov, E. S., Moskalenko, N. G., Talbot, S. S., Yurtsev, B. A. (†), & The other members of the CAVM Team. (2005). The Circumpolar Arctic vegetation map. *Journal of Vegetation Science*, *16*(3), 267–282. https://doi.org/10.1111/j.1654-1103.2005.tb02365.x

Walker, D. A., Leibman, M. O., Epstein, H. E., Forbes, B. C., Bhatt, U. S., Raynolds, M. K., Comiso, J. C., Gubarkov, A. A., Khomutov, A. V., Jia, G. J., Kaarlejärvi, E., Kaplan, J. O., Kumpula, T., Kuss, P., Matyshak, G., Moskalenko, N. G., Orekhov, P., Romanovsky, V. E., Ukraientseva, N. G., & Yu, Q. (2009). Spatial and temporal patterns of greenness on the Yamal Peninsula, Russia: Interactions of ecological and social factors affecting the Arctic normalized difference vegetation index. *Environmental Research Letters*, *4*(4), 045004. https://doi.org/10.1088/1748-9326/4/4/045004

Walker, D.A., Forbes, B. C., Leibman, M. O., Epstein, H. E., Bhatt, U. S., Comiso, J. C., Drozdov, D. S., Gubarkov, A. A., Jia, G. J., Kaarlejärvi, E., Kaplan, J. O., Khomutov, A. V., Kofinas, G. P., Kumpula, T., Kuss, P., Moskalenko, N. G., Meschtyb, N. A., Pajunen, A., Raynolds, M. K., … Yu, Q. (2010). Cumulative Effects of Rapid Land-Cover and Land-Use Changes on the Yamal Peninsula, Russia. In G. Gutman & A. Reissell (Eds.), *Eurasian Arctic Land Cover and Land Use in a Changing Climate* (pp. 207–236).

Springer Netherlands. DOI: 10.1007/978-90-481-9118-5_9

Walker, D.A., & M.K. Raynolds. 2018. Circumpolar Arctic Vegetation, Geobotanical, Physiographic Maps, 1982-2003. ORNL DAAC, Oak Ridge, Tennessee, USA. DOI: 10.3334/ORNLDAAC/1323.

Walker, M. D., Wahren, C. H., Hollister, R. D., Henry, G. H. R., Ahlquist, L. E., Alatalo, J. M., Bret-Harte, M. S., Calef, M. P., Callaghan, T. V., Carroll, A. B., Epstein, H. E., Jonsdottir, I.S., Klein, J.A., Magnusson, B., Molau, U., Oberbauer, S.F., Rewa, S.P., Robinson, C.H., … Wookey, P.A. (2006). Plant community responses to experimental warming across the tundra biome. *Proceedings of the National Academy of Sciences*, 103(5), 1342-1346. DOI: 10.1073/pnas.0503198103.

Wan, Z., Hook, S., Hulley, G. (2015). MOD11A1 MODIS/Terra Land Surface Temperature/Emissivity Daily L3 Global 1km SIN Grid V006 [Data set]. NASA EOSDIS Land Processes DAAC. DOI: 10.5067/MODIS/MOD11A1.006

Yu, Q., Epstein, H. E., Walker, D. A., Frost, G. V., & Forbes, B. C. (2011). Modeling dynamics of tundra plant communities on the Yamal Peninsula, Russia, in response to climate change and grazing pressure. *Environmental Research Letters*, *6*(4), 045505. https://doi.org/10.1088/1748-9326/6/4/045505

Yu, Q., Epstein, H., Engstrom, R., & Walker, D. (2017). Circumpolar arctic tundra biomass and productivity dynamics in response to projected climate change and herbivory. *Global Change Biology*, *23*(9), 3895–3907. https://doi.org/10.1111/gcb.13632

Zhang, T., Osterkamp, T. E., and Stamnes, K. (1997). Effects of Climate on the Active Layer and Permafrost on the North Slope of Alaska, U.S.A. *Permafrost and Periglacial Processes*, *8*, 23.

Zhang, T. (2005). Influence of the seasonal snow cover on the ground thermal regime: An overview. *Reviews of Geophysics*, *43*(4), RG4002. https://doi.org/10.1029/2004RG000157

Chapter 2: Drivers of Spatial and Temporal Heterogeneity in Vegetation Function and Functional Diversity on the Yamal Peninsula, Siberia, Russia

1.0 Abstract

Combinations of seasonal Normalized Difference Vegetation Index (NDVI) metrics that serve as proxies for aboveground biomass and phenology can be used to define Ecosystem Functional Types (EFTs), discrete areas with similar carbon gain dynamics. EFT richness, the number of unique EFTs within a prescribed area, represents the spatial heterogeneity in the seasonal dynamics of primary productivity across a landscape, and can be used as an index of functional diversity. EFTs and EFT richness can be used to gain a more comprehensive understanding of how carbon cycling, climate feedbacks, and ecosystem resistance will be altered under projected warming; however, the potential drivers of EFT distribution and EFT richness have not yet been evaluated for the Arctic. In this study, I used recently developed NDVI-based Arctic EFTs and a suite of climatic, geologic, biologic, and anthropogenic variables to determine the drivers of ecosystem function and functional diversity on the Yamal Peninsula, Siberia, Russia between 2001 and 2018.

EFTs represented spatially distinct functional niches on the Yamal Peninsula that were primarily driven by long-term climate patterns, and their classification probabilities indicated that summer warming, earlier snowmelt, and greater moisture availability could eventually result in functional convergence driven by shifts towards greater aboveground biomass and earlier peak biomass. EFT richness values ranged from 1 to 11 (out of a possible 30), and increased across 30% of the Peninsula (7% significant trends, p-value < 0.05). The spatial and temporal dynamics of EFT richness were primarily driven by landscape heterogeneity and continentality that facilitate variable vegetation responses. These findings demonstrate how Arctic EFTs and EFT richness are useful tools for monitoring shifting carbon gain dynamics in response to multiple driving forces in complex Arctic ecosystems, and how Arctic regions with heterogeneous landscapes shaped by permafrost disturbance regimes could experience increases in functional

diversity under changing climate conditions. Additional research is needed to further disentangle the drivers of vegetation function and functional diversity for the entire Arctic.

2.0 Introduction

Over recent decades, climate change has impacted the seasonal dynamics of Arctic vegetation productivity through shifts in aboveground biomass (Berner et al., 2020; Elmendorf et al., 2012; Frost et al., 2020) and phenology (Post et al., 2016; Prevéy et al., 2019; Zeng et al., 2011). The seasonal dynamics of primary productivity can be monitored using the Normalized Difference Vegetation Index (NDVI), a satellite-derived proxy for primary productivity that is driven by photosynthetically-active green vegetation (Jia et al., 2006; Reichle et al., 2018) and has a strong relationship with aboveground biomass (Berner et al., 2018; Epstein et al., 2012, 2021; Jia et al., 2006; Raynolds et al., 2012). Combinations of seasonal NDVI metrics can be used to define Ecosystem Functional Types (EFTs), discrete areas with similar carbon gain dynamics that may or may not have similar vegetation structure or composition (Alcaraz-Segura et al., 2013; Armstrong et al., in prep.; Cabello et al., 2013; Cazorla et al., 2021; Ivits et al., 2013; Paruelo et al., 2001; Pérez-Hoyos et al., 2014; Villarreal et al., 2018). EFT richness, the number of unique EFTs within a prescribed area, represents the spatial heterogeneity in the seasonal dynamics of primary productivity across a landscape, and can be used as an index of functional diversity (Alcaraz-Segura et al., 2013; Cabello et al., 2013; Cazorla et al., 2021; Paruelo et al., 2001). Similar to structural and compositional diversity, functional diversity provides for ecosystem stability through differential responses to environmental changes or disturbances (Oliver et al., 2015). Evaluating the drivers of spatial and temporal heterogeneity in Arctic ecosystem functioning is necessary to gain a comprehensive understanding of how carbon cycling and climate feedbacks will be altered under projected warming (Fernández et al., 2010; IPCC, 2021; Oliver et al., 2015; Pearson et al., 2013).

NDVI-based EFTs have recently been developed for the circumpolar Arctic tundra as part of a NASA-funded project (Armstrong et al., in prep.), generating the capacity to evaluate Arctic ecosystem functional diversity. The effects of warming on the seasonal dynamics of Arctic vegetation productivity (and therefore EFTs and EFT richness) can be mediated by other climatic (Bhatt et al., 2021; Campbell et al., 2021; Gamon et al., 2013; Li et al., 2016), geologic (Lara et al., 2018; Macias-Fauria et al., 2012; Raynolds et al., 2006; Raynolds and Walker, 2009), biologic (Elmendorf et al., 2012; Epstein et al., 2021), and anthropogenic factors (Forbes, 1999; Johnstone and Kokelj, 2008; Walker et al., 2010); however, the potential drivers of EFT distribution and EFT richness have not yet been evaluated for the Arctic. The goal of this study was to provide the first regional-scale assessment of EFTs and EFT richness in the Arctic by determining the drivers of ecosystem function and functional diversity on the Yamal Peninsula between 2001 and 2018.

The Yamal Peninsula, located in the northwestern Siberian tundra, is representative of other Arctic regions, with its steep climate and geologic gradients, ice-rich continuous permafrost, diverse Arctic vegetation, indigenous reindeer herding, and natural resource (gas) operations (Figures 1 and 2; Walker et al., 2009). I used the EFTs developed by Armstrong et al. (in prep.) and a suite of climatic, geologic, biologic, and anthropogenic drivers (Table 1) to answer the following questions:

1) Which drivers best predicted the spatial distribution of EFTs and EFT richness across the Yamal Peninsula between 2001 and 2018?
2) What were the temporal trends in EFT richness across the Yamal Peninsula between 2001 and 2018?

3) Which drivers best predicted temporal trends in EFT richness between 2001 and 2018?

Climatic drivers included Summer Warmth Index (SWI, sum of April – September monthly mean temperatures > 0 °C), mean growing season (April – September) precipitation and soil moisture (hereafter, precipitation and soil moisture), and snow-free period onset date (first day of the year with 0% snow cover). Geologic drivers included coast distance (a proxy for continentality and sea ice influence), water distance (distance from nearest permanent or seasonal inland water body), elevation, landscape age (time since last glaciation), percent water (percent coverage of permanent and seasonal water bodies), soil texture, and substrate chemistry. The biologic driver considered was the Circumpolar Arctic Vegetation Map physiognomic vegetation unit (Walker and Raynolds 2018). Reindeer herbivory has been found to influence Yamal Peninsula vegetation productivity (Forbes et al., 2009; Olofsson et al., 2009); however, limited quantitative data and exclusion areas prevented the inclusion of reindeer herbivory as a biologic driver in this analysis (Walker et al., 2009). The anthropogenic driver considered was human modification (percent area impacted by natural resource extraction, infrastructure, and settlements) (Kennedy et al., 2019).

Climate patterns were expected to be the primary drivers of EFT distribution, because of their influence on Arctic aboveground biomass accumulation and phenology (Bieniek et al., 2015; Jia et al., 2006; Raynolds et al., 2006). Vegetation unit could be a driver of EFT distribution due to the influence of climate on the distribution of Arctic vegetation types (Raynolds et al., 2008; Walker et al., 2002); however, functioning can vary within vegetation units, and different vegetation units can function similarly (Armstrong et al., in prep.; Euskirchen et al., 2017a, 2017b; Lara et al., 2020). Spatial and temporal variation in EFT richness were

expected to be primarily influenced by landscape-scale variations in geologic, biological, and anthropogenic drivers that result in differential functionality by mediating the effects of climate on vegetation productivity (Bhatt et al., 2021; Campbell et al., 2021; Elmendorf et al., 2012; Epstein et al., 2021; Forbes, 1999; Gamon et al., 2013; Johnstone and Kokelj, 2008; Lara et al., 2018; Li et al., 2016; Macias-Fauria et al., 2012; Raynolds et al., 2006; Raynolds and Walker, 2009; Walker et al., 2010). Last, I expected the strongest positive EFT richness trends to occur where high landscape heterogeneity facilitated differential vegetation responses to climate change (Oliver et al., 2015). Specifically, I expected positive EFT richness trends to be strongest further inland (where there is higher continentality and more topographic variability), where there is a high percentage of seasonal and permanent water bodies present, and where multiple vegetation, soil texture, substrate chemistry, and landscape age classes occurred.

3.0 Methods

3.1 Study Area

A detailed description of the Yamal Peninsula is included in Chapter 1, Section 3.1.

3.2 Data Sources and Pre-Processing

Pre-processing was completed using a combination of Google Earth Engine (GEE), ArcGIS version 10.6 (Redlands, CA), and R version 4.0.0 (R Core Team, 2020). EFTs, EFT richness, human modification, percent water, precipitation, soil moisture, snow-free period onset date, SWI, and water distance datasets were derived from products available through GEE (Table 1). All other datasets were manually uploaded to GEE for pre-processing. Methods were unique to each dataset; however, pre-processing generally required evaluating pixel quality, resampling to a 1-km spatial resolution for EFT analyses) or 1.4-km resolution (for EFT richness analyses), masking (permanent and seasonal water bodies), and developing georeferenced tables for statistical analysis.

When applicable, product developers removed low-quality pixels affected by cloud cover, aerosols, and viewing angle (Abatzoglou et al., 2018; Didan, 2015; FAO et al., 2012; Hall et al., 2016; Kennedy et al., 2019; Rizzoli et al., 2017; Walker and Raynolds, 2018; Wan et al., 2015). Marginal quality pixels were used to supplement the spatial and temporal coverage of EFTs, snow-free period onset date, and SWI datasets when the highest quality data were unavailable. When required, mean aggregation was used to decrease spatial resolution in GEE, while bilinear interpolation or nearest neighbor resampling was used to increase spatial resolution in ArcGIS. The water mask derived by Armstrong et al. (in prep.) for EFT calculation was modified and applied to each finalized dataset. The water mask removed large permanent water bodies (ESA and UC Louvain, 2010) and pixels where 20% or more of the area was covered by permanent or seasonal water bodies (Armstrong et al., in prep.; Pekel et al., 2016). In this study, we reprojected the water mask to a 1-km resolution (for EFT analyses) or 1.4-km resolution (for EFT richness analyses) to ensure that pixels with greater than 20% water coverage were masked after resampling. Last, georeferenced tables were developed using the terra package in R (Hijmans, 2021).

3.3 EFT and EFT Richness Calculation

Yamal Peninsula 2001-2018 EFTs and EFT richness were derived following methods outlined in Armstrong et al. (in prep.) (Figure 3). Ecosystem Functional Attributes (EFAs), or seasonal NDVI metrics, were used to construct EFTs and were calculated using the Moderate Resolution Imaging Spectroradiometer (MODIS) NDVI product (MOD13Q1.006), which uses the equation (NIR – R)/(NIR + R), where NIR equals the spectral reflectance of near-infrared radiation (0.7 - 1.1 μm), and R equals the spectral reflectance of visible red radiation (0.6 - 0.7 μm) (Didan, 2015). For each year, the MODIS growing season data were comprised of multiple 16-day maximum value composites (i.e., images comprised of the maximum NDVI value over a

defined 16-day period) that minimize the effect of clouds, smoke, and viewing angle on reflectance values (Didan, 2015; Raynolds et al., 2008; Verbyla, 2008). The 2001-2018 means of each 16-day composite were used to calculate EFAs for each pixel.

Using spatial principal components analysis and Pearson's correlations, Armstrong et al. (in prep.) determined the three EFAs that captured the greatest variability in the seasonal dynamics of Arctic NDVI: 1) mean growing season (March – October) NDVI, 2) date of the greatest positive NDVI slope (start of season [SOS] date), and 3) date of the maximum NDVI value (max date). Mean NDVI provides information on growing season primary productivity, whereas SOS and max date provide information on phenology. The water mask (described in Section 2.2) was applied to EFA images to minimize the potential effects of water on EFA values and therefore EFT classification. Next, EFAs were divided into classes based on their distributions across the Arctic (quintiles for mean NDVI, and three classes each for SOS and max date), defining 45 (5 x 3 x 3) possible Arctic EFTs. Mean NDVI quintiles correspond to high, mid-high, mid, mid-low, and low mean NDVI values, while SOS and max date categories correspond to early, mid, or late dates. EFTs were numbered by the combination of EFA classes (e.g., EFT 523 represents high mean NDVI [5], mid SOS date [2], and a late season Max NDVI date [3]) (Armstrong et al., in prep.). EFTs were calculated for the entire Arctic tundra (and clipped to the Yamal Peninsula) to facilitate comparison with future analyses of other Arctic regions.

The number of unique EFTs within 6x6 pixel windows (covering a 2 km^2 area) were counted to determine EFT richness values. This window size ensured that all 30 EFTs on the Yamal Peninsula could be counted if present (albeit highly unlikely). Overall 2001-2018 EFT richness was used in spatial analyses, and annual EFT richness was used in temporal analyses.

To calculate annual EFT richness, the previous steps were repeated for each year in the study period. EFA classes used to define the Arctic EFTs remained constant when calculating annual EFT richness to facilitate the interpretation of temporal analyses (Alcaraz-Segura et al., 2013).

3.4 Spatial Analyses

Drivers of EFT distribution

A pairwise Spearman's correlation between continuous drivers found that mean precipitation, mean snow-free period onset date, and mean SWI were highly spatially correlated ($r > 0.75$ or < -0.75). Arctic vegetation is generally limited by summer warmth (Raynolds et al., 2008); therefore, mean precipitation and mean snow-free period onset date were removed from the analysis. All remaining drivers were included as explanatory variables in the spatial analysis (Table 1). Random Forest classification was used to determine which drivers best predicted the spatial distribution of the most common EFTs on the Yamal Peninsula (322, 323, 422, 423, 522, 523). The frequencies of the EFTs were variable; therefore, the input dataset was balanced by randomly sampling each EFT class to have the same number of occurrences. Random Forest classification is a non-parametric machine-learning method that utilizes independent decision tree models of bootstrapped data to rank the predictive power of explanatory variables (Breiman, 2001; Liaw and Wiener, 2002). First, data were randomly partitioned into model training (2/3 of the data) and testing (1/3 of the data) sets. Models constructed using the training data were repeatedly fit to determine the number of randomized drivers considered at each tree node (mtry) that resulted in the highest out-of-bag (OOB) classification accuracy (Berner et al., 2020). Classification accuracy was cross-validated using testing data. Variable importance was determined by the mean decrease in accuracy metric, which measures the decrease in classification accuracy when OOB data for a given variable is permuted in the model (Berner et

al., 2020; Han et al., 2016; Liaw and Wiener, 2002). Last, for the six most important drivers, partial dependence plots were used to evaluate the classification probability of each EFT across the range of driver values while still considering the average effects of the other drivers (Goldstein et al., 2014). The Spearman's correlation was implemented using the psych package in R (Revelle, 2020). Random Forest classification and evaluation with partial dependence plots was completed using the University of Virginia's high-performance computing system (Rivanna) along with the caret (Kuhn, 2020), randomForest (Liaw and Wiener, 2002), doParallel (Microsoft and Weston, 2020), and pdp packages (Greenwell, 2017) in R.

Spatial correlations among EFT richness and continuous drivers

Pairwise Spearman's correlation was used to determine the direction and significance of the spatial relationships among EFT richness and the continuous drivers (Table 1). The overall EFT richness values and means of climatic drivers were included as inputs. All other included variables (coast distance, elevation, human modification, percent water, and water distance) were constant over the study period. The Bonferroni correction was applied to account for multiple comparisons. Spearman's correlations were also run on stratified random samples using 2/3 and 1/2 of the input dataset. Spearman's correlations were implemented using the psych package in R (Revelle, 2020).

Spatial correlations among EFT richness and categorical drivers

Chi-Square (χ^2) Tests of Independence were employed to determine if there were significant spatial associations among EFT richness and categorical drivers (Table 1). Overall EFT richness was divided into high and low categories using the Jenk's natural breaks classification method (implemented using the BAMMtools package in R) (Rabosky et al., 2014).

Chi-Square Tests of Independence were also run on stratified random samples using 2/3 and 1/2 of the input datasets. The χ^2 test statistics and residuals were compared to determine the direction and significance of the spatial associations.

3.5 Temporal Analysis

EFT richness and climatic driver trends

Pixel-scale monotonic trends in EFT richness and climatic drivers between 2001 and 2018 were detected using Mann-Kendall trend tests. Pixels with 15+ years of data were included in the analyses, and time series residuals were tested for lag-1 serial autocorrelation using the Durbin-Watson test. Pre-whitened Mann-Kendall trend tests were also run to verify that pixels with significant serial autocorrelation did not affect trend significance (Kulkarni and von Storch, 1995). Non-parametric Sen's slope estimation was used to determine the direction and magnitude of EFT richness and climatic driver trends. Trend detection analyses were completed using the car (Fox and Weisberg, 2019), Kendall (McLeod, 2011), modifiedmk (Patakamuri and O'Brien, 2020), and trend packages (Pohlert, 2020) in R.

Drivers of EFT richness trends

Random Forest regression was used to determine the most important drivers (i.e., the best predictors) of EFT richness trends (Sen's slopes). EFT richness Sen's slopes = 0.000 were excluded from the analysis. All drivers were included as explanatory variables in the model, including the Sen's slopes of climatic drivers (Table 1). A pairwise Spearman's correlation was used to confirm that multicollinearity ($r > 0.75$ or < -0.75) was not present among the continuous drivers (Berner et al., 2020; Oliveira et al., 2012). The Random Forest regression algorithm and procedure is similar to that described for Random Forest classification in Section 2.4; however, the division of data into training and testing sets was not required (Cutler et al., 2007; Oliveira et

al., 2012). Prediction accuracy was determined by the OOB mean square error (MSE), and variable importance was assessed with the mean decrease in accuracy metric (% IncMSE), which measures the decrease in prediction accuracy when the OOB data for a given driver is permuted in the model (Liaw and Wiener, 2002; Oliveira et al., 2012).

4.0 Results

4.1 Spatial Analyses

Drivers of EFT distribution

Thirty of the 45 Arctic tundra EFTs were present on the Yamal Peninsula. Six EFTs (322, 323, 422, 423, 522, 523) with mid- to high mean NDVI, mid SOS dates, and mid to late season max dates covered > 99% of the Peninsula (Figure 4). The most common EFT was 423, which corresponds to mid-high mean NDVI, a mid SOS date, and a late season max date. The least common of the 6 EFTs was 322, which corresponds to a mid-mean NDVI, a mid SOS date, and a mid max date.

The Random Forest classification model had an overall accuracy of 48%; however, the balanced classification accuracy was 68% for EFT 322, 72% for EFT 323, 67% for EFT 422, 65% for EFT 423, 72% for EFT 522, and 71% for EFT 523. The six most important predictors of EFT distribution were mean SWI, mean soil moisture, coast distance, human modification, elevation, and percent water (Figure 5). Mean SWI exhibited strong correlations with mean precipitation ($r = 0.89$) and mean snow-free period onset date ($r = -0.85$); therefore, mean precipitation and mean snow-free period onset date were also important predictors of EFT distribution. The presence of each EFT was influenced by a unique combination of driver conditions; however, EFTs with the same mean NDVI and max date classifications had similar relationships with some drivers (Figure 6). EFTs with mid- mean NDVI (322 and 323) most

often occurred where mean SWI and precipitation were lower, where snowmelt occurred later, and where human modification did not exceed 2.5% of the pixel area. EFTs with mid-high mean NDVI (422 and 423) most often occurred where mean soil moisture was lower. EFTs with high mean NDVI (522 and 523) most often occurred where mean SWI, mean precipitation, and mean soil moisture were higher; where snowmelt occurred earlier; closer to the coast; at low elevations; and where percent water was lower. EFTs with mid- max dates (322, 422, and 522) most often occurred at low elevations associated with inland drainages, whereas EFTs with late max dates (323, 423, and 523) most often occurred closer to the coast and where percent water was lower.

Spatial correlations among EFT richness and continuous drivers

Overall EFT richness values ranged from 1 to 11 (out of a possible 30) across the Yamal Peninsula (Figure 7). EFT richness values of 2 and 3 were the most common (29.8% and 32.0% of the Peninsula, respectively), and values between 6 and 11 were rare (3.3% of the Peninsula). EFT richness exhibited significant (p-value < 0.05) spatial correlations with all of the continuous drivers (Figure 8). The strongest correlations were with percent water (r = 0.57) and water distance (r = -0.56, Figure 9). Mean snow-free period onset date exhibited the strongest correlation with EFT richness of the climatic drivers (r = -0.44, Figure 10), indicating that EFT richness was higher where snow melt occurred earlier. EFT richness was also positively correlated with mean precipitation (r = 0.35), mean SWI (r = 0.24), human modification (r = 0.22), coast distance (r = 0.06) and mean soil moisture (r = 0.01), but negatively correlated with elevation (r = -0.27). Among the continuous drivers, notable correlations were present between mean SWI and mean precipitation (r = 0.90), mean SWI and mean snow-free period onset date (r = -0.83), mean precipitation and mean snow-free period onset date (r = -0.86), mean soil

moisture and coast distance (r = -0.73), as well as coast distance and elevation (r = 0.65). In addition to being negatively correlated with each other (r = -0.75), water distance and percent water exhibited opposing relationships with elevation (r = 0.44 and -0.43, respectively). Similar to EFT richness, human modification was negatively correlated with mean snow-free period onset date (r = -0.46) and positively correlated with both mean precipitation and mean SWI (r = 0.46 and 0.35, respectively). Results were similar for analyses run on stratified random samples using 2/3 and 1/2 of the input dataset.

Spatial correlations among EFT richness and categorical drivers

Overall EFT richness had significant spatial associations with all of the categorical drivers (p-value < 0.05). The association with vegetation unit was the strongest (χ^2 = 6,759), followed by substrate chemistry (χ^2 = 2,269), landscape age (χ^2 = 584), and soil texture (χ^2 = 295, Table 2). High EFT richness (4 – 11) was associated with erect shrub and wetland vegetation (a combination of sedges, mosses, and erect shrubs) (Raynolds et al., 2006); acidic and saline substrates; younger (~25,000 years old) and recently disturbed landscapes (~1,000 years old); as well as clay loam, loam, sand, and sandy loam soils. Low EFT richness (1 – 3) was associated with graminoid and prostrate shrub vegetation, circumneutral substrates, older landscapes (~70,000 years old), and silt loam soils.

4.2 Temporal Analysis

EFT richness and climatic driver trends

The direction and magnitude of 2001-2018 EFT richness trends were heterogeneous across the Yamal Peninsula (Figure 11). There was no trend (Sen's slope = 0.000, p-value > 0.05) in EFT richness across a majority of the Peninsula (67.1%). However, 30.0% of pixels exhibited positive EFT richness trends, 7.0% of which were significant (p-value ≤ 0.05) and

2.9% of pixels exhibited a negative EFT richness trend (0.3% significant). EFT richness Sen's slopes ranged from -0.400 to 0.620 yr^{-1}, with the mode between -0.100 and 0.000 yr^{-1}. EFT richness Sen's slopes below -0.107 yr^{-1} and greater than 0.178 yr^{-1} were outliers.

The direction and magnitude of climatic driver trends were also heterogeneous (Figure 12). SWI trends were positive across 83.1% of the Peninsula (1.3% significant), while precipitation trends were positive across 50.9% (no significant trends). Generally, positive precipitation trends were stronger where SWI increased (r = 0.46). Snow-free period onset date trends were negative across 85.0% of the Peninsula (4.1% significant), indicating trends toward earlier snow melt. Negative snow-free period onset date trends were stronger where SWI increased (r = -0.44). Soil moisture trends were negative across 85.0% of the Peninsula (3.8% significant) and were less negative where SWI increased (r = 0.43).

Drivers of EFT richness trends

The EFT richness Random Forest regression model explained 51% of EFT richness Sen's slope variance. The six most important drivers of EFT richness trends were coast distance, elevation, human modification, precipitation trends, summer warmth trends, and water distance (Figure 13). On average, positive EFT richness trends were stronger further inland, where human modification was greater, where precipitation increased, and where SWI increased (Figure 14). Positive EFT richness trends were also stronger at lower elevations and closer to inland water bodies.

5.0 Discussion

5.1. Spatial Drivers of EFT Distribution

The use of Arctic tundra EFTs based on seasonal vegetation productivity dynamics allowed for the characterization of functional variability across the Yamal Peninsula. Although

30 of the 45 EFTs were present, 6 EFTs distinguished by varying mean NDVI values and max dates (322, 323, 422, 423, 522, 523) covered more than 99% of the Peninsula. Each of these EFTs were most likely to occur under a unique set of driver conditions, indicating the presence of distinct functional niches. The occurrence of each EFT was best predicted by climatic drivers (mean SWI, mean precipitation, mean snow-free period onset date, and mean soil moisture), and patterns emerged when EFTs grouped by similar mean NDVI and max classes were compared.

EFTs with high mean NDVI (522 and 523) occurred where summers were warmer, precipitation and soil moisture were higher, and where snowmelt occurred earlier. Conversely, EFTs with mid- mean NDVI (322 and 323) occurred where summers were cooler, precipitation was lower, and snowmelt occurred later, and EFTs with mid-high mean NDVI (422 and 423) occurred where soil moisture was lower. These findings are consistent with previous research that found aboveground biomass was higher where Arctic vegetation growth was not limited by low summer temperatures, low water availability, and/or shorter growing seasons due to prolonged snow cover (Elmendorf et al., 2012; Epstein et al. 2021; Jia et al., 2006; Myers-Smith et al., 2015; Raynolds et al., 2006). EFT-climate driver relationships show how variable climate conditions facilitated functional heterogeneity on the Yamal Peninsula; however, observed changes in SWI, precipitation, the timing of snowmelt, and soil moisture could eventually alter long-term climate patterns. Summer warming, earlier snow melt, and increased water availability could cause shifts in functionality and the loss of less common EFTs (322 and 422), which could decrease ecosystem resistance and diversity in ecosystem services (Cazorla et al., 2021; Manning et al., 2018; Oliver et al., 2015).

Although infrastructure and settlements are largely confined to areas surrounding gas operations on the Yamal Peninsula, human modification was an important driver of EFT

distribution. EFTs with the lowest mean NDVI (322 and 323) were most likely to occur where human modification was limited, whereas human modification had mixed effects on EFTs with higher mean NDVI (422, 423, 522, and 523). Human modification could have a positive relationship with EFTs characterized by mid-high and high mean NDVI (422 and 523), because human modification was greater where climate conditions favored these EFTs. However, re-vegetated off-road vehicle tracks near Yamal Peninsula gas fields and settlements have been found to have higher aboveground biomass than surrounding undisturbed areas approximately 20 years after revegetation (Forbes et al., 2009).

Geologic drivers (coast distance, elevation, and percent water) also influenced EFT distribution. EFTs with mid-season max dates (322, 422, and 522) occurred at low elevations, whereas EFTs with late season max dates (323, 423, and 523) occurred closer to the coast and where percent water was lower (i.e., where fewer water bodies were present). Elevation is generally lower closer to the coast on the Yamal Peninsula; however, low elevation landforms (drainages, landslide depressions, ice-wedge troughs, and drained thermokarst lakes) are present inland where summer temperatures are higher. Although not detectable at the 1-km spatial resolution used in this analysis, these landforms can have higher soil moisture than surrounding areas (Walker et al., 2009), which in conjunction with warmer temperatures may have facilitated peak aboveground biomass earlier in the growing season (May et al., 2020). Later peak aboveground biomass seemed to occur where either temperature or soil moisture conditions were not optimal. Summer temperatures were lower closer to the coastline due to the influence of sea ice (Bhatt et al., 2010) and maritime air flow (Bhatt et al., 2021), and areas with fewer water bodies generally have lower soil moisture (Raynolds et al., 2006) and occur at higher elevations (where soil moisture is lower) on the Yamal Peninsula. If coastal temperatures on the Yamal

Peninsula rise, decreases in EFTs with later max dates (323, 423, and 523) could occur; however, the draining of coastal thermokarst lakes (Nitze et al., 2018) could limit shifts towards earlier peak aboveground biomass by decreasing percent water and soil moisture.

5.2 Spatial Drivers of EFT Richness

Calculating EFT richness at a 1.4-km resolution allowed for the evaluation of functional diversity patterns across the Yamal Peninsula. EFT richness was generally higher in the south and values ranged from 1 to 11, with 2 and 3 occurring the most frequently. Of the continuous drivers considered, percent water and water distance had the strongest spatial relationships with EFT richness. The occurrence of higher EFT richness where lakes and drainages were more abundant was likely due to the landscape heterogeneity in these areas that allows for micro-habitats distinguished by fine-scale differences in temperature, soil conditions, and topography (Oliver et al., 2015; Raynolds et al., 2006, 2008).

The occurrence of higher EFT richness where snow melted earlier, where precipitation was higher, and where summers were warmer (primarily in the southern region of the Peninsula) was possibly related to the north-south gradients in percent water and water distance. These conditions also facilitate higher species richness (Billings, 1987; Walker et al., 2019) and permafrost disturbances on the Yamal Peninsula (e.g., thermokarst lake formation/draining, ice-wedge degradation, landslides, erosion) that increase landscape heterogeneity (Ardelean et al., 2020; Leibman et al., 2014; Nitze et al., 2018; Verdonen et al., 2020; Walker et al., 2009; Zhang, 2005). Further, vegetation less limited by summer temperature, growing season length (influenced by the timing of snow melt), and precipitation could exhibit more variable growth and phenology in response to landscape conditions (Bieniek et al. 2015; Billings, 1987; Elmendorf et al., 2012; Keenan and Riley, 2018). *In situ* observations and/or high-resolution

imagery that can detect changes in fine-scale (< 1-km) conditions (e.g., temperature, soil moisture, topography, species richness, extent of permafrost degradation) are needed to verify their effects on the spatial distribution of EFT richness across the Yamal Peninsula. Although fine-scale variability cannot be resolved at the 1.4-km resolution used here, these results suggest that the percent water and water distance metrics may be useful proxies for remotely capturing landscape heterogeneity at coarser resolutions (Lara et al., 2020).

Of the categorical drivers considered, vegetation type had the strongest spatial association with functional diversity. While each vegetation unit on the Yamal Peninsula (erect shrub, graminoid, prostrate shrub, and wetland) is characterized by multiple species, EFT richness was higher in erect shrub and wetland vegetation units. Both erect shrub and wetland vegetation units occurred closer to water bodies and where percent water was high, whereas graminoid and prostrate shrub units occurred further from water bodies and where percent water was low (results not shown), indicating that the landscape heterogeneity associated with lakes and drainages likely drove higher functional diversity within erect shrub and wetland vegetation units. However, there are three other potential explanations for the higher variability in aboveground biomass and phenology in these vegetation units: 1) higher vascular species richness in the southern region where these units are dominant (Walker et al., 2019), 2) variable climate sensitivity of erect shrubs (also present in some wetlands) (Myers-Smith et al., 2015; Raynolds et al., 2006), and 3) reindeer grazing of deciduous shrubs (Olofsson et al., 2009; Yu et al., 2011). Therefore, the variability in aboveground biomass accumulation and phenology within erect shrub and wetland vegetation units may demonstrate how functional diversity can be independent of compositional or structural diversity, but additional research would be needed to confirm this.

Substrate chemistry, landscape age, and soil texture also exhibited significant spatial associations with EFT richness. Circumneutral substrates with higher nutrient availability generally support greater vegetation diversity in the Arctic (Raynolds et al., 2006; Walker et al., 2001). However, acidic and saline substrates with lower nutrient availability were associated with high EFT richness on the Yamal Peninsula. The high EFT richness on acidic substrates could have been driven by an abundance of acidophilic shrub species (Raynolds et al., 2006; Walker et al., 2001), and the high EFT richness on saline substrates (associated with floodplains and marshes) could have been driven by landscape heterogeneity (Moskovchenko et al., 2017). High EFT richness on younger and recently disturbed landscapes that have been less developed by erosion, peat accumulation, and vegetation succession was also likely facilitated by landscape heterogeneity (Walker et al., 1995). Of the five soil texture classes present on the Yamal Peninsula, silt loam and sandy loam drove the significant spatial association between EFT richness and soil texture. Again, EFT richness was unexpectedly higher where nutrient availability was likely lower (on sandy loam soils) than where nutrient availability was likely higher (on silty loam soils). The concentration of sandy loam soils along drainages (Figure 2) could have resulted in the association with high EFT richness.

5.3. Temporal Drivers of EFT Richness

The six drivers that best predicted EFT richness trends were a combination of geologic (coast distance, elevation, and water distance), anthropogenic (human modification), and climatic drivers (precipitation trends and SWI trends). The most important driver, coast distance, captured coastal-inland gradients in continentality and topographic variability on the Yamal Peninsula. Stronger positive EFT richness trends further inland indicate that greater seasonal temperature fluctuations and landscape heterogeneity facilitated increases in functional diversity, particularly in areas with low-elevation inland drainages, landslide depressions, degraded ice-wedge troughs,

and/or drained thermokarst lake basins. Decreasing continentality across the Arctic due to melting sea ice (Bhatt et al., 2021) could eventually reverse the positive EFT richness trends on the Yamal Peninsula. However, inland topographic variability along with increasing precipitation and SWI that facilitates permafrost disturbances and the formation of inland low-elevation landforms could mitigate the effect of decreasing continentality on functional diversity (Ardelean et al., 2020; Becker et al., 2016; Leibman et al., 2014; Jorgenson et al., 2015; Walker et al., 2009). Vegetation succession that occurs in landslide depressions, ice-wedge troughs, and drained thermokarst lakes likely contributed to the stronger positive EFT richness trends at lower inland elevations (Jorgenson et al., 2015; Lantz, 2017; Loiko et al., 2020; Walker et al., 2009). Additionally, landslides often occur along the banks of lakes and drainages, and human modification has been found to exacerbate permafrost degradation on the Yamal Peninsula (Ardelean et al., 2020).

Although positive EFT richness trends were strongest where SWI increased, SWI increases exceeding 0.2 °C months yr^{-1} (3.6 °C months increase over 18-year study period) exhibited a negative relationship with positive EFT richness trends. Summer warming exceeding this threshold may have weakened positive EFT richness trends by causing shifts towards higher aboveground biomass, earlier SOS dates, and earlier max dates (Elmendorf et al., 2012; Post et al., 2016; Prevéy et al., 2019; Walker et al., 2006). Increases in shrub and graminoid aboveground biomass have been linked to warming (Elmendorf et al., 2012; Walker et al., 2006), and warming has been found to advance the phenology of Arctic vegetation species that flower later in the growing season more than those that flower earlier (Prevéy et al., 2019). Reindeer grazing on the Yamal Peninsula could maintain functional diversity by limiting aboveground biomass increases (Olofsson et al., 2009; Yu et al., 2011); however, phenological convergence

towards earlier SOS and max dates could result in a trophic mismatch that would negatively impact reindeer (Kerby and Post, 2013; Post et al., 2008). Future research is needed to better understand the interacting effects of warming and herbivory on Arctic vegetation in order to better predict shifts in aboveground biomass and the timing of resource availability for reindeer.

5.4. Summary and Conclusions

This study demonstrates the usefulness of Arctic EFTs for identifying distinct functional niches and evaluating both the spatial and temporal drivers of functional diversity. EFT distribution was primarily influenced by long-term climate patterns, while the spatial and temporal dynamics of EFT richness were primarily driven by landscape heterogeneity and continentality that facilitate variable vegetation responses. Warming, earlier snowmelt, and greater moisture availability could eventually result in functional convergence driven by shifts towards higher aboveground biomass and earlier max dates on the Yamal Peninsula (and potentially elsewhere in the Arctic), thereby reducing ecosystem resistance (Cazorla et al., 2021). These shifts could be mitigated by reductions in soil moisture following the draining of thermokarst lakes (Nitze et al., 2018). Additionally, potential decreases in EFT richness due to decreasing continentality (Bhatt et al., 2021) could be offset by inland topographic variability and a climate-induced increase in permafrost disturbances that help maintain landscape heterogeneity (Ardelean et al., 2020; Becker et al., 2016; Jorgenson et al., 2015; Loiko et al., 2020; Walker et al., 2009). However, SWI increases exceeding a 0.2 °C months yr^{-1} threshold may facilitate increased aboveground biomass and advanced phenology that weaken positive EFT richness trends (Elmendorf et al., 2012; Post et al., 2016; Prevéy et al., 2019; Walker et al., 2006). At existing levels, human modification on the Yamal Peninsula had mixed effects on EFT distribution and positive effects on EFT richness, but extensive vegetation removal would be expected to reduce functional diversity. Overall, I found that Arctic EFTs and EFT richness are

useful tools for monitoring shifting carbon gain dynamics in response to multiple driving forces in complex Arctic ecosystems, and that Arctic regions with heterogeneous landscapes shaped by permafrost disturbance regimes are more likely to experience increases in functional diversity under changing climate conditions. Future research utilizing high-resolution imagery that can capture fine-scale landscape features, *in situ* species richness measurements, and/or herbivory data is needed to further disentangle the drivers of Arctic functioning and functional diversity.

6.0 Figures

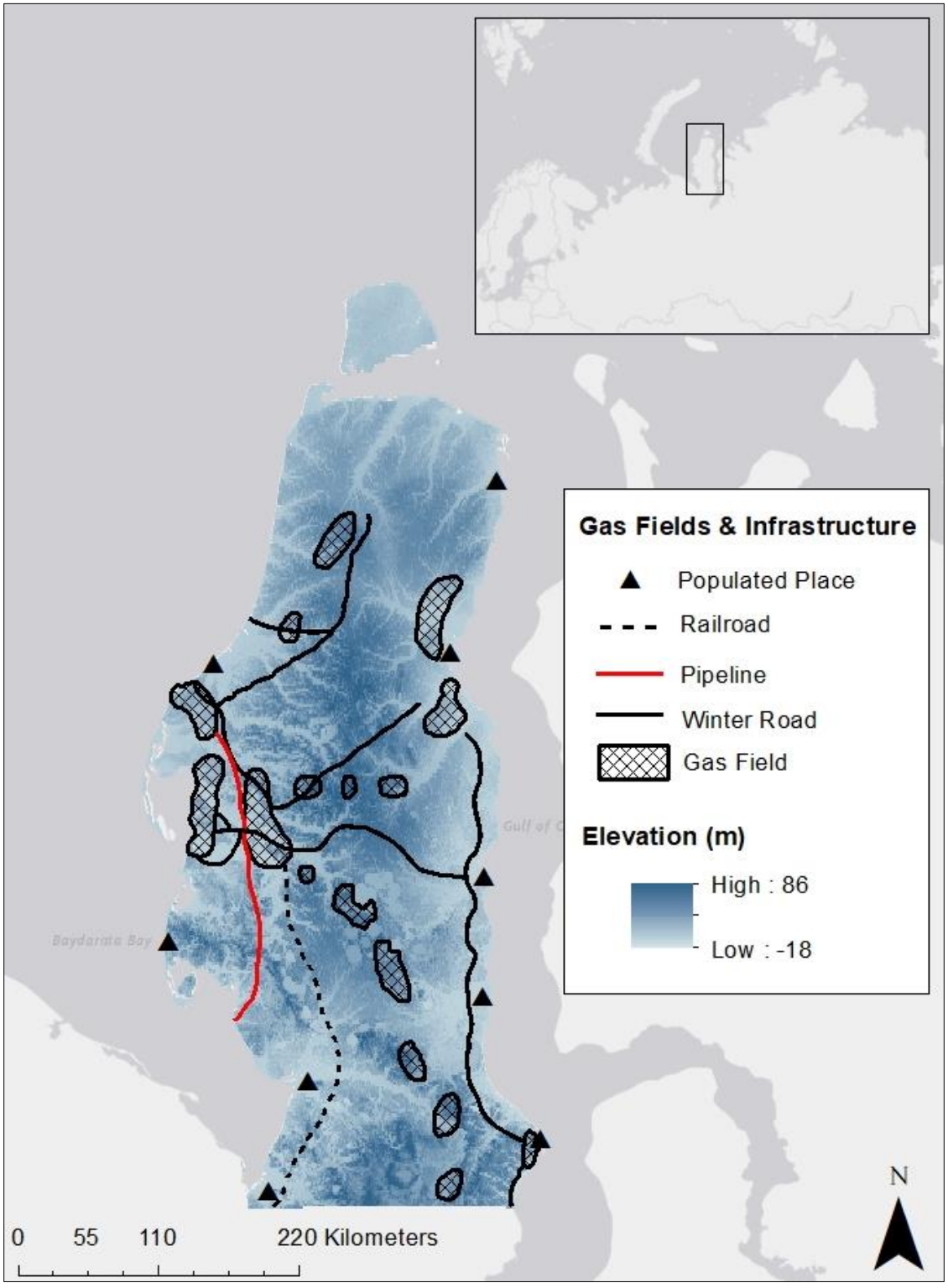

Figure 1. The Yamal Peninsula with elevation (m above sea level) and locations of population centers, infrastructure, and gas fields (adapted from Forbes 1999 and Gazprom 2021). The inset map shows the location of the Yamal Peninsula (outlined by the black box).

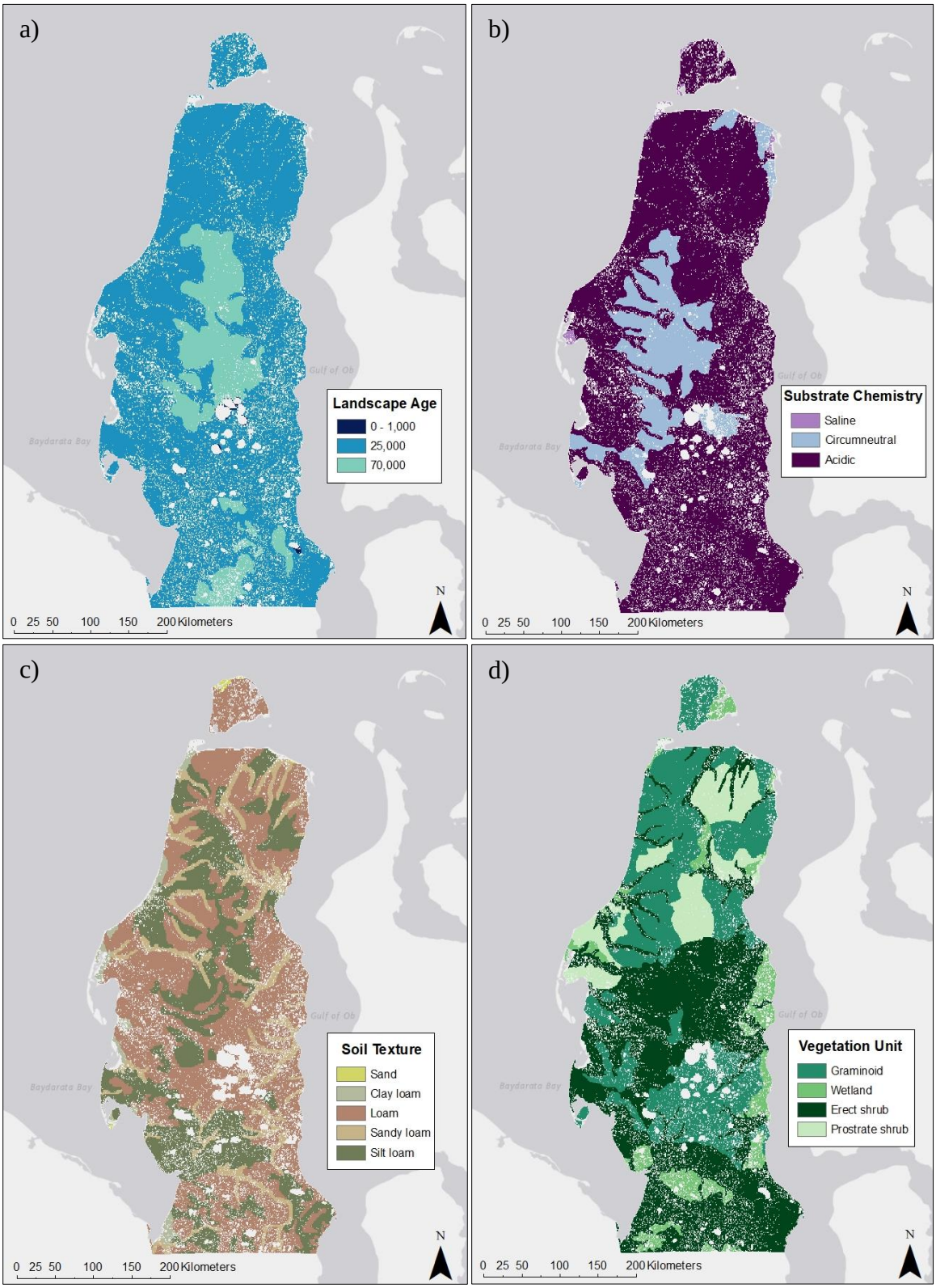

Figure 2. Yamal Peninsula (a) landscape age, or time since last glaciation, (b) substrate chemistry, (c) soil texture, and (d) physiognomic vegetation unit representing the dominant vegetation type. Permanent surface water bodies and pixels with > 20% water coverage are masked.

Table 1. Datasets included in the analyses and their respective types, years collected, native spatial resolutions, and sources.

Data Type	Year(s) Collected	Dataset(s)	Native Resolution	Source
Continuous	NA	Distance from the Coast	1 kilometer	Circumpolar Arctic Vegetation Map
	1984-2019	Distance from Inland Waterbodies	250 meters	Water Mask derived from GlobCover Land Cover and Joint Research Center (JRC) Global Surface Water Map
	2010 - 2015	Elevation	90 meters	TanDEM-X 90m Digital Elevation Model
	2014, 2016	Human Modification	1 kilometer	Conservation Science Partners
	2000-2019	EFTs	250 meters	Terra MODIS Vegetation Indices (MOD13Q1.006)
	1958-2018	Mean Growing Season Precipitation and Soil Moisture	2.5 arc minutes	TerraClimate: Monthly Climate and Climatic Water Balance for Global Terrestrial Surfaces, University of Idaho
	1984-2019	Percent Water in Pixel (0 - 20%)	250 meters	Water Mask derived from GlobCover Land Cover and Joint Research Center (JRC) Global Surface Water Map
	2000-2019	Snow-Free Period Onset	500 meters	Terra MODIS Snow Cover (MOD10A1.006)
	2000-2019	Summer Warmth Index	1 kilometer	Terra MODIS Land Surface Temperature and Emissivity (MOD11A1.006)
Categorical	2009	Landscape Age	1 kilometer	Circumpolar Arctic Vegetation Map
	2003	Physiognomic Vegetation Unit	1 kilometer	Circumpolar Arctic Vegetation Map
	1971 - 2010	Soil Texture	1 kilometer	Harmonized World Soil Database
	2003	Substrate Chemistry	1 kilometer	Circumpolar Arctic Vegetation Map

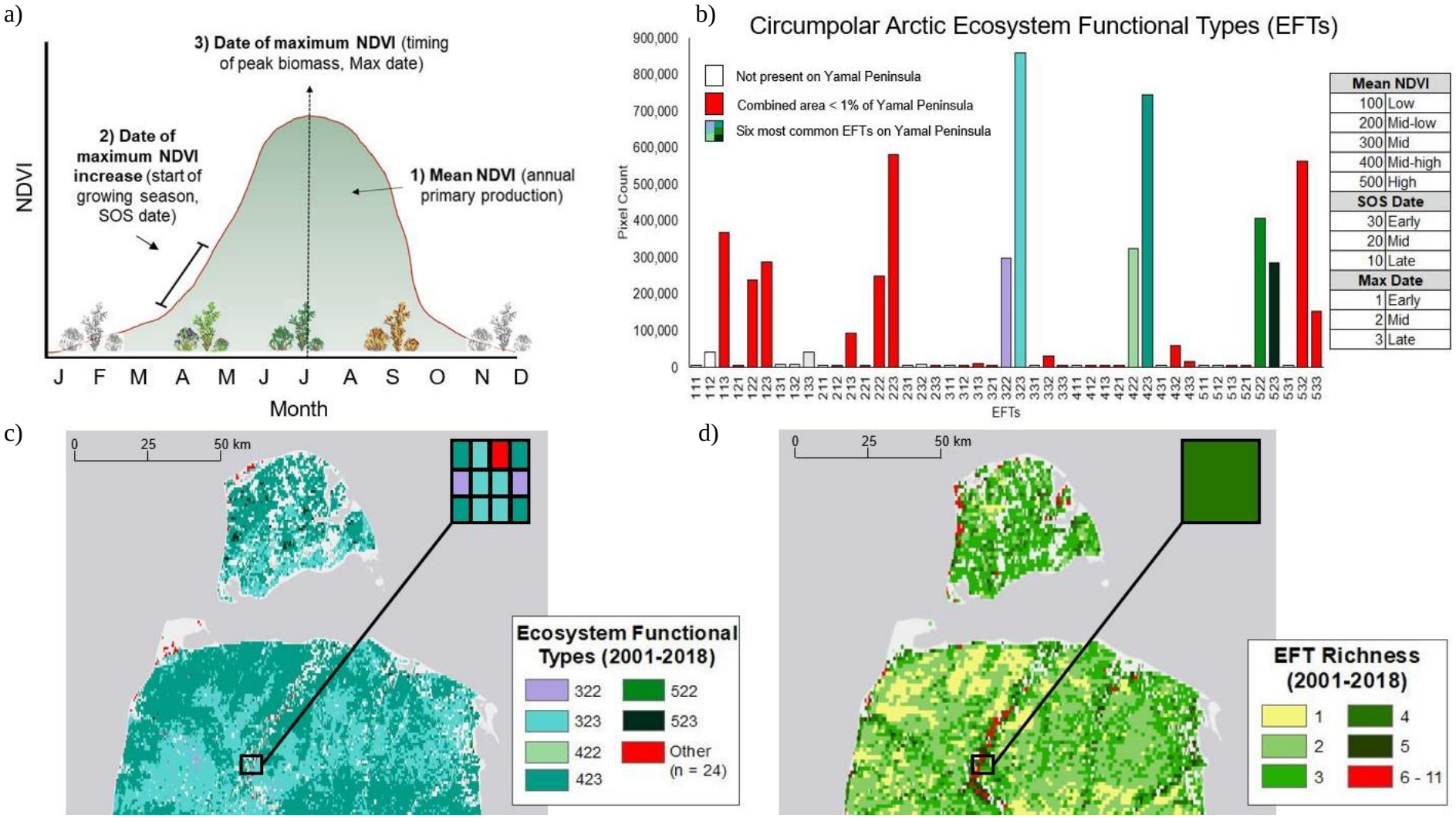

Figure 3. Ecosystem Functional Attribute (EFA), Ecosystem Functional Type (EFT), and EFT richness calculation. a) Derive EFAs (mean NDVI, SOS date, and max date) from the mean intra-annual NDVI curve of each pixel. b) Divide the EFAs into classes. The frequency distribution of mean NDVI was divided into quintiles representing low, mid-low, mid, mid-high, and high mean NDVI values. SOS and max dates were divided into 3 classes (early, mid, and late) based on natural breaks in their frequency distributions. The EFT of each pixel is determined by a combination of these classes. c) Map the EFTs to evaluate their spatial distribution. d) Calculate EFT richness by counting the number of EFTs within a 6x6 pixel window, which is conceptually represented by the inset maps. The use of the 6x6 pixel window (containing 36 pixels) allows for all 30 EFTs on the Yamal Peninsula to be counted if present. Both the EFT and EFT richness images display the northernmost point of the Yamal Peninsula. Permanent surface water bodies and pixels with > 20% water coverage are masked

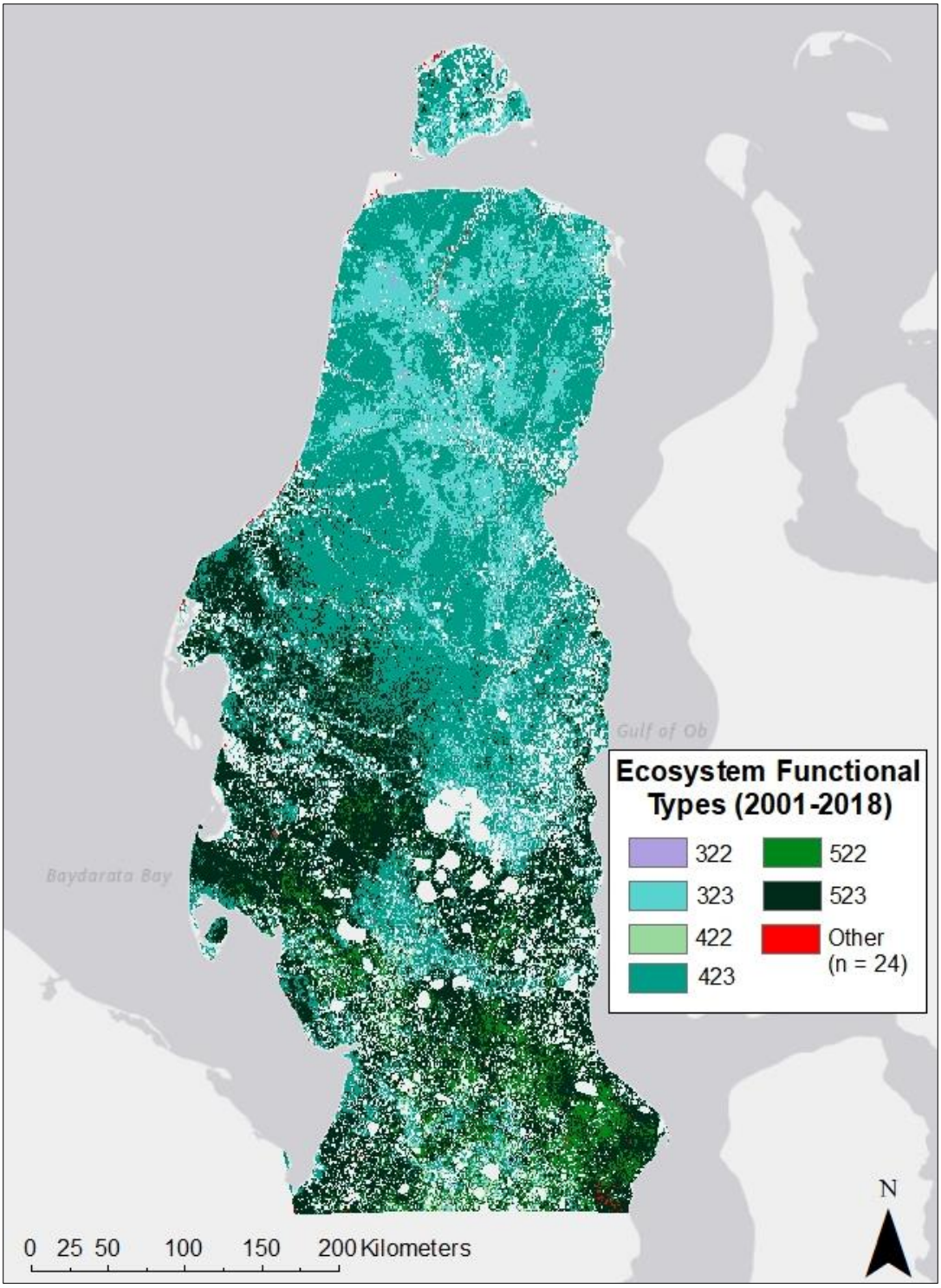

Figure 4. Yamal Peninsula Ecosystem Functional Types (EFTs) for 2001-2018. Red pixels represent an EFT that occurred across < 1% of the Yamal Peninsula. Permanent surface water bodies and pixels with > 20% water coverage are masked.

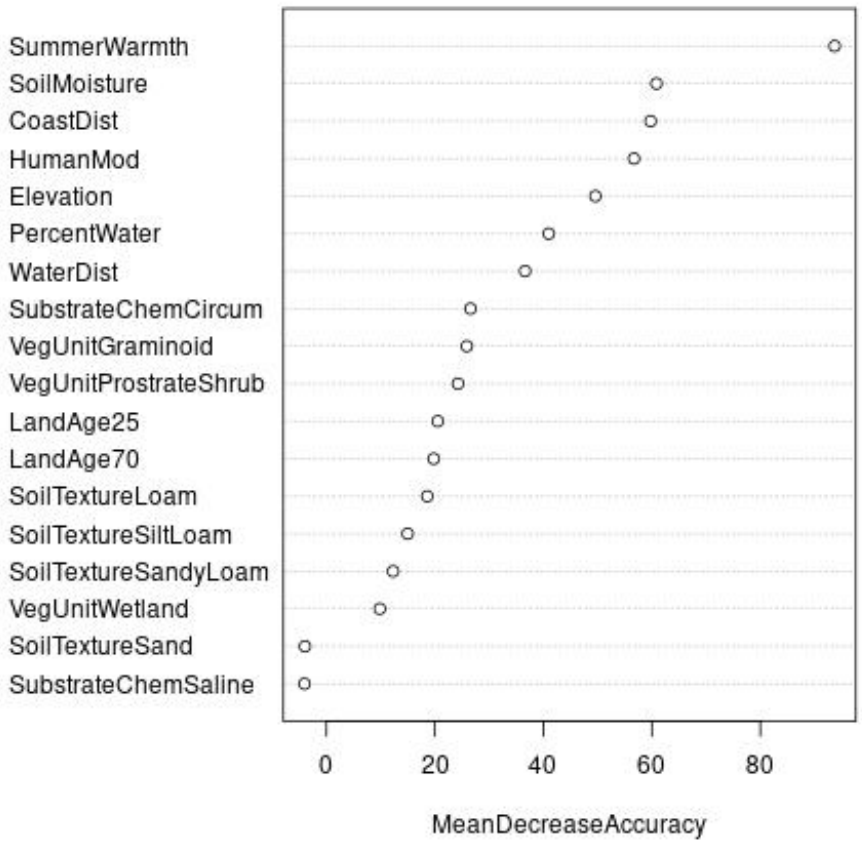

Figure 5. Variable importance for the prediction of EFT spatial distribution. Variable importance was determined by the Random Forest classification model and quantified with the mean decrease in accuracy metric, which measures the decrease in classification accuracy when out-of-bag (OOB) data for a given variable is permuted in the model (Berner et al., 2020; Han et al., 2016; Liaw and Wiener, 2002). A higher mean decrease in accuracy value indicates greater importance.

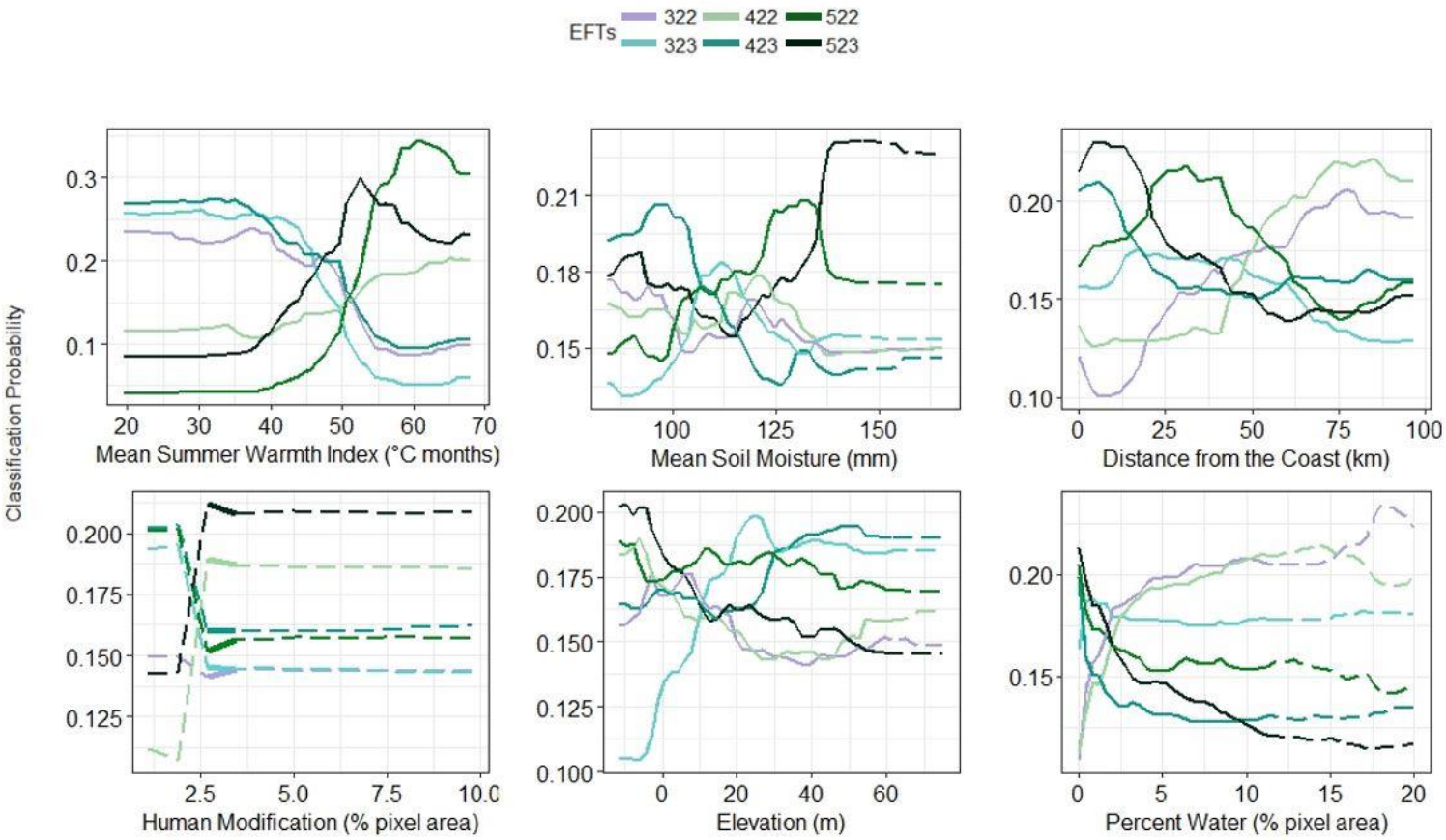

Figure 6. Partial dependence plots for the six most important drivers of EFT spatial distribution: mean Summer Warmth Index (SWI), mean growing season soil moisture, distance from the coast, human modification, elevation, and percent water in a pixel (0 – 20%). Partial dependence plots display the classification probability of each EFT across the range of driver values while still considering the average effects of the other drivers (Goldstein et al., 2014). Dashed lines indicate outlier drive variable values.

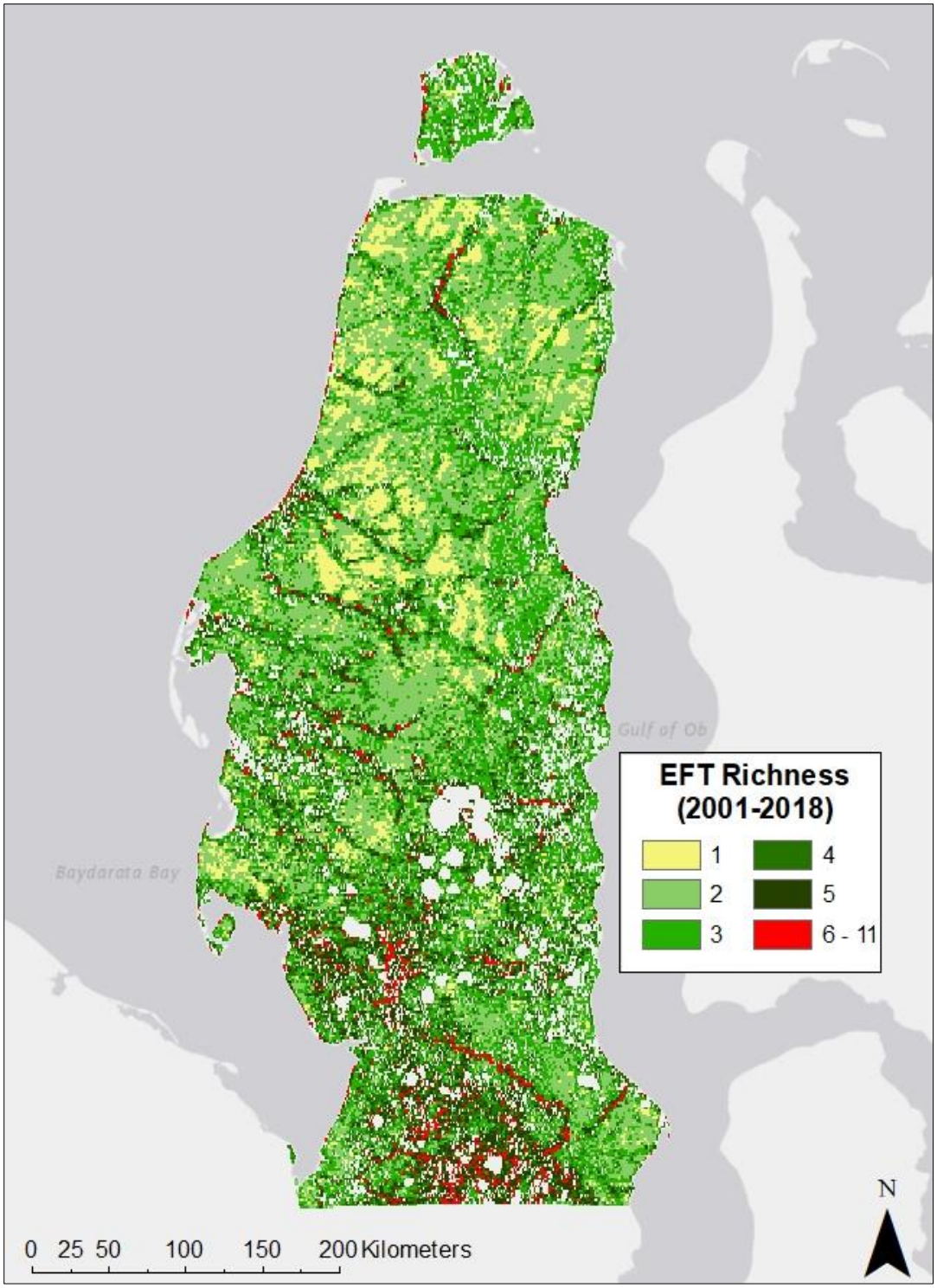

Figure 7. Yamal Peninsula overall EFT richness (2001-2018). EFT richness values 6 – 11 occurred across 3.3% of the Peninsula. Permanent surface water bodies and pixels with > 20% water coverage are masked.

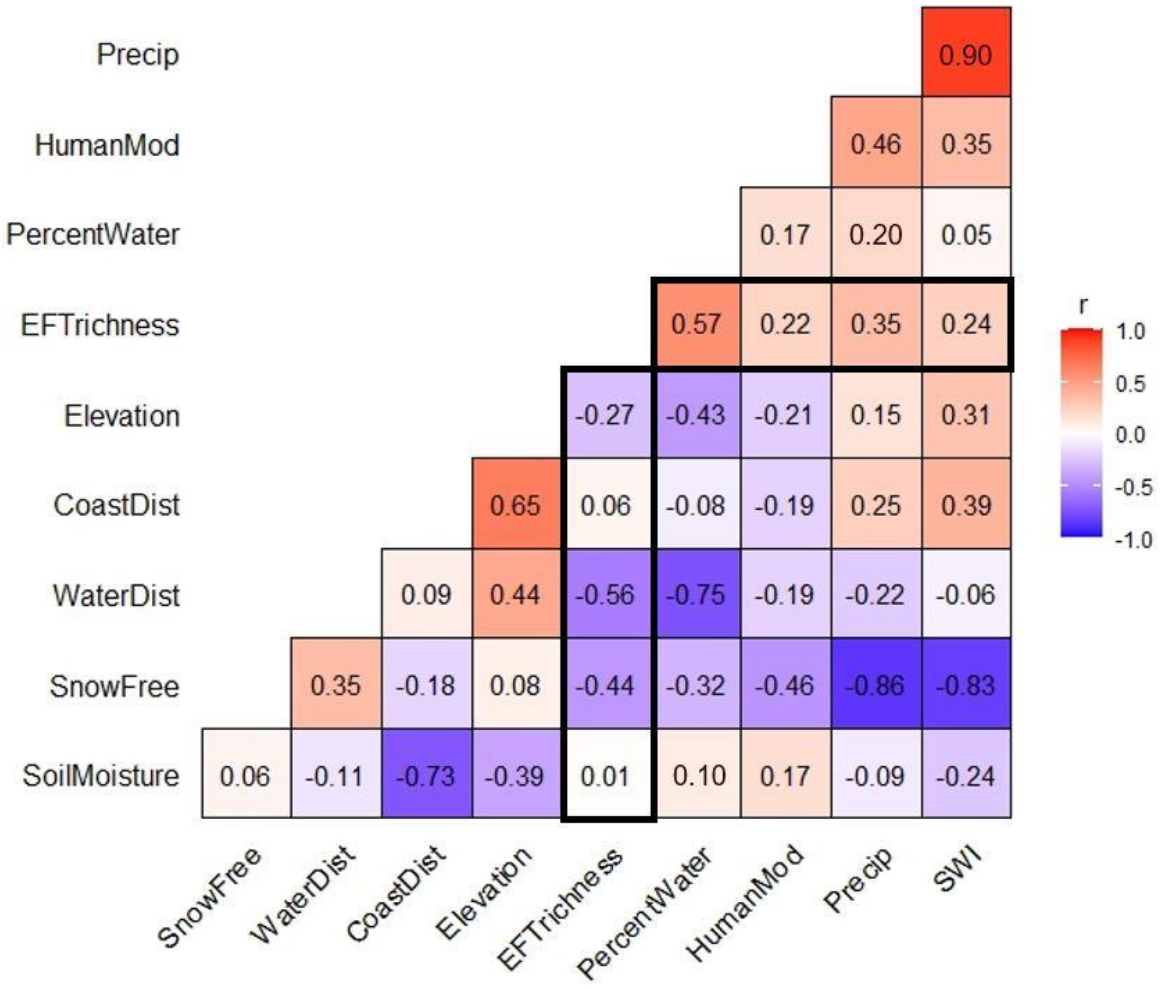

Figure 8. Spearman's correlation coefficients (r) for correlations between overall EFT richness (2001-2018) and continuous drivers. The 2001-2018 means of precipitation (Precip), snow-free period onset date (SnowFree), soil moisture, and Summer Warmth Index (SWI) were used. Distance from the coast (CoastDist), human modification (HumanMod), elevation, percent water, and distance from inland water bodies (WaterDist) were constant over the study period. EFT richness correlations are highlighted by the thicker black boxes. All correlations were significant at the 95% confidence level.

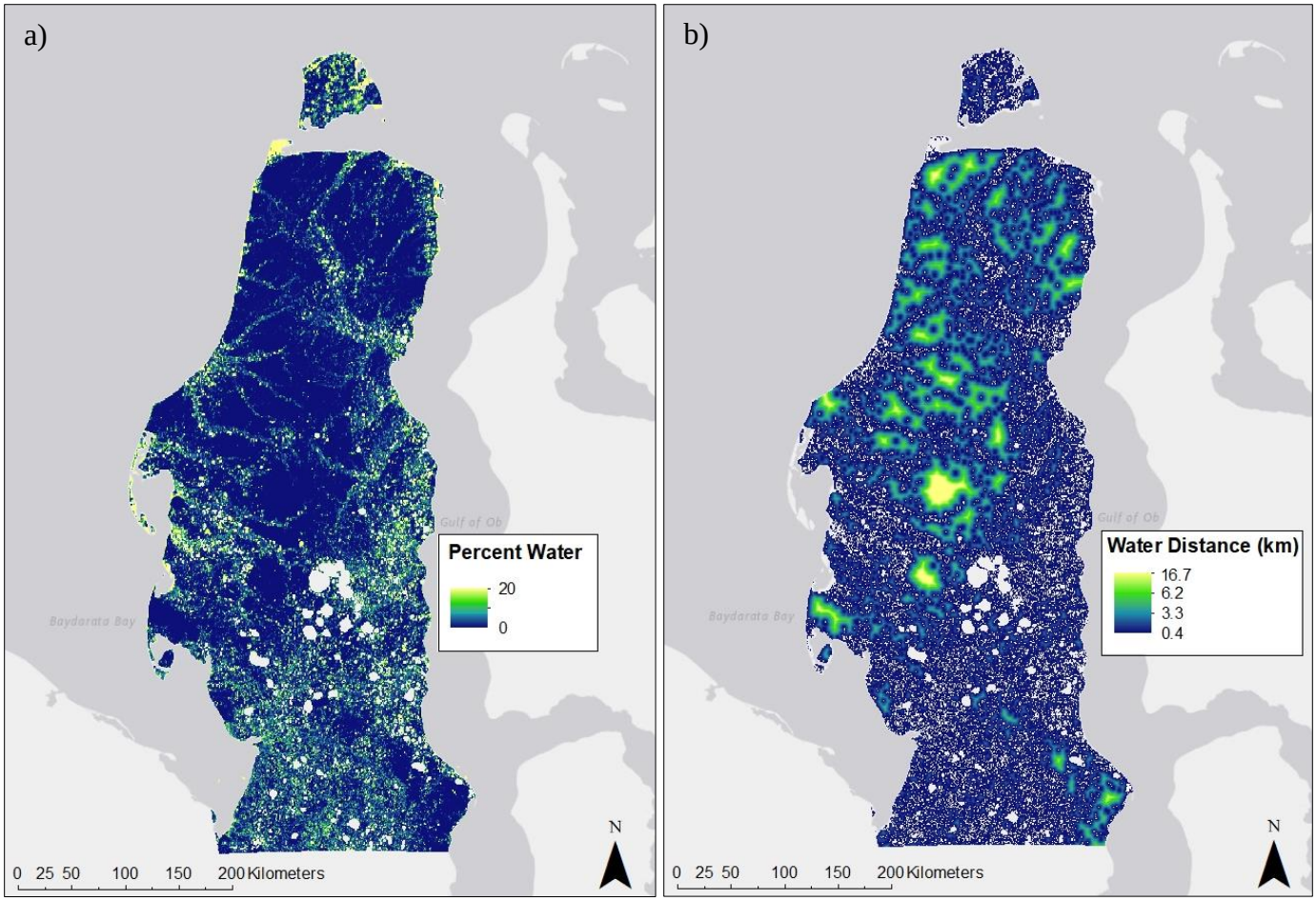

Figure 9. Yamal Peninsula (a) percent water in a pixel, and (b) distance from inland water bodies. Permanent surface water bodies and pixels with > 20% water coverage are masked.

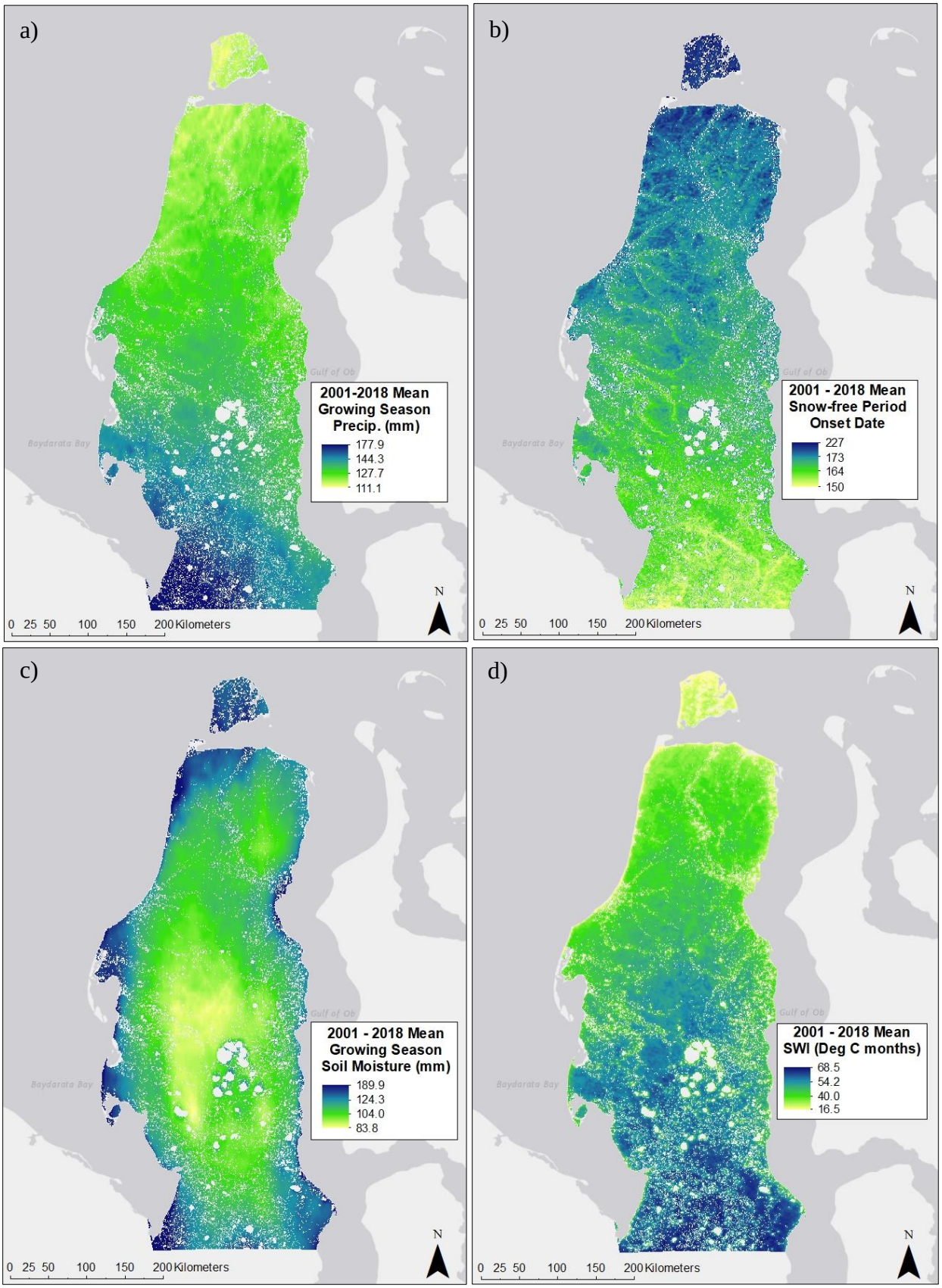

Figure 10. Yamal Peninsula 2001-2018 mean (a) mean growing season precipitation, (b) snow-free period onset date (Julian date), (c) mean growing season soil moisture, and (d) Summer Warmth Index (SWI). Permanent surface water bodies and pixels with > 20% water coverage are masked.

Table 2. Chi-Square Test of Independence results. All tests were significant at the 95% confidence level. A larger $\chi 2$ value indicates a stronger spatial association. Bolded residual values with the largest absolute values had the greatest influence on the spatial associations. Positive residuals indicate a positive relationship, and negative residuals indicate a negative relationship.

Drivers		Residuals	
		EFT Richness	
		High	Low
Vegetation Unit (χ^2 = 6,759)	Erect Shrub	**39.8**	-25.1
	Graminoid	-29.9	18.8
	Prostrate Shrub	**-45.1**	28.4
	Wetland	18.1	-11.4
Substrate Chemistry (χ^2 = 2,269)	Acidic	16.9	-10.2
	Circumnuetral	**-36.6**	**22.0**
	Saline	6.1	-3.7
Landscape Age (χ^2 = 584)	Older	**-18.4**	**11.1**
	Younger	8.4	-5.0
	Recently Disturbed	4.3	-2.6
Soil Texture (χ^2 = 295)	Clay Loam	1.4	-0.8
	Loam	1.6	-1.0
	Sand	1.8	-1.1
	Sandy Loam	**11.0**	-6.9
	Silt Loam	**-9.1**	5.7

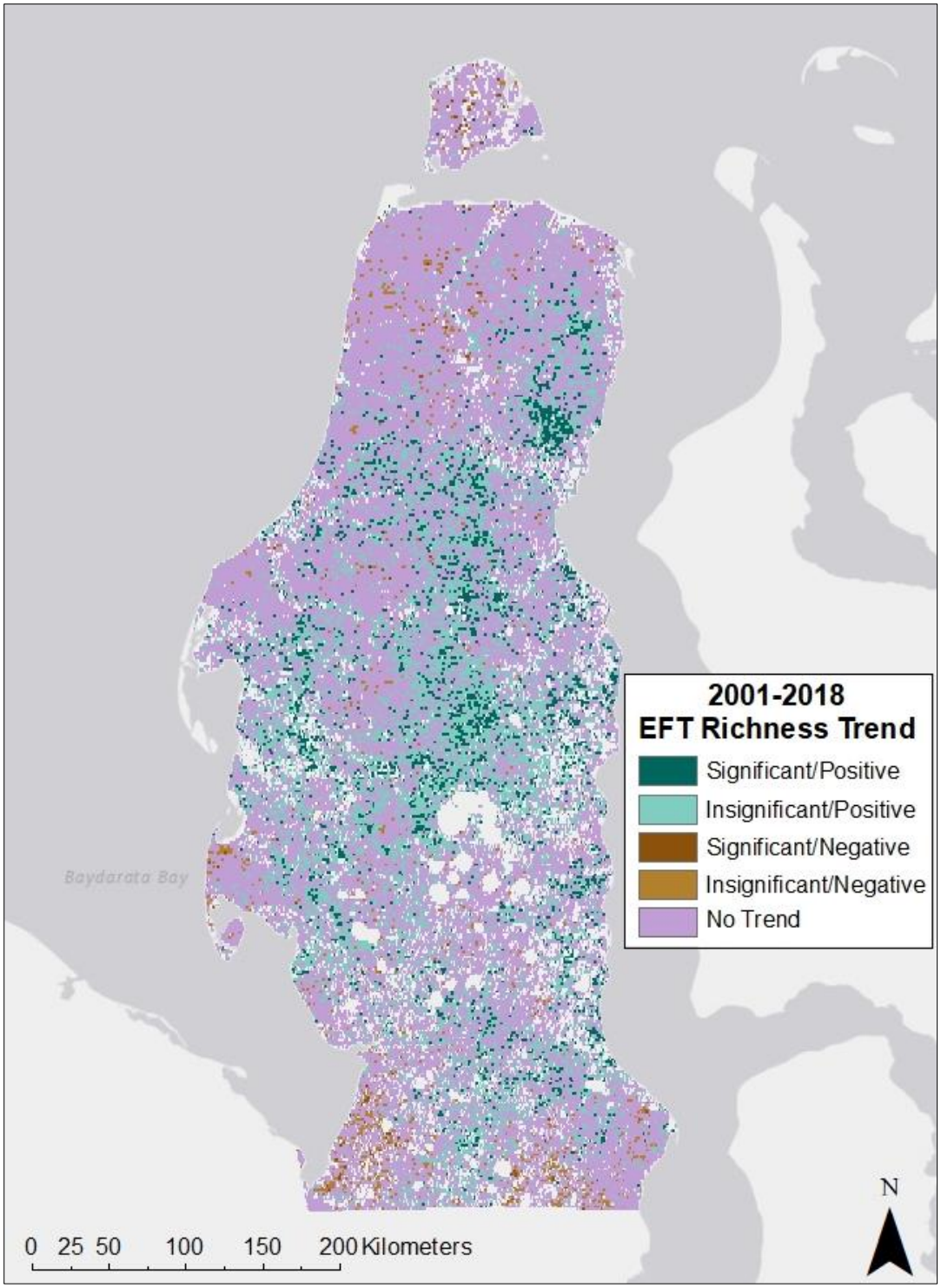

Figure 11. EFT richness trends inferred from Mann-Kendall trend tests and Sen's slope estimation. Pixels were classified based on trend significance at the 95% confidence level and Sen's slope direction. Pixels classified as no trend had insignificant trends and Sen's slopes = 0.000. Pixels with > 20% water coverage and pixels with < 15 years of data (due to low quality data or conditions preventing vegetation growth) were masked.

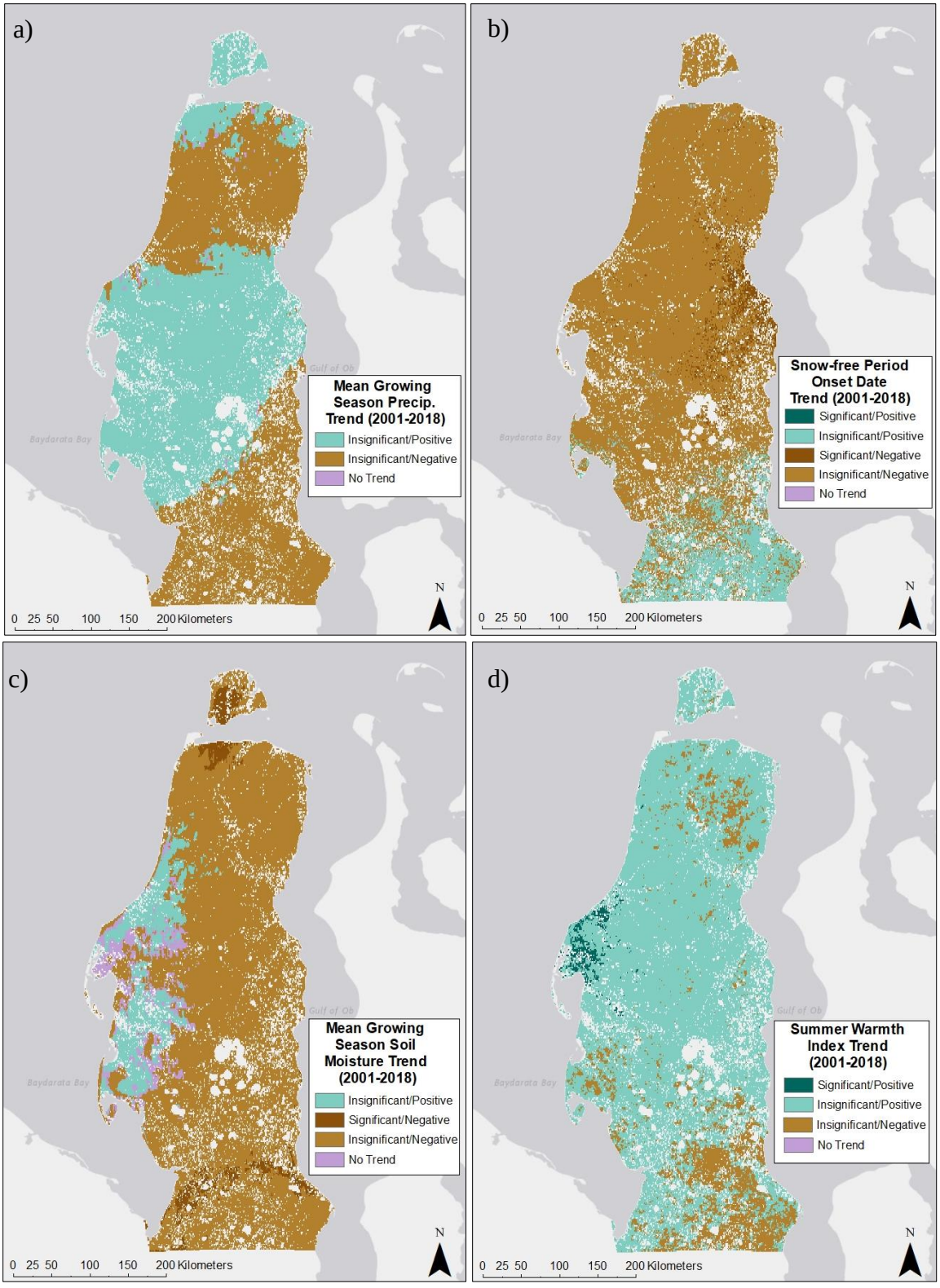

Figure 12. Trends in (a) mean growing season precipitation, (b) snow-free period onset date, (c) mean growing season soil moisture, and (d) Summer Warmth Index (SWI) inferred from Mann-Kendall trend tests and Sen's slope estimation. Pixels were classified based on trend significance at the 95% confidence level and Sen's slope direction. Pixels classified as no trend had insignificant trends and Sen's slopes = 0.000. Pixels with > 20% water coverage and pixels with < 15 years of data (due to low quality data or conditions preventing vegetation growth) were masked.

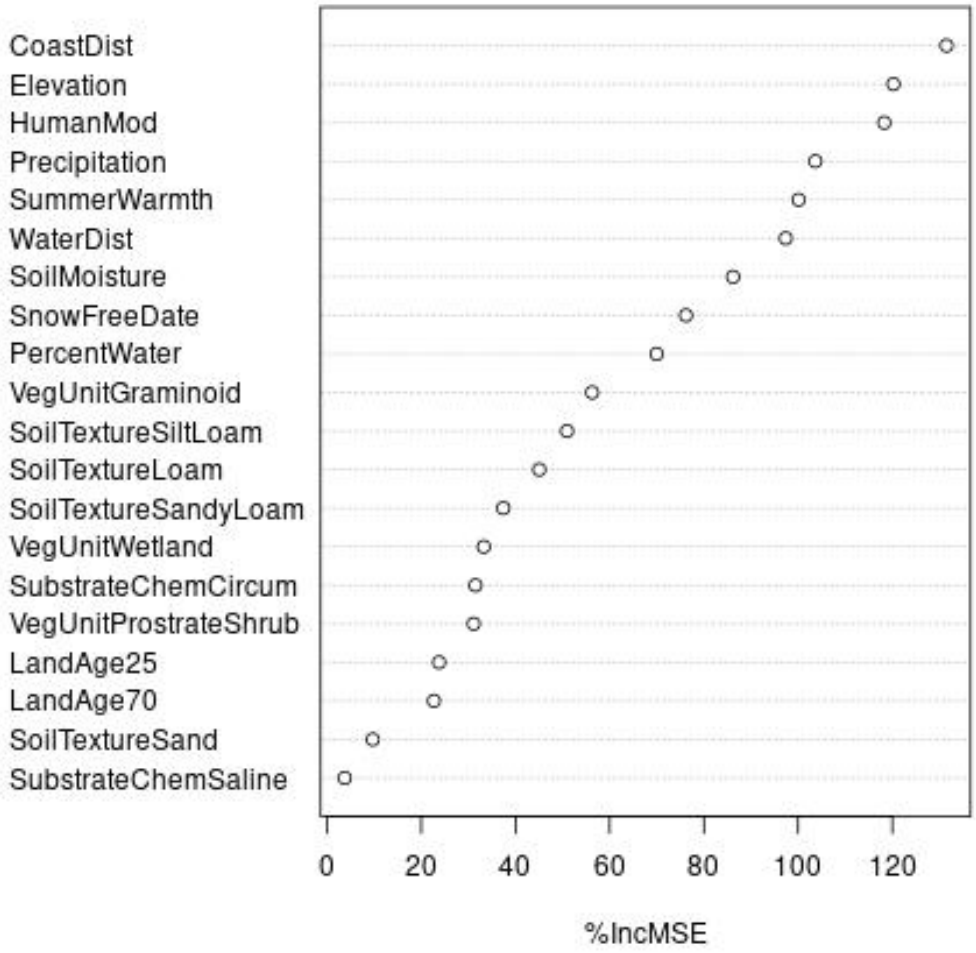

Figure 13. Variable importance for the prediction of EFT richness Sen's slope. Variable importance was determined by the Random Forest regression model and quantified with %Inc MSE parameter. %Inc MSE measures the percent increase in MSE when a predictor variable is permuted in the out-of-bag (OOB) data while all other predictor variables remain unchanged (Liaw and Wiener 2002). A higher %Inc MSE value indicates greater importance.

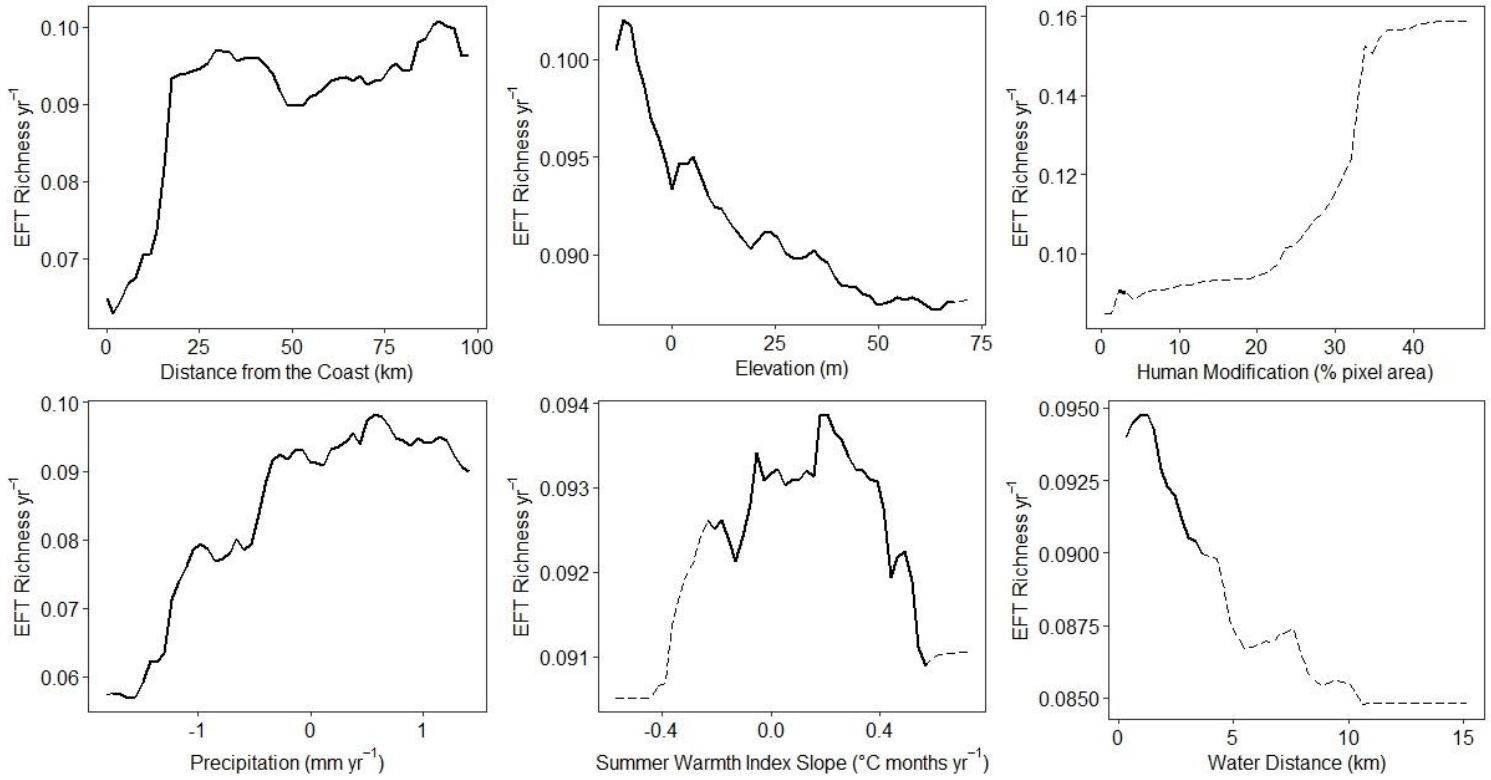

Figure 14. Partial dependence plots for the six most important drivers of EFT richness Sen's slope: coast distance, elevation, human modification, mean growing season precipitation Sen's slope, mean SWI Sen's slope, and water distance. Partial dependence plots display the average predicted relationships between EFT richness trends and individual drivers across their range of values while still considering the average effects of the other drivers (Goldstein et al., 2014). Dashed lines indicate outlier driver variable values.

7.0 References

Abatzoglou, J. T., Dobrowski, S. Z., Parks, S. A., & Hegewisch, K. C. (2018). TerraClimate, a high-resolution global dataset of monthly climate and climatic water balance from 1958–2015. *Scientific Data*, *5*(1), 170191. https://doi.org/10.1038/sdata.2017.191

Alcaraz-Segura, D., Paruelo, J., Epstein, H., & Cabello, J. (2013). Environmental and Human Controls of Ecosystem Functional Diversity in Temperate South America. *Remote Sensing*, *5*(1), 127–154. https://doi.org/10.3390/rs5010127

Ardelean, F., Onaca, A., Chețan, M.-A., Dornik, A., Georgievski, G., Hagemann, S., Timofte, F., & Berzescu, O. (2020). Assessment of Spatio-Temporal Landscape Changes from VHR Images in Three Different Permafrost Areas in the Western Russian Arctic. *Remote Sensing*, 12(23), 3999. https://doi.org/10.3390/rs12233999

Armstrong et al. (in preparation). Ecosystem Functional Types of the circumpolar arctic tundra based on the seasonal dynamics of vegetation productivity.

Becker, M. S., Davies, T. J., & Pollard, W. H. (2016). Ground ice melt in the high Arctic leads to greater ecological heterogeneity. *Journal of Ecology*, 104(1), 114–124. https://doi.org/10.1111/1365-2745.12491

Berner, L. T., Jantz, P., Tape, K. D., & Goetz, S. J. (2018). Tundra plant above-ground biomass and shrub dominance mapped across the North Slope of Alaska. *Environmental Research Letters*, 13(3), 035002. https://doi.org/10.1088/1748-9326/aaaa9a

Berner, L. T., Massey, R., Jantz, P., Forbes, B. C., Macias-Fauria, M., Myers-Smith, I., Kumpula, T., Gauthier, G., Andreu-Hayles, L., Gaglioti, B. V., Burns, P., Zetterberg, P., D'Arrigo, R., & Goetz, S. J. (2020). Summer warming explains widespread but not uniform greening in the Arctic tundra biome. *Nature Communications*, 11(1), 4621. https://doi.org/10.1038/s41467-020-18479-5

Bhatt, U. S., Walker, D. A., Raynolds, M. K., Comiso, J. C., Epstein, H. E., Jia, G., Gens, R., Pinzon, J. E., Tucker, C. J., Tweedie, C. E., & Webber, P. J. (2010). Circumpolar Arctic Tundra Vegetation Change Is Linked to Sea Ice Decline. *Earth Interactions*, 14(8), 1–20. https://doi.org/10.1175/2010EI315.1

Bhatt, U. S., Walker, D. A., Raynolds, M. K., Walsh, J. E., Bieniek, P. A., Cai, L., Comiso, J. C., Epstein, H. E., Frost, G. V., Gersten, R., Hendricks, A. S., Pinzon, J. E., Stock, L., & Tucker, C. J. (2021). Climate drivers of Arctic tundra variability and change using an indicators framework. *Environmental Research Letters*, *16*(5), 055019. https://doi.org/10.1088/1748-9326/abe676

Bieniek, P. A., Bhatt, U. S., Walker, D. A., Raynolds, M. K., Comiso, J. C., Epstein, H. E., Pinzon, J. E., Tucker, C. J., Thoman, R. L., Tran, H., Mölders, N., Steele, M., Zhang, J., & Ermold, W. (2015). Climate Drivers Linked to Changing Seasonality of Alaska Coastal Tundra Vegetation Productivity. *Earth Interactions*, *19*(19), 1–29.

https://doi.org/10.1175/EI-D-15-0013.1

Billings, W. D. (1987). Constraints to Plant Growth, Reproduction, and Establishment in Arctic Environments. *Arctic and Alpine Research*, 19(4), 357. https://doi.org/10.2307/1551400

Breiman, L. (2001). Random Forests. Machine Learning, 45, pp. 5-32.

Cabello, J., Lourenço, P., Reyes, A., Alcaraz-Segura, D. (2013). Chapter 9: Ecosystem Services Assessment of National Parks Networks for Functional Diversity and Carbon Conservation Strategies Using Remote Sensing, Earth Observation of Ecosystem Services (1st ed). CRC Press. https://doi.org/10.1201/b15628

Campbell, T. K. F., Lantz, T. C., Fraser, R. H., & Hogan, D. (2021). High Arctic Vegetation Change Mediated by Hydrological Conditions. *Ecosystems*, *24*(1), 106–121. https://doi.org/10.1007/s10021-020-00506-7

Cazorla, B. P., Cabello, J., Peñas, J., Garcillán, P. P., Reyes, A., & Alcaraz-Segura, D. (2021). Incorporating Ecosystem Functional Diversity into Geographic Conservation Priorities Using Remotely Sensed Ecosystem Functional Types. *Ecosystems*, 24(3), 548–564. https://doi.org/10.1007/s10021-020-00533-4

Cutler, D. R., Edwards, T. C., Beard, K. H., Cutler, A., Hess, K. T., Gibson, J., & Lawler, J. J. (2007). Random Forests For Classification in Exology. *Ecology*, 88(11), 2783–2792. https://doi.org/10.1890/07-0539.1

Didan, K. (2015). MOD13Q1 MODIS/Terra Vegetation Indices 16-Day L3 Global 250m SIN Grid V006 [Data set]. NASA EOSDIS Land Processes DAAC. DOI: 10.5067/MODIS/MOD13Q1.006

Elmendorf, S. C., Henry, G. H. R., Hollister, R. D., Björk, R. G., Boulanger-Lapointe, N., Cooper, E. J., Cornelissen, J. H. C., Day, T. A., Dorrepaal, E., Elumeeva, T. G., Gill, M., Gould, W. A., Harte, J., Hik, D. S., Hofgaard, A., Johnson, D. R., Johnstone, J. F., Jónsdóttir, I. S., Jorgenson, J. C., … Wipf, S. (2012). Plot-scale evidence of tundra vegetation change and links to recent summer warming. *Nature Climate Change*, *2*(6), 453–457. https://doi.org/10.1038/nclimate1465

Epstein, H. E., Raynolds, M. K., Walker, D. A., Bhatt, U. S., Tucker, C. J., & Pinzon, J. E. (2012). Dynamics of aboveground phytomass of the circumpolar Arctic tundra during the past three decades. *Environmental Research Letters*, *7*(1), 015506. https://doi.org/10.1088/1748-9326/7/1/015506

Epstein, H. E., Walker, D. A., Frost, G. V., Raynolds, M. K., Bhatt, U., Daanen, R., Forbes, B., Geml, J., Kaärlejarvi, E., Khitun, O., Khomutov, A., Kuss, P., Leibman, M., Matyshak, G., Moskalenko, N., Orekhov, P., Romanovsky, V. E., & Timling, I. (2021). Spatial

patterns of arctic tundra vegetation properties on different soils along the Eurasia Arctic Transect, and insights for a changing Arctic. *Environmental Research Letters*, *16*(1), 014008. https://doi.org/10.1088/1748-9326/abc9e3

European Space Agency (ESA) and Université Catholique de Louvain (UC Louvain). (2010). GlobCover 2009 (Global Land Cover Map). http://due.esrin.esa.int/page_globcover.php.

Euskirchen, E. S., Bret-Harte, M. S., Shaver, G. R., Edgar, C. W., & Romanovsky, V. E. (2017a). Long-Term Release of Carbon Dioxide from Arctic Tundra Ecosystems in Alaska. *Ecosystems*, *20*(5), 960–974. https://doi.org/10.1007/s10021-016-0085-9

Euskirchen, E. S., Edgar, C. W., Syndonia Bret-Harte, M., Kade, A., Zimov, N., & Zimov, S. (2017b). Interannual and Seasonal Patterns of Carbon Dioxide, Water, and Energy Fluxes From Ecotonal and Thermokarst-Impacted Ecosystems on Carbon-Rich Permafrost Soils in Northeastern Siberia. *Journal of Geophysical Research: Biogeosciences*, *122*(10), 2651–2668. https://doi.org/10.1002/2017JG004070

FAO/IIASA/ISRIC/ISS-CAS/JRC (2012). Harmonized World Soil Database (version 1.2). FAO, Rome, Italy and IIASA, Laxenburg, Austria.

Fernández, N., Paruelo, J. M., & Delibes, M. (2010). Ecosystem functioning of protected and altered Mediterranean environments: A remote sensing classification in Doñana, Spain. *Remote Sensing of Environment*, *114*(1), 211–220. https://doi.org/10.1016/j.rse.2009.09.001

Forbes, B. C. (1999). Land use and climate change on the Yamal Peninsula of north-west Siberia: Some ecological and socio-economic implications. *Polar Research*, *18*(2), 367–373. https://doi.org/10.3402/polar.v18i2.6597

Forbes, B. C., Stammler, F., Kumpula, T., Meschtyb, N., Pajunen, A., & Kaarlejärvi, E. (2009). High resilience in the Yamal-Nenets social–ecological system, West Siberian Arctic, Russia. *Proceedings of the National Academy of Sciences*, *106*(52), 22041–22048. https://doi.org/10.1073/pnas.0908286106

Forbes, B. C., & Kumpula, T. (2009). The Ecological Role and Geography of Reindeer (*Rangifer tarandus*) in Northern Eurasia: Ecology/geography of Eurasian reindeer. *Geography Compass*, *3*(4), 1356–1380. https://doi.org/10.1111/j.1749-8198.2009.00250.x

Fox, J. and Weisberg, S. (2019). An {R} Companion to Applied Regression, Third Edition. Thousand Oaks CA: Sage. URL: https://socialsciences.mcmaster.ca/jfox/Books/Companion/

Frost, G. V., Bhatt, U. S., Epstein, H. E., Myers-Smith, I., Phoenix, G. K., Berner, L. T., Bjerke, J. W., Forbes, B. C., Goetz, S. J., Kerby, J. T., Macander, M. J., Park, T., Raynolds, M. K., Tommervik, H., and Walker, D. A. (2020). Tundra Greenness. In: Arctic Report Card: Update for 2020. NOAA, Silver Spring, MD. Retrieved from

https://arctic.noaa.gov/Report-Card/Report-Card-2020/ArtMID/7975/ArticleID/879/Tundra-Greenness

Gamon, J. A., Huemmrich, K. F., Stone, R. S., & Tweedie, C. E. (2013). Spatial and temporal variation in primary productivity (NDVI) of coastal Alaskan tundra: Decreased vegetation growth following earlier snowmelt. *Remote Sensing of Environment*, *129*, 144–153. https://doi.org/10.1016/j.rse.2012.10.030

Gazprom. (2021). Yamal. https://www.gazprom.com/projects/yamal/

Goldstein, A., Kapelner, A., Bleich, J., & Pitkin, E. (2014). Peeking Inside the Black Box: Visualizing Statistical Learning with Plots of Individual Conditional Expectation. *ArXiv:1309.6392 [Stat]*. http://arxiv.org/abs/1309.6392

Greenwell, B.M. (2017). pdp: An R Package for Constructing Partial Dependence Plots. The R Journal, 9(1), 421--436. URL: https://journal.r-project.org/archive/2017/RJ-2017-016/index.html.

Hall, D. K., et al. (2016). MODIS/Terra Snow Cover Daily L3 Global 500m Grid. Version 6. Boulder, Colorado USA: NASA National Snow and Ice Data Center Distributed Active Archive Center.

Hijmans, R.J. (2021). terra: Spatial Data Analysis. R package version 1.0-10. https://CRAN.R-project.org/package=terra

Hong Han, Xiaoling Guo, & Hua Yu. (2016). Variable selection using Mean Decrease Accuracy and Mean Decrease Gini based on Random Forest. *2016 7th IEEE International Conference on Software Engineering and Service Science (ICSESS)*, 219–224. https://doi.org/10.1109/ICSESS.2016.7883053

IPCC, 2021: *Climate Change 2021: The Physical Science Basis. Contribution of Working Group I to the Sixth Assessment Report of the Intergovernmental Panel on Climate Change* [Masson-Delmotte, V., P. Zhai, A. Pirani, S. L. Connors, C. Péan, S. Berger, N. Caud, Y. Chen, L. Goldfarb, M. I. Gomis, M. Huang, K. Leitzell, E. Lonnoy, J. B.R. Matthews, T. K. Maycock, T. Waterfield, O. Yelekçi, R. Yu and B. Zhou (eds.)]. Cambridge University Press. In Press.

Ivits, E., Cherlet, M., Horion, S., & Fensholt, R. (2013). Global Biogeographical Pattern of Ecosystem Functional Types Derived From Earth Observation Data. *Remote Sensing*, *5*(7), 3305–3330. https://doi.org/10.3390/rs5073305

Jia, G. J., Epstein, H. E., & Walker, D. A. (2006). Spatial heterogeneity of tundra vegetation response to recent temperature changes: SPATIAL HETEROGENEITY OF TUNDRA DYNAMICS. *Global Change Biology*, *12*(1), 42–55. https://doi.org/10.1111/j.1365-2486.2005.01079.x

Johnstone, J. F., & Kokelj, S. V. (2009). Environmental Conditions and Vegetation Recovery at

Abandoned Drilling Mud Sumps in the Mackenzie Delta Region, Northwest Territories, Canada. *ARCTIC*, *61*(2), 199–211. https://doi.org/10.14430/arctic35

Jorgenson, M. T., Kanevskiy, M., Shur, Y., Moskalenko, N., Brown, D. R. N., Wickland, K., Striegl, R., & Koch, J. (2015). Role of ground ice dynamics and ecological feedbacks in recent ice wedge degradation and stabilization. *Journal of Geophysical Research: Earth Surface*, 120(11), 2280–2297. https://doi.org/10.1002/2015JF003602

Keenan, T. F., & Riley, W. J. (2018). Greening of the land surface in the world's cold regions consistent with recent warming. *Nature Climate Change*, 8(9), 825–828. https://doi.org/10.1038/s41558-018-0258-y

Kennedy, C.M., et al. (2019). Managing the middle: A shift in conservation priorities based on the global human modification gradient. *Global Change Biology*, 25, pp. 811-826. https://doi.org/10.1111/gcb.14549

Kerby, J. T. & Post, E. (2013). Advancing plant phenology and reduced herbivore production in a terrestrial system associated with sea ice decline. *Nature Communications*, 4, 2514. https://doi.org/10.1038/ncomms3514

Kuhn, M. (2020). caret: Classification and Regression Training. R package version 6.0-86. https://CRAN.R-project.org/package=caret

Kulkarni, A., & Storch, H. V. (1995). Monte Carlo experiments on the effect of serial correlation on the Mann-Kendall test of trend. *Kurzberichte*, 4.

Lantz, T. C. (2017). Vegetation Succession and Environmental Conditions following Catastrophic Lake Drainage in Old Crow Flats, Yukon. *ARCTIC*, 70(2), 177. https://doi.org/10.14430/arctic4646

Lara, M. J., Nitze, I., Grosse, G., Martin, P., & McGuire, A. D. (2018). Reduced arctic tundra productivity linked with landform and climate change interactions. *Scientific Reports*, *8*(1), 2345. https://doi.org/10.1038/s41598-018-20692-8

Lara, M. J., McGuire, A. D., Euskirchen, E. S., Genet, H., Yi, S., Rutter, R., Iversen, C., Sloan, V., & Wullschleger, S. D. (2020). Local-scale Arctic tundra heterogeneity affects regional-scale carbon dynamics. *Nature Communications*, *11*(1), 4925. https://doi.org/10.1038/s41467-020-18768-z

Leibman, M., Khomutov, A., & Kizyakov, A. (2014). Cryogenic Landslides in the West-Siberian Plain of Russia: Classification, Mechanisms, and Landforms. In W. Shan, Y. Guo, F. Wang, H. Marui, & A. Strom (Eds.), Landslides in Cold Regions in the Context of Climate Change. Springer International Publishing. https://doi.org/10.1007/978-3-319-00867-7_11

Li, B., Heijmans, M. M. P. D., Berendse, F., Blok, D., Maximov, T., & Sass-Klaassen, U.

(2016). The role of summer precipitation and summer temperature in establishment and growth of dwarf shrub Betula nana in northeast Siberian tundra. *Polar Biology*, *39*(7), 1245–1255. https://doi.org/10.1007/s00300-015-1847-0

Liaw, A., & Wiener, M. (2002). Classification and Regression by randomForest. R News, 2(3).

Loiko, S., Klimova, N., Kuzmina, D., & Pokrovsky, O. (2020). Lake Drainage in Permafrost Regions Produces Variable Plant Communities of High Biomass and Productivity. *Plants*, *9*(7), 867. https://doi.org/10.3390/plants9070867

Macias-Fauria, M., Forbes, B. C., Zetterberg, P., & Kumpula, T. (2012). Eurasian Arctic greening reveals teleconnections and the potential for structurally novel ecosystems. *Nature Climate Change*, *2*(8), 613–618. https://doi.org/10.1038/nclimate1558

Manning, P., van der Plas, F., Soliveres, S., Allan, E., Maestre, F. T., Mace, G., Whittingham, M. J., Fischer, M. (2018). Redefining ecosystem multifunctionality. *Nature Ecology & Evolution*, 2(3):427–36.

May, J. L., Hollister, R. D., Betway, K. R., Harris, J. A., Tweedie, C. E., Welker, J. M., Gould, W. A., & Oberbauer, S. F. (2020). NDVI Changes Show Warming Increases the Length of the Green Season at Tundra Communities in Northern Alaska: A Fine-Scale Analysis. *Frontiers in Plant Science*, *11*, 1174. https://doi.org/10.3389/fpls.2020.01174

McLeod, A.I. (2011). Kendall: Kendall rank correlation and Mann-Kendall trend test. R package version 2.2. https://CRAN.R-project.org/package=Kendall

Microsoft Corporation (Microsoft) and Weston, S. (2020). doParallel: Foreach Parallel Adaptor for the 'parallel' Package. R package version 1.0.16. https://CRAN.R-project.org/package=doParallel

Moskovchenko, D. V., Kurchatova, A. N., Fefilov, N. N., & Yurtaev, A. A. (2017). Concentrations of trace elements and iron in the Arctic soils of Belyi Island (the Kara Sea, Russia): patterns of variation across landscapes. *Environ Monit Assesss*, 189-210.

Myers-Smith, I. H., Elmendorf, S. C., Beck, P. S. A., Wilmking, M., Hallinger, M., Blok, D., Tape, K. D., Rayback, S. A., Macias-Fauria, M., Forbes, B. C., Speed, J. D. M., Boulanger-Lapointe, N., Rixen, C., Lévesque, E., Schmidt, N. M., Baittinger, C., Trant, A. J., Hermanutz, L., Collier, L. S., … Vellend, M. (2015). Climate sensitivity of shrub growth across the tundra biome. *Nature Climate Change*, 5(9), 887–891. https://doi.org/10.1038/nclimate2697

Nitze, I., Grosse, G., Jones, B. M., Romanovsky, V. E., & Boike, J. (2018). Remote sensing quantifies widespread abundance of permafrost region disturbances across the Arctic and Subarctic. *Nature Communications*, 9(1), 5423. https://doi.org/10.1038/s41467-018-07663-3

Oliveira, S., Oehler, F., San-Miguel-Ayanz, J., Camia, A., & Pereira, J. M. C. (2012). Modeling

spatial patterns of fire occurrence in Mediterranean Europe using Multiple Regression and Random Forest. *Forest Ecology and Management*, *275*, 117–129. https://doi.org/10.1016/j.foreco.2012.03.003

Oliver, T. H., Heard, M. S., Isaac, N. J. B., Roy, D. B., Procter, D., Eigenbrod, F., Freckleton, R., Hector, A., Orme, C. D. L., Petchey, O. L., Proença, V., Raffaelli, D., Suttle, K. B., Mace, G. M., Martín-López, B., Woodcock, B. A., & Bullock, J. M. (2015). Biodiversity and Resilience of Ecosystem Functions. *Trends in Ecology & Evolution*, *30*(11), 673–684. https://doi.org/10.1016/j.tree.2015.08.009

Olofsson, J., Oksanen, L., Callaghan, T., Hulme, P. E., Oksanen, T., & Suominen, O. (2009). Herbivores inhibit climate-driven shrub expansion on the tundra: *Global Change Biology*, *15*(11), 2681–2693. https://doi.org/10.1111/j.1365-2486.2009.01935.x

Paruelo, J. M., Jobbágy, E. G., & Sala, O. E. (2001). Current Distribution of Ecosystem Functional Types in Temperate South America. *Ecosystems*, *4*(7), 683–698. https://doi.org/10.1007/s10021-001-0037-9

Patakamuri, S.K. and O'Brien, N. (2020). modifiedmk: Modified Versions of Mann Kendall and Spearman's Rho Trend Tests. R package version 1.5.0. https://CRAN.R-project.org/package=modifiedmk

Pearson, R. G., Phillips, S. J., Loranty, M. M., Beck, P. S. A., Damoulas, T., Knight, S. J., & Goetz, S. J. (2013). Shifts in Arctic vegetation and associated feedbacks under climate change. *Nature Climate Change*, *3*(7), 673–677. https://doi.org/10.1038/nclimate1858

Pekel, J.-F., Cottam, A., Gorelick, N., & Belward, A. S. (2016). High-resolution mapping of global surface water and its long-term changes. *Nature*, *540*(7633), 418–422. https://doi.org/10.1038/nature20584

Pérez-Hoyos, A., Martínez, B., García-Haro, F., Moreno, Á., & Gilabert, M. (2014). Identification of Ecosystem Functional Types from Coarse Resolution Imagery Using a Self-Organizing Map Approach: A Case Study for Spain. *Remote Sensing*, *6*(11), 11391–11419. https://doi.org/10.3390/rs61111391

Pohlert, T. (2020). trend: Non-Parametric Trend Tests and Change-Point Detection. R package version 1.1.2. https://CRAN.R-project.org/package=trend

Post, E., Pederson, C., Wilmers, C. C., & Forchhammer, M. C. (2008). Warming, plant phenology and the spatial dimension of trophic mismatch for large herbivores. *Proc. R. Soc. B.*, 275, 2005–2013. http://doi.org/10.1098/rspb.2008.0463

Post, E., Kerby, J., Pedersen, C., & Steltzer, H. (2016). Highly individualistic rates of plant phenological advance associated with arctic sea ice dynamics. Biology Letters, 12(12), 20160332. https://doi.org/10.1098/rsbl.2016.0332

Prevéy, J. S., Rixen, C., Rüger, N., Høye, T. T., Bjorkman, A. D., Myers-Smith, I. H., Elmendorf, S. C., Ashton, I. W., Cannone, N., Chisholm, C. L., Clark, K., Cooper, E. J., Elberling, B., Fosaa, A. M., Henry, G. H. R., Hollister, R. D., Jónsdóttir, I. S., Klanderud, K., Kopp, C. W., … Wipf, S. (2019). Warming shortens flowering seasons of tundra plant communities. *Nature Ecology & Evolution*, *3*(1), 45–52. https://doi.org/10.1038/s41559-018-0745-6

R Core Team (2020). R: A language and environment for statistical computing. R Foundation for Statistical Computing, Vienna, Austria. URL https://www.R-project.org/.

Rabosky, D.L., et al. (2014). BAMMtools: an R package for the analysis of evolutionary dynamics on phylogenetic trees. Methods in Ecology and Evolution 5:701-707.

Raynolds, M. K., Walker, D. A., & Maier, H. A. (2006). NDVI patterns and phytomass distribution in the circumpolar Arctic. *Remote Sensing of Environment*, *102*(3–4), 271–281. https://doi.org/10.1016/j.rse.2006.02.016

Raynolds, M., Comiso, J., Walker, D., & Verbyla, D. (2008). Relationship between satellite-derived land surface temperatures, arctic vegetation types, and NDVI. *Remote Sensing of Environment*, *112*(4), 1884–1894. https://doi.org/10.1016/j.rse.2007.09.008

Raynolds, M. K., Walker, D. A., Epstein, H. E., Pinzon, J. E., and Tucker C. J. (2012). A new estimate of tundra-biome phytomass from trans-Arctic field data and AVHRR NDVI *Remote Sens. Lett.* 3, 403–11. https://doi.org/10.1080/01431161.2011.609188

Raynolds, M. K., & Walker, D. A. (2009). Effects of deglaciation on circumpolar distribution of arctic vegetation. *Canadian Journal of Remote Sensing*, *35*(2), 12.

Reichle, L. M., Epstein, H. E., Bhatt, U. S., Raynolds, M. K., & Walker, D. A. (n.d.). Spatial Heterogeneity of the Temporal Dynamics of Arctic Tundra Vegetation. *Geophysical Research Letters*, 10.

Revelle, W. (2020). psych: Procedures for Personality and Psychological Research, Northwestern University, Evanston, Illinois, USA, https://CRAN.R-project.org/package=psych Version = 2.0.9.

Rizzoli, P. et al. (2017). Generation and performance assessment of the global TanDEM-X digital elevation model. ISPRS Journal of Photogrammetry and Remote Sensing, 132, pp. 119-139.

Verbyla, D. (2008). The greening and browning of Alaska based on 1982–2003 satellite data. *Global Ecology and Biogeography*, *17*(4), 547–555. https://doi.org/10.1111/j.1466-8238.2008.00396.x

Verdonen, M., Berner, L. T., Forbes, B. C., & Kumpula, T. (2020). Periglacial vegetation dynamics in Arctic Russia: Decadal analysis of tundra regeneration on landslides with

time series satellite imagery. *Environmental Research Letters*, *15*(10), 105020. https://doi.org/10.1088/1748-9326/abb500

Villarreal, S., Guevara, M., Alcaraz-Segura, D., Brunsell, N. A., Hayes, D., Loescher, H. W., & Vargas, R. (2018). Ecosystem functional diversity and the representativeness of environmental networks across the conterminous United States. *Agricultural and Forest Meteorology*, 262, 423–433. https://doi.org/10.1016/j.agrformet.2018.07.016

Walker, D. A., Auerbach, N. A., & Shippert, M. M. (1995). NDVI, biomass, and landscape evolution of glaciated terrain in northern Alaska. *Polar Record*, 31(177), 169–178. https://doi.org/10.1017/S003224740001367X

Walker, D. A., Bockheim, J. G., Chapin III, F. S., Eugster, W., Nelson, F. E., & Ping, C. -L. (2001). Calcium-rich tundra, wildlife, and the "Mammoth Steppe". *Quaternary Science Reviews*, 20, 149−163.

Walker, D. A., Gould, W. A., Maier, H. A., & Raynolds, M. K. (2002). The Circumpolar Arctic Vegetation Map: AVHRR-derived base maps, environmental controls, and integrated mapping procedures. *International Journal of Remote Sensing*, *23*(21), 4551–4570. https://doi.org/10.1080/01431160110113854

Walker, D. A., Leibman, M. O., Epstein, H. E., Forbes, B. C., Bhatt, U. S., Raynolds, M. K., Comiso, J. C., Gubarkov, A. A., Khomutov, A. V., Jia, G. J., Kaarlejärvi, E., Kaplan, J. O., Kumpula, T., Kuss, P., Matyshak, G., Moskalenko, N. G., Orekhov, P., Romanovsky, V. E., Ukraientseva, N. G., & Yu, Q. (2009). Spatial and temporal patterns of greenness on the Yamal Peninsula, Russia: Interactions of ecological and social factors affecting the Arctic normalized difference vegetation index. *Environmental Research Letters*, *4*(4), 045004. https://doi.org/10.1088/1748-9326/4/4/045004

Walker, Donald A., Forbes, B. C., Leibman, M. O., Epstein, H. E., Bhatt, U. S., Comiso, J. C., Drozdov, D. S., Gubarkov, A. A., Jia, G. J., Kaarlejärvi, E., Kaplan, J. O., Khomutov, A. V., Kofinas, G. P., Kumpula, T., Kuss, P., Moskalenko, N. G., Meschtyb, N. A., Pajunen, A., Raynolds, M. K., … Yu, Q. (2010). Cumulative Effects of Rapid Land-Cover and Land-Use Changes on the Yamal Peninsula, Russia. In G. Gutman & A. Reissell (Eds.), *Eurasian Arctic Land Cover and Land Use in a Changing Climate* (pp. 207–236). Springer Netherlands. DOI: 10.1007/978-90-481-9118-5_9

Walker, D. A., Epstein, H. E., Šibík, J., Bhatt, U., Romanovsky, V. E., Breen, A. L., Chasníková, S., Daanen, R., Druckenmiller, L. A., Ermokhina, K., Forbes, B. C., Frost, G. V., Geml, J., Kaärlejarvi, E., Khitun, O., Khomutov, A., Kumpula, T., Kuss, P., Matyshak, G., … Timling, I. (2019). Vegetation on mesic loamy and sandy soils along a 1700-km maritime Eurasia Arctic Transect. *Applied Vegetation Science*, 22(1), 150–167. https://doi.org/10.1111/avsc.12401

Walker, D.A., & M.K. Raynolds. 2018. Circumpolar Arctic Vegetation, Geobotanical, Physiographic Maps, 1982-2003. ORNL DAAC, Oak Ridge, Tennessee, USA. DOI:

10.3334/ORNLDAAC/1323.

Walker, M. D., Wahren, C. H., Hollister, R. D., Henry, G. H. R., Ahlquist, L. E., Alatalo, J. M., Bret-Harte, M. S., Calef, M. P., Callaghan, T. V., Carroll, A. B., & Epstein, H. E. (2006). Plant community responses to experimental warming across the tundra biome. *PNAS*, 103(5).

Wan, Z., Hook, S., Hulley, G. (2015). MOD11A1 MODIS/Terra Land Surface Temperature/Emissivity Daily L3 Global 1km SIN Grid V006 [Data set]. NASA EOSDIS Land Processes DAAC. DOI: 10.5067/MODIS/MOD11A1.006

Yu, Q., Epstein, H. E., Walker, D. A., Frost, G. V., & Forbes, B. C. (2011). Modeling dynamics of tundra plant communities on the Yamal Peninsula, Russia, in response to climate change and grazing pressure. *Environmental Research Letters*, 6(4), 045505. https://doi.org/10.1088/1748-9326/6/4/045505

Zeng, H., Jia, G., & Epstein, H. (2011). Recent changes in phenology over the northern high latitudes detected from multi-satellite data. *Environmental Research Letters*, *6*(4), 045508. https://doi.org/10.1088/1748-9326/6/4/045508

Zhang, T. (2005). Influence of the seasonal snow cover on the ground thermal regime: An overview: Snow Cover and Ground Thermal Regime. *Reviews of Geophysics*, *43*(4). https://doi.org/10.1029/2004RG000157

Summary and Conclusions

Assessing the drivers of peak aboveground biomass (Max NDVI), total productivity (TI-NDVI), ecosystem function (EFTs), and functional diversity (EFT richness) provided multiple perspectives on how vegetation communities were influenced by persistent and changing conditions on the Yamal Peninsula between 2001 and 2018. Spatial analyses found that Max NDVI, TI-NDVI, and EFT distribution were primarily influenced by long-term climate patterns (particularly SWI) on the Yamal Peninsula, while spatial patterns of EFT richness were best predicted by the degree of landscape heterogeneity in an area (captured by the percent water and water distance drivers). Higher SWI and earlier snowmelt facilitated higher Max and TI-NDVI, and spatial gradients in these drivers (in addition to soil moisture and precipitation) allowed for the formation of distinct functional niches on the Yamal Peninsula that were captured by EFTs. EFT-driver relationships indicated that climate change could eventually result in functional convergence driven by shifts towards higher aboveground biomass and earlier max dates, thereby increasing carbon uptake but reducing ecosystem resistance (Cazorla et al., 2021). Higher SWI and longer growing seasons also supported erect shrub and wetland vegetation units with higher Max NDVI, TI-NDVI, and EFT richness. However, it was unclear if the high EFT richness in erect shrub and wetland units was driven by higher landscape heterogeneity, or favorable climate conditions that facilitate more variable vegetation responses and higher species richness (Bieniek et al., 2015; Billings, 1987; Elmendorf et al., 2012; Keenan and Riley, 2018; Walker et al., 2019).

The direction and magnitude of peak aboveground biomass, total productivity, and functional diversity trends were variable across the Yamal Peninsula. Max and TI-NDVI increased across a majority of the Yamal Peninsula between 2001 and 2018, and comparisons to previous studies indicate a recent shift from negative to positive TI-NDVI trends in some areas

(Bhatt et al., 2021; Frost et al., 2020). The discrepancy between this study and previous findings could be due to the timeframe considered, data product used, or the method used for calculating TI-NDVI. Here, TI-NDVI was only calculated for pixels with all growing season composites available to eliminate bias towards low TI-NDVI values due to variable intra-annual coverage. Divergent peak aboveground biomass and total productivity trends (concurrent increases in TI-NDVI and decreases in Max NDVI) observed across 26.7% of the Peninsula were likely caused by a shift from shrub to graminoid dominance (Forbes et al., 2009; Kumpula et al., 2011; Magnússon et al., 2021; Raynolds et al., 2006; van der Kolk et al., 2016). Although this study did not utilize *in situ* vegetation observations to verify this, shifts from shrub to graminoid dominance following disturbance from off-road vehicle tracks and heavy reindeer grazing have been observed on the Yamal Peninsula (Forbes et al., 2009; Kumpula et al., 2011). EFT richness exhibited no trend across a majority of the Peninsula, but 30.0% did exhibit positive EFT richness trends. These findings indicate that functional diversity was maintained despite increases in peak aboveground biomass and total aboveground productivity; however, areas exhibiting divergent trends could be contributing to increasing functional diversity.

Max NDVI, TI-NDVI, and EFT richness trends were best predicted by coast distance, which captured gradients in continentality and SWI due to the influence of sea ice, as well as soil moisture and topographic variability. Higher mean SWI and lower mean soil moisture further inland resulted in stronger positive Max NDVI trends and weaker positive TI-NDVI trends, whereas greater continentality and topographic variability further inland drove stronger positive EFT richness trends by facilitating variable vegetation responses. Melting sea ice is driving coastal increases in SWI (Bhatt et al., 2010) and decreases in continentality (Bhatt et al., 2021), which could facilitate increased shrub growth closer to coastlines and reduce the functional

diversity of inland areas; however, the effect of decreasing continentality could be mitigated by inland topographic variability. Additionally, the Max NDVI, TI-NDVI, and EFT richness trend relationships with climatic driver trends pointed to the influence of climate-induced permafrost disturbances that alter hydrological conditions and increase landscape heterogeneity (Becker et al., 2016; Jorgenson et al., 2015). SWI increases below 0.2 - 0.5 °C months yr^{-1} seemed to primarily impact Max NDVI, TI-NDVI, and EFT richness trends via effects on permafrost disturbances, while more extreme SWI increases exceeding these thresholds likely resulted in increased shrub and graminoid growth (Elmendorf et al., 2012; Walker et al., 2006) that caused stronger positive Max and TI-NDVI trends, but weaker positive EFT richness trends. Shifts toward higher aboveground biomass as warming intensifies is expected to result in positive climate feedbacks that further increase warming by altering albedo and evapotranspiration (Pearson et al., 2013), and advancing phenology could result in trophic mismatch between Arctic vegetation and herbivores (Kerby and Post, 2013; Post et al., 2008). While greater human modification weakened positive Max and TI-NDVI trends and strengthened positive EFT richness trends, extensive vegetation removal associated with infrastructure and permanent settlement expansion would be expected to eventually reduce functional diversity.

As a whole, this thesis provides a comprehensive assessment of vegetation dynamics across the Yamal Peninsula between 2001 and 2018 and highlights the importance of coast distance, elevation, permafrost disturbances, and human modification in addition to climatic drivers. Chapter 1 provides insight into the potential future of other Arctic regions undergoing warming, moisture regime shifts, and increasing human modification, and demonstrates the usefulness of considering multiple NDVI metrics to disentangle the effects of individual drivers across heterogeneous landscapes. Chapter 2 found that Arctic EFTs and EFT richness are useful

tools for monitoring shifting carbon gain dynamics in response to multiple driving forces in complex Arctic ecosystems, and that Arctic regions with heterogeneous landscapes shaped by permafrost disturbance regimes are more likely to experience increases in functional diversity under changing climate conditions. Additional research utilizing *in situ* vegetation data, reindeer herd numbers and migration patterns, and high-resolution imagery that can discern fine-scale landscape features (such as permafrost disturbances) is needed to further elucidate driver effects on Yamal Peninsula vegetation productivity, functioning, and functional diversity. Further, understanding how productivity and functional diversity trends are related could provide insight into how ecosystem resistance may be altered as productivity increases or decreases.

References

Becker, M. S., Davies, T. J., & Pollard, W. H. (2016). Ground ice melt in the high Arctic leads to greater ecological heterogeneity. *Journal of Ecology*, 104(1), 114–124. https://doi.org/10.1111/1365-2745.12491

Bhatt, U. S., Walker, D. A., Raynolds, M. K., Comiso, J. C., Epstein, H. E., Jia, G., Gens, R., Pinzon, J. E., Tucker, C. J., Tweedie, C. E., & Webber, P. J. (2010). Circumpolar Arctic Tundra Vegetation Change Is Linked to Sea Ice Decline. *Earth Interactions*, 14(8), 1–20. https://doi.org/10.1175/2010EI315.1

Bhatt, U. S., Walker, D. A., Raynolds, M. K., Walsh, J. E., Bieniek, P. A., Cai, L., Comiso, J. C., Epstein, H. E., Frost, G. V., Gersten, R., Hendricks, A. S., Pinzon, J. E., Stock, L., & Tucker, C. J. (2021). Climate drivers of Arctic tundra variability and change using an indicators framework. *Environmental Research Letters*, *16*(5), 055019. https://doi.org/10.1088/1748-9326/abe676

Bieniek, P. A., Bhatt, U. S., Walker, D. A., Raynolds, M. K., Comiso, J. C., Epstein, H. E., Pinzon, J. E., Tucker, C. J., Thoman, R. L., Tran, H., Mölders, N., Steele, M., Zhang, J., & Ermold, W. (2015). Climate Drivers Linked to Changing Seasonality of Alaska Coastal Tundra Vegetation Productivity. *Earth Interactions*, *19*(19), 1–29. https://doi.org/10.1175/EI-D-15-0013.1

Billings, W. D. (1987). Constraints to Plant Growth, Reproduction, and Establishment in Arctic Environments. *Arctic and Alpine Research*, 19(4), 357. https://doi.org/10.2307/1551400

Elmendorf, S. C., Henry, G. H. R., Hollister, R. D., Björk, R. G., Boulanger-Lapointe, N.,

Cooper, E. J., Cornelissen, J. H. C., Day, T. A., Dorrepaal, E., Elumeeva, T. G., Gill, M., Gould, W. A., Harte, J., Hik, D. S., Hofgaard, A., Johnson, D. R., Johnstone, J. F., Jónsdóttir, I. S., Jorgenson, J. C., … Wipf, S. (2012). Plot-scale evidence of tundra vegetation change and links to recent summer warming. *Nature Climate Change*, *2*(6), 453–457. https://doi.org/10.1038/nclimate1465

Forbes, B. C., & Stammler, F. (2009). Arctic climate change discourse: The contrasting politics of research agendas in the West and Russia. *Polar Research*, 28(1), 28–42. https://doi.org/10.1111/j.1751-8369.2009.00100.x

Frost, G. V., Bhatt, U. S., Epstein, H. E., Myers-Smith, I., Phoenix, G. K., Berner, L. T., Bjerke, J. W., Forbes, B. C., Goetz, S. J., Kerby, J. T., Macander, M. J., Park, T., Raynolds, M. K., Tommervik, H., and Walker, D. A. (2020). Tundra Greenness. In: Arctic Report Card: Update for 2020. NOAA, Silver Spring, MD. Retrieved from https://arctic.noaa.gov/Report-Card/Report-Card-2020/ArtMID/7975/ArticleID/879/Tundra-Greenness

Jorgenson, M. T., Kanevskiy, M., Shur, Y., Moskalenko, N., Brown, D. R. N., Wickland, K., Striegl, R., & Koch, J. (2015). Role of ground ice dynamics and ecological feedbacks in recent ice wedge degradation and stabilization. *Journal of Geophysical Research: Earth Surface*, 120(11), 2280–2297. https://doi.org/10.1002/2015JF003602

Keenan, T. F., & Riley, W. J. (2018). Greening of the land surface in the world's cold regions consistent with recent warming. *Nature Climate Change*, 8(9), 825–828. https://doi.org/10.1038/s41558-018-0258-y

Kumpula, T., Pajunen, A., Kaarlejarvi, E., Forbes, B. C., Stammler, F. (2011). Land use and land cover change in Arctic Russia: Ecological and social implications of industrial development. *Global Environmental Change*, 21(2), 550-562. https://doi.org/10.1016/j.gloenvcha.2010.12.010

Magnússon, R. Í., Limpens, J., Kleijn, D., van Huissteden, K., Maximov, T. C., Lobry, S., & Heijmans, M. M. P. D. (2021). Shrub decline and expansion of wetland vegetation revealed by very high resolution land cover change detection in the Siberian lowland tundra. *Science of The Total Environment*, *782*, 146877. https://doi.org/10.1016/j.scitotenv.2021.146877

Martin, A. C., Jeffers, E. S., Petrokofsky, G., Myers-Smith, I., & Macias-Fauria, M. (2017). Shrub growth and expansion in the Arctic tundra: An assessment of controlling factors using an evidence-based approach. *Environmental Research Letters*, *12*(8), 085007. https://doi.org/10.1088/1748-9326/aa7989

Oliver, T. H., Heard, M. S., Isaac, N. J. B., Roy, D. B., Procter, D., Eigenbrod, F., Freckleton, R., Hector, A., Orme, C. D. L., Petchey, O. L., Proença, V., Raffaelli, D., Suttle, K. B., Mace, G. M., Martín-López, B., Woodcock, B. A., & Bullock, J. M. (2015). Biodiversity and Resilience of Ecosystem Functions. *Trends in Ecology & Evolution*, *30*(11), 673–

684. https://doi.org/10.1016/j.tree.2015.08.009

Pearson, R. G., Phillips, S. J., Loranty, M. M., Beck, P. S. A., Damoulas, T., Knight, S. J., & Goetz, S. J. (2013). Shifts in Arctic vegetation and associated feedbacks under climate change. *Nature Climate Change*, *3*(7), 673–677. https://doi.org/10.1038/nclimate1858

Raynolds, M. K., Walker, D. A., & Maier, H. A. (2006). NDVI patterns and phytomass distribution in the circumpolar Arctic. *Remote Sensing of Environment*, *102*(3–4), 271–281. https://doi.org/10.1016/j.rse.2006.02.016

van der Kolk, H.J., Heijmans, M. M. P. D., van Huissteden, J., Pullens, J. W. M., & Berendse, F. (2016). Potential Arctic tundra vegetation shifts in response to changing temperature, precipitation and permafrost thaw. *Biogeosciences*, *13*(22), 6229–6245. https://doi.org/10.5194/bg-13-6229-2016

Walker, D. A., Epstein, H. E., Šibík, J., Bhatt, U., Romanovsky, V. E., Breen, A. L., Chasníková, S., Daanen, R., Druckenmiller, L. A., Ermokhina, K., Forbes, B. C., Frost, G. V., Geml, J., Kaärlejarvi, E., Khitun, O., Khomutov, A., Kumpula, T., Kuss, P., Matyshak, G., … Timling, I. (2019). Vegetation on mesic loamy and sandy soils along a 1700-km maritime Eurasia Arctic Transect. *Applied Vegetation Science*, 22(1), 150–167. https://doi.org/10.1111/avsc.12401

Walker, M. D., Wahren, C. H., Hollister, R. D., Henry, G. H. R., Ahlquist, L. E., Alatalo, J. M., Bret-Harte, M. S., Calef, M. P., Callaghan, T. V., Carroll, A. B., & Epstein, H. E. (2006). Plant community responses to experimental warming across the tundra biome. *PNAS*, 103(5).